AN ABSTRACT OF THE DISSERTATION OF

Katherine A. Adams for the degree of Doctor of Philosophy in Oceanography presented on September 4, 2014.

Title: Influence of Upwelling-season Coastal Currents on Near-bottom Dissolved Oxygen Concentrations over a Submarine Bank

Abstract approved:

_____

John A. Barth

Wind-driven coastal upwelling brings subsurface water onto the central-Oregon shelf after the spring transition each year. This cold and salty source water is oxygen-poor, yet above the hypoxic threshold, dissolved oxygen < 1.4 ml l^{-1}. Once on the shelf, dissolved oxygen (DO) concentrations of upwelled near-bottom waters are modified by physical and biological shelf processes, such as advection, mixing and microbial respiration. The influences of shelf processes on near-bottom DO concentrations on tidal, event and seasonal time scales are investigated using moored continuous time series and underwater glider cross-shelf transects over the Heceta and Stonewall Bank complex (HSBC) off central Oregon.

A linear, seasonal decline rate of ~0.01 ml l^{-1} day^{-1} is observed from moored near-bottom continuous time series on the mid shelf over HSBC. This seasonal decline rate is only 30% of the expected draw down from calculated respiration rates over the shelf (0.026 ± 0.013 ml l^{-1} day^{-1}). The severity of low-oxygen concentrations in a given year is a combined result of the biological consumption rate, the physical replenishment rate due to advection and mixing and the length of the season.

Along the Newport Hydrographic (NH) line (44.65°N), cross-shelf variability of hypoxic measurements sampled in over 100 underwater glider cross-shelf transects (2006 – 2012) is investigated. Prevalent near-bottom hypoxic areas are identified on the mid (50-80-m isobaths) and the outer (120-150-m isobaths) shelf regions. The gap in between the two regions is just north of Stonewall Bank, an area of enhanced mixing where higher-DO water is likely mixed into the bottom mixed layer. A seasonal change in near-bottom currents is observed on the mid shelf. In early July of 2011, equatorward along-shelf currents weaken and near-bottom cross-shelf currents change from strongly onshore to weakly onshore and offshore. This change is likely due to the offshore movement of the coastal jet during the upwelling season. Consequently, bottom Ekman transport decreases significantly throughout the upwelling season. Low along-shelf and cross-shelf flow, or flushing, of near-bottom shelf waters increases the risk for hypoxia. Cross-shelf advection cannot account for the large decrease in outer-shelf DO observed in a sequence of 10 glider lines in late-summer 2011. This decrease is attributed to an along-shelf DO gradient of -0.72 ml l^{-1} over 2.58 km, or 0.28 ml l^{-1} per km, such that equatorward near-bottom flow brings low-DO water south past the NH line.

The effect of the Heceta and Stonewall Bank complex on along-shelf variability of shelf and slope waters is investigated during the 2008 upwelling season by comparing the NH glider line with a glider line located just south of the Bank (Umpqua River – UR, 43.7°N). Spicy, subsurface poleward flows, characteristic of the California Undercurrent (CU), are observed along both lines in September 2008. Spice values are proportional to a salinity anomaly and thus can be positive and negative. High spice values indicate transport from the southern CCS via the CU. A poleward core of 0.05 m s^{-1} is observed against the continental slope of the NH line, however the spiciness of this poleward flow is diffuse and reaches a maximum of -0.1 kg m^{-3}. The UR-line poleward core, 0.1 m s^{-1}, and spice maximum, 0.05 kg m^{-3}, are much stronger signals. The average spice field from

64 summertime Seaglider lines collected along the NH line from 2008 to 2012, also show a wide, diffuse subsurface spice signal of magnitude -0.1 kg m^{-3}. Mixing of CU water induced by flow around the Bank is likely resulting in the weak signal observed on the NH line. To investigate the along-shelf difference in shelf water properties, spice-density and DO-density relationships over the 300-m isobath are investigated. Spice along isopycnals which upwell onto the shelf, 26.4 – 26.6 kg m^{-3}, are much higher on the UR line. DO concentrations along isopycnals are similar on the NH and UR lines. This indicates that spicier source water does not equate to lower DO concentrations on the UR line. Near-bottom shelf waters, 10 m above the 100-m isobath, are also spicier on the UR line than the NH line in 2008. A spice-DO relationship for shelf waters indicates the influence of source water variability on shelf DO concentrations is small in comparison to the shelf respiration signal on shelf DO concentrations.

Influence of Upwelling-season Coastal Currents on Near-Bottom Dissolved Oxygen Concentrations over a Submarine Bank

by
Katherine A. Adams

A DISSERTATION

submitted to

Oregon State University

in partial fulfillment of
the requirements for the
degree of

Doctor of Philosophy

Presented September 4, 2014
Commencement June 2015

Doctor of Philosophy dissertation of Katherine A. Adams presented on September 4, 2014.

APPROVED:

Major Professor, representing Oceanography

Dean of the College of Earth, Ocean, and Atmospheric Sciences

Dean of the Graduate School

I understand that my dissertation will become part of the permanent collection of Oregon State University libraries. My signature below authorizes release of my dissertation to any reader upon request.

Katherine A. Adams, Author

ACKNOWLEDGEMENTS

I'm very grateful to Dr. John A. Barth for providing his time, guidance, encouragement and resources over the last 5 years. Dr. Barth leads by example and has been a wonderful mentor, teacher and scientist to work alongside. I also thank my committee members, Drs. Francis Chan, R. Kipp Shearman, James Lerczak, Andrew Valls and the late Murray Levine, for their time, comments and insights.

Several entities contributed to student and research support. The MI_LOCO mooring program was funded by the Betty and Gordon Moore Foundation, Grant #1661. The PISCO program is primarily funded by the Moore Foundation and the David and Lucile Packard Foundation. Oregon State University glider group operations were funded through NSF Grants OCE-0527168 and OCE-0961999. Oregon Sea Grant agreement number NA10OAR4170059 also provided student support.

The faculty of the College of Earth, Ocean and Atmospheric Sciences expertly executed a transfer of knowledge and skills. Both, the formal and informal instruction received throughout the PhD program were instrumental in my journey to become an oceanographer.

I'm very grateful for my experience as a student member of the OSU glider group. Special thanks to Anatoli Erofeev for teaching me how to remotely pilot Slocum gliders. Thanks to Dr. Barth and Dr. Shearman for entrusting me with such a responsibility.

Many folks ensured the work at sea was carried out safely and competently. I especially thank Walt Waldorf, Tully Rohrer and Captain Mike Kriz for teaching me how to deploy and recover instruments off the Oregon coast.

My office mates Craig Risien, Ata Suanda and Piero Mazzini helped tremendously in keeping morale high and in assisting with data analysis

techniques. Many friends in Corvallis provided encouragement and support during this process.

I'm very grateful to my hard working parents, Judy and Harry, who always checked my homework and indulged my early interests in math and science. Thank you for encouraging me not to give up when times were hard and for celebrating even my smallest accomplishments. To my grandmother Dottie, whose perseverance and beauty never fades, thank you for always keeping me in your thoughts. And to my sisters thousands of miles apart for always making time and making me feel at home.

CONTRIBUTION OF AUTHORS

Dr. John A. Barth contributed significantly to the analysis and writing of each manuscript in this dissertation. Dr. Francis Chan was involved with the analysis and writing of the manuscript in Chapter 2. Dr. R. Kipp Shearman was involved with the analysis presented in Chapters 3 and 4.

TABLE OF CONTENTS

TABLE OF CONTENTS (Continued)

Page

LIST OF FIGURES

LIST OF FIGURES (Continued)

LIST OF TABLES

Influence of Upwelling-season Coastal Currents on Near-bottom Dissolved Oxygen Concentrations over a Submarine Bank

1. Introduction

Summertime wind-driven coastal upwelling currents along the California Current System bring source water that is cold, salty and oxygen-poor onto the continental shelf [Hickey, 1979] commencing with the spring transition [Huyer et al., 1979] each year. Equatorward winds drive offshore transport in a surface Ekman layer and a compensatory onshore return flow brings source water up on to the shelf. Upwelled water rich in nutrients reaches the photic zone, promoting phytoplankton blooms in the surface. The subsequent organic matter that is produced rains down through the water column where microbial respiration consumes dissolved oxygen (DO). Near-bottom DO concentrations are further lowered from source water levels due to shelf respiration. At this point it is a balance between physical advection and mixing and biological respiration on the shelf that determines local near-bottom DO variability. However, the relative importance of each of these processes throughout the upwelling season is not well understood or constrained.

Previous observational studies of dissolved oxygen (DO) variability along the western coast of the U.S. reveal decadal changes. These long-term studies show a significant decline in DO concentration and a shoaling of the hypoxic (DO < 1.4 ml l^{-1}) boundary in the eastern subarctic Pacific [Whitney, *et al.*, (2007)] and the continental shelf waters off Oregon [Pierce, *et al.*, (2012)] and California [Bograd, *et al.*, (2008)] over a span of 50 years. Less is known about DO variability and its response to physical drivers on finer time scales over the shelf. *Connolly et al.* (2010) identify advective currents and microbial respiration as drivers of near-bottom DO for the Washington shelf on seasonal to event time scales. Wind relaxations and shelf width were found to drive DO variability on

event scales off California [Send and Nam, 2012]. Oregon-shelf studies have not identified drivers of near-bottom DO variability on these fine time scales.

Specifically, near-bottom flows have not been well addressed in the continental shelf DO variability literature. Near-bottom currents can affect DO concentrations by either mixing or advection. In a 2-dimensional flow regime, where along-shelf variations are small, onshore and offshore transports in the surface and bottom Ekman layers balance one another. In a simplified modeling study, increases in the bottom slope and stratification of the water column can alter the return flow depth from in the bottom boundary layer to just below the surface boundary layer (Lentz and Chapman, 2004). The return flow depth may be important for near-bottom DO variability since a change flow depth in the interior may diminish near-bottom advection, or flushing, which increases the risk for hypoxia. Resolving and identifying the drivers of near-bottom DO variability is necessary to understand what triggers low-DO events and how future changes to ocean climate will affect DO concentrations.

Hypoxia has varying effects on marine organisms [Diaz and Rosenberg, 1995; Gray et al., 2002; Keller et al., 2010; Rankin et al., 2013]. On the central-Oregon coast, hypoxic [Grantham et al, 2004; Hales et al., 2006] and anoxic [Chan et al., 2008] events have resulted in fish and invertebrate deaths, however lethal effects are not observed each year hypoxic levels are recorded. Previous studies of near-bottom DO variability have not incorporated continuous time series, thus the cumulative time that marine organisms are exposed to hypoxic concentrations is unknown. Spatially, DO observations have been limited to a few cross-shelf sections along the Oregon shelf. Recent maps of near-bottom DO along the northern California Current system has identified hypoxic areas from ship transects spaced 40 km apart. However, information on smaller spatial scales is unknown. High-resolution data presented in this dissertation come from the Newport-Hydrographic line (44.65°N), the Umpqua River line (43.7°N) and over

Heceta and Stonewall Bank. The Bank has been identified as a potential vulnerable location from a few cross-shelf transects in 2001 [Hales, et al. 2006]. Barth et al., [2005] also found retentive currents and a high primary productivity signal over the Bank.

Off the central-Oregon shelf, near-bottom potential density anomalies observed during upwelling, 26.4 – 26.5 kg m^{-3}, are observed ~200 m depth offshore. Dissolved oxygen (DO) concentrations along these isopycnals are above the hypoxic threshold (DO < 1.4 ml l^{-1}) which is located around 400-m depth [Pierce et al., 2012]. Hence near-bottom, onshore return flow is low in DO but not hypoxic. Slope waters along upwelling isopycnals is a combination, ~40% at 200-m depth, of North Pacific Upper water and oxygen-depleted Pacific Equatorial water (PEW) [Thomson and Krassovski, 2010]. PEW is transported poleward via the California Undercurrent during the summer [Thomson and Krassovski, 2010; Hickey, 1979]. Observations of the poleward velocities and spice [Flament, 2002] of the CU exist along the NH line [Huyer et al., 2002; Huyer et al., 2007] where a diffuse spice signal and a weak 0.05 m s^{-1} poleward core is observed above the continental slope. However, the influence this signal may have on upwelling source water properties and subsequent shelf DO variability has not been well investigated or constrained. Along-shelf gradients in spice have been reported from a long-term decadal study [Meinvielle and Johnson, 2013] as well as a single along-shelf transect [Pierce et al., 2000]. However, the associated along-shelf DO variability and possible shelf influence has not been well investigated.

In the following chapters, the first continuous time series analysis for the Oregon shelf is presented in Chapter 2. A comparison between the inner and mid shelf is drawn on tidal, event and interannual time scales. In Chapter 3, high-resolution cross-shelf glider transects are used to investigate the drivers of cross-shelf DO variability across the shelf. In Chapter 4, along-shelf differences in slope and shelf water mass properties are presented over Heceta Bank to test the hypothesis that a

stronger California Undercurrent signal may have implications for shelf DO concentrations. In Chapter 5 we summarize and identify future needs for modeling and observations.

2. Temporal variability of near-bottom dissolved oxygen during upwelling off central Oregon

Katherine Adams, John A. Barth, and Francis Chan

Journal of Geophysical Research
2000 Florida Avenue, N.W., Washington DC 20009, USA
Vol. 118, 2013

2.1. Abstract

In the productive central-Oregon coastal upwelling environment, wind-driven upwelling, tides and topographic effects vary across the shelf, setting the stage for varied biogeochemical responses to physical drivers. Current, temperature, salinity and dissolved oxygen (DO) measurements from three moorings deployed during the upwelling seasons of 2009 - 2011 off the central-Oregon coast are analyzed over three time bands (interannual, subtidal, tidal) to explore the relationship between mid- (70 m) and inner-shelf (15 m) upwelling dynamics and the associated effect on DO. Topographic effects are observed in each time band due to the Heceta and Stonewall Bank complex. Seasonal cumulative hypoxia (DO < 1.4 ml l^{-1}) calculations identify two regions, a well-ventilated inner shelf and a mid shelf vulnerable to hypoxia (98 ± 15 days annually). On tidal timescales, intensification of along-shelf diurnal (K1) velocities are intensified over the Bank, 0.08 m s^{-1} compared with 0.03 m s^{-1} to the north. Interannual variability in the timing of spring and fall transitions, defined using glider-measured continental slope source water temperature, is observed on the mid shelf. Interannual source water DO concentrations vary on the order of 0.1 ml l^{-1}. Each spring and summer, DO decline rates are modulated by physical and biological processes. The net observed decrease is about 30% of the expected draw down due to water-column respiration. Physical processes initiate low-oxygen conditions on the shelf through coastal upwelling and subsequently prevent the system via advection and mixing from reaching the potential anoxic levels anticipated from respiration rates alone.

2.2. Introduction

Dissolved oxygen concentrations of continental shelf waters are modulated by physical and biological processes. Wind-driven coastal upwelling currents bring cold, salty, oxygen-poor and nutrient-rich waters onto the Oregon shelf each spring and summer, commencing with the spring transition [*Huyer et al.*, 1979].

The delivery of nutrients via onshore flow of upwelled source water fuels photic-zone productivity and subsequent sub-surface microbial respiration over the shelf. The relative contribution of processes, such as wind-driven advection and microbial respiration, to oxygen variability on the shelf is unknown. Here, we relate continuous time series of near-bottom dissolved oxygen (DO) concentrations to forcing mechanisms across the Oregon shelf and across time bands to identify drivers of oxygen variability. Understanding the drivers of DO spatiotemporal variability is a critical step to understanding the past and predicting the future of low-oxygen events on the Oregon shelf.

Dissolved oxygen (DO) concentrations on the Oregon shelf range between high, ventilated values during winter (> 6 ml l^{-1}, 260 μmol kg^{-1}) and minimum values during the summertime upwelling season (< 2 ml l^{-1}, 87 μmol kg^{-1}) [*Pierce et al.*, 2012]. Recently, oxygen minimum values on the Oregon shelf have fallen below the hypoxic threshold (< 1.4 ml l^{-1}, 60 μmol kg^{-1}) [*Chan et al.*, 2008]. Recent observational studies of DO variability along the western coast of the U.S. reveal changes occurring over several decades based on ship or, more recently, glider measurements. These long-term studies show a significant decline in DO concentration and a shoaling of the hypoxic (DO < 1.4 ml l^{-1}) boundary over a span of 50 years in the eastern subarctic Pacific [*Whitney et al.*, 2007] and the continental shelf waters off Oregon [*Pierce et al.*, 2012] and California [*Bograd et al.*, 2008]. Less is known about dissolved oxygen variability and its response to mechanisms on shorter time scales over the Oregon shelf as the temporal resolution of previous studies do not allow for sub-seasonal scale analysis. Along the California Current system, known drivers of DO temporal variability on shorter timescales than decadal include advective currents and biochemical consumption [*Connolly et al.*, 2010; Washington], shelf width [*Send and Nam*, 2012; Southern California], and El Niño/Southern Oscillation (ENSO) [*Nam et al.*, 2011; Southern California].

The response to upwelling along the Oregon shelf varies with alongshelf bottom topography [*Castelao and Barth*, 2005; *Barth et al.*, 2005]. In a region of complex bottom topography, such as the submarine Heceta and Stonewall Bank Complex (HSBC) (44-44.25°N, Fig 2.1), a 3-D flow regime has been established indicating an intermittent recirculation around the Bank [*Barth et al.,* 2005]. In the along-shelf direction, the coastal upwelling jet (0.25 – 0.50 m s^{-1}) is deflected offshore due to the geometry of the Bank. On the lee, or onshore, side of the Bank, a high chlorophyll signal coincident with weak currents has been observed [*Barth et al.,* 2005]. Here, we expand on this finding by relating upwelling and dissolved oxygen dynamics at locations on the mid and inner shelf, over and north of the Bank (44.25°N).

Biological responses to low-oxygen waters vary by species and oxygen concentration [*Gray et al.,* 2002; *Diaz and Rosenberg*, 1995]. Typical low DO water categorizations include hypoxic (1.4 ml l^{-1}), severely hypoxic (0.5 ml l^{-1}) or anoxic (0 ml l^{-1}). Although long-term biological effects are largely unknown, low-oxygen events have devastating immediate effects on biological communities as evidenced off Oregon by the unprecedented crab mortalities in 2002 [*Grantham et al.*, 2004] and anoxia observed in 2006 [*Chan et al.,* 2008]. Hypoxia has become more frequent since the early 2000s on the central Oregon shelf [*Chan et al.*, 2008], although with high temporal variability and to varying degrees of severity. With continuous time series data we quantify the exposure to hypoxia (< 1.4 ml l^{-1}) on local biological communities not yet reported due to the coarse temporal resolution of previous observational studies. Additionally, bottle respiration rate data is presented from the Oregon mid shelf to quantify the contribution of biological processes on low-oxygen events.

In this paper, we investigate the variability in dissolved oxygen concentrations along the inner- and mid-shelf areas of the central Oregon coast and estimate the relative importance of physical and biological drivers. Continuous moored time

series collected from three consecutive upwelling seasons (2009 – 2011) off the central Oregon mid shelf (44.25°N, 70-m isobath) and inner shelf (44.25°N and 44.75°N, 15-m isobath) (see Fig 2.1) are analyzed in three time bands: subtidal, tidal, and interannual. In section 2.3, we present data sources and processing methods. In Section 2.4, results from investigating drivers of oxygen variability at each time band through correlation analysis, harmonic regression analysis, and oxygen decline analysis are presented. Section 2.5 contains a discussion explaining the results within the context of previous findings and theories. We conclude and identify future research in Section 2.6.

2.3. Data Sources and Processing

2.3.1. Data Sources

The mooring component of the MI_LOCO (Microbial Initiative in Low-Oxygen areas off Concepción and Oregon) Oregon State University (OSU) program focused on collecting near-bottom data from the 70-m isobath off Strawberry Hill (SH70; 44.25°N, 124.25°W), near Yachats, Oregon (Fig 2.1), during the upwelling seasons of 2009 and 2010. An additional year of sampling was conducted in 2011 with partial support of the MI_LOCO program. Three deployments were conducted each season with turnarounds ranging from 2-9 days (Fig 2.2). Instruments measuring temperature, conductivity, dissolved oxygen (DO), and currents were attached to an all-aluminum frame on platforms approximately 0.5 m above the ocean floor. Sea-Bird Electronics, Inc. SBE16plus CTD (conductivity, temperature, depth) and SBE43 (DO) sensors collected measurements on 30-min intervals. Current measurements were made using a Teledyne RD Instruments 300-kHz Workhorse Sentinel Acoustic Doppler Current Profiler (ADCP) on 5-min sampling intervals.

CTD and DO sensors were factory calibrated before and after each field season. ADCP instruments passed all pre-deployment tests including internal compass calibration for hard and soft iron corrections for each deployment. Mooring data

were field calibrated using the weekly-biweekly MI_LOCO ship-based CTD+DO program cast data from the SH70 site [*F. Chan* unpublished]. Calibration casts were also performed on the DO sensor at the end of each deployment. During a calibration cast the moored CTD+DO instrument is attached to a profiling instrument (Sea-Bird Electronics, Inc. SBE25 with SBE43) and data are collected for 5 min at 5-m, 25-m and 50-m water depths. The profiling DO sensor is calibrated periodically through in-lab Winkler titrations of water samples taken throughout the field season. Data from calibration casts were plotted against each other to determine inaccuracies in the moored instrument measurements, e.g. drift. Based on analysis of field calibrations, all factory calibration constants for the moored DO sensor were proven accurate throughout the field season with little to no observed drift between annual factory calibrations.

Since 1998, the Partnership for Interdisciplinary Studies of the Coastal Ocean (PISCO) program at OSU has maintained inner-shelf moorings along the 15-m isobath during the upwelling season along the central Oregon coast. *Kirincich and Barth* [2009] analyzed physical data from the 2004 season. During the 2009 – 2011 field seasons, observations at the Lincoln Beach (LB15, 44.8°N) and Strawberry Hill (SH15, 44.25°N) locations were maintained from April – September (Fig 2.2). Each mooring was outfitted with a Teledyne RD Instruments 600-kHz Workhorse Sentinel ADCP sampling at 2-min intervals, a Sea-Bird Electronics, Inc. SBE16plus CTD and SBE43 DO sensor both with a 15-min sampling interval. Calibration of instruments on the LB15 and SH15 moorings is similar to the SH70 (MI_LOCO) mooring calibration.

Scalar and current data collected in 2009 from 10 miles offshore on the Newport Hydrographic Line (NH10, 44.6°N; Fig 2.1) buoy program are included in this analysis (Fig 2.2). Data from NH10 are available through the NDBC program as station 46094: http://www.ndbc.noaa.gov. Temperature, salinity and dissolved oxygen measurements were made at a depth of 73-m in 80-m of water by a Sea-Bird Electronics, Inc. SBE16plus with a SBE43. Data were collected on 2-hr

intervals. Scalar data from this location are used to extend the SH70 mid-shelf mooring record of 2009 before year day 100 (Fig 2.2) in order to capture the spring transition. Current records at this location, measured by a downward-looking Teledyne RD Instruments 300-kHz ADCP, cover approximately 8 – 70 m of the water column.

Current data from the Coastal Ocean Advances in Shelf Transport (COAST) program in 2001 are included to give context both north and south of the Bank spanning the inner shelf, mid shelf and shelf break (Fig 2.1 & 2) [*Boyd et al.,* 2002].

Hourly-averaged wind speed and direction are from the National Data Buoy Center (NDBC) buoy 46050 (44.64° N, 124.53°W) (Fig 2.1). *Kirincich et al.,* [2005] calculated the correlation between meteorological wind stations off and on shore and found winds at buoy 46050 were strongly correlated to the winds on the coast (> 0.87 correlation coefficient). North-south and east-west components of wind stress were calculated per *Large et al.,* [1994]. Ordinal directions were used rather than principal axis directions (Table 2.1). Gaps in the 2011 NDBC 46050 record were filled by applying regression coefficients (slope = 0.90, offset = -0.34 ms^{-1}) to the onshore C-MAN station NWP03 (44.61°N, 124.07°W) wind data. The correlation coefficient between the measured north-south velocity at 46050 and NWP03 is 0.76 at zero lag with maximum correlation of 0.77 at 1-hr lag (offshore 46050 leading onshore NWP03).

Data collected along the Newport Hydrographic line (NH line) by Teledyne Webb Research Slocum gliders, operated by the OSU glider research group, are used as a proxy for upwelling source water. Near-bottom shelf waters originate from water depths between 100 to 200 m off shore during upwelling (σ_t: 26.4 – 26.6 kg m^{-3}, DO: 1.84 to 2.30 ml l^{-1}) [*Pierce et al.,* 2012]. We define glider-measured source water as $\sigma_t = 26.5 \pm 0.01$ kg m^{-3}, 100 to 200 m between the 250- and 300-

m isobaths, within ± 0.2 degrees of latitude (22 km) of the NH line. This region surrounds NH25 (44.65°N 124.65°W, approx. bottom depth 285 m; Fig 2.1) located 46 km (25 nautical miles) off shore of Newport, Oregon.

At the SH-70 station, near-bottom water samples were collected at 10 time points over the course of the upwelling season in 2009 in order to determine water column oxygen utilization rate measurements. Water was collected from depth via large volume (20 liter) Niskin bottles and immediately dispensed into duplicate, acid-washed, ground glass stoppered 300ml borosilicate bottles. Each bottle was equipped with internal polymer-embedded oxygen-sensitive platinum porphyrine fluorophore pigment spots to enable oxygen concentration determination via a lifetime-based oxygen optode system (Presens GmbH, Regensburg, Germany) [*Steindler et al.,* 2011]. Briefly, oxygen concentration is calculated from the phase shift between pulsed excitation light and pigment fluorescence [*Tenberg et al.,* 2006] as compensated by temperature. This approach enables high-precision determination of oxygen change in individual bottles without breaching the gas-tight seal. The sensor was calibrated pre-cruise with air-saturated (100% DO) and sodium sulfite enriched (0% DO) bottles. Initial oxygen concentrations were determined within 2 to 4 hrs of collection and bottles were held in a dark on-deck temperature-adjusted water bath until transfer to a temperature-controlled (within 1°C of in-situ temperature) dark incubator in the lab. Reference 100% and 0% DO saturation bottles were incubated along side to control for potential sensor drift. Subsequent oxygen concentration readings were taken approximately 18hr and 42hr from initial time zero measurements to calculate water column respiration rates (Table 2.2).

2.3.2. Data Processing

The 5-min (MI_LOCO) and 2-min (PISCO) current records were averaged to 1-hr ensembles. The sea-surface was detected using maximum intensity and pressure measurements for the PISCO moorings. Since pressure measurements were not

recorded by the MI_LOCO mooring ADCP, beam intensity measurements were used as an indicator of the surface; removal of the closest eight bins to the sea surface and deepest bin sufficiently masked feedback from the ocean surface and bottom. Along- and cross-shelf velocity components were derived from the north and east velocity measurements by principal axes rotation. Angles of rotation (Table 2.1) at LB15 and SH15 agree with previous analysis [*Kirincich et al.*, 2005].

Temperature, salinity and dissolved oxygen records were cleaned for erroneous values and hourly averaged. Density anomaly values, $\sigma_t = \rho(S,T,0) - 1000$, are calculated from CTD-measured temperature and salinity. Scalar and current records for each deployment were low-pass filtered (loess filter with 40-hour cutoff window) [Schlax and Chelton 1992], concatenated and gap-filled using a MATLAB boundary value solver [*D'Errico* 2004]. This low-frequency data product is used in the event-scale and interannual analysis (Sections 2.4.1, 2.4.2, and 2.4.4). The residual of the raw data and low-frequency data product for a single deployment in 2009 is used for the high-frequency analysis (Section 2.4.3).

For the interannual analysis, we align DO and density time series by spring transition dates, since the onset of upwelling varies between years. We use two methods to estimate the spring transition. Based solely on wind forcing, *Pierce et al.*, [2006] selects the spring transition date using a statistical change-point detection method to indicate the regime shift from downwelling-favorable winds in wintertime to upwelling-favorable winds in the summertime. For the interannual analysis, low-pass filtered density, dissolved oxygen and cross-shelf and along-shelf current records from SH70 are shifted to begin on the spring transition date (year: Julian Day, 2009:134, 2010:161, 2011:106) for each respective year. Cumulative wind stress and the spring and fall transition dates are currently available: http://damp.coas.oregonstate.edu/windstress/.

As an alternative to the wind forcing-based spring transition, we define the start of the upwelling season based on *in situ* measurements. As isopycnals tilt upward and the onshore flow of source water reaches the shelf, values of temperature and salinity on the shelf reflect offshore values. A spring transition date is determined by the intersection of shelf mooring temperature and salinity time series (SH70 supplemented with NH10 in early 2009) with the glider-measured NH25 source water time series annual average (7.4°C, 33.9 psu) within one standard deviation (year :Julian Day, 2009: 96, 2010: 167, 2011: 127). This index identifies the arrival of upwelling waters onto the shelf which influence near-bottom biogeochemical processes and early-season ecosystem dynamics.

The rate of oxygen decline during each upwelling season is analyzed by fitting linear regression lines to DO time series. Each DO time series is first shifted by the source water-based spring transition date, described above. The fall transition, or end of upwelling season, date marks the increase from source water to wintertime shelf temperatures. DO values less than the source water average concentration (2.3 ml l^{-1}) of each time series are used in the analysis in order to exclude events with elevated measurements (e.g., day 18 and 60 in 2009) and to capture the lower frequency secular trend due to shelf processes over a season. Minimum DO values corresponding to σ_t 26.5 ± 0.1 kg m^{-3} are used in the least-squares linear regression line calculation. The minimum values are selected using a change-point detection algorithm with a tolerance of 0.2 ml l^{-1}.

2.4. Results

2.4.1. Current and density structure

Off the central-Oregon coast, upwelling-favorable winds drive an equatorward coastal jet that is deflected around the submarine Heceta and Stonewall Bank complex [*Castelao and Barth* 2005]. Moored current records from SH15, LB15, SH70 and NH10 (2009) and COAST (2001) locations are analyzed to compare the mean and variability of currents (Fig 2.3). Depth-average current vectors show

the mean equatorward flow at all locations except for SH70, located in the lee of the Bank, confirming previous results [*Barth et al.,* 2005]. Currents at the inner shelf site east of the Bank (SH15) agrees strongly with the inner shelf site north of the Bank (LB15) demonstrating the effect on currents from the Bank does not translate to the inner shelf. This also suggests connectivity between inner shelf sites (SH15, LB15). *Kirincich and Barth* [2009] introduce the idea of a second upwelling jet on the inner shelf, inshore of the Bank. Current variability ellipses (Fig 2.3) show strong north-south variability north of the Bank and an increase in the cross-shelf component of current variability over the Bank except for the inner shelf sites (SH15, COAST SIS). This supports the deflection of the coastal jet moving offshore [*Barth et al.,* 2005] as the upwelling season develops. Mean and fluctuation states of the mid-shelf location, SH70, are anomalously weak and less polarized compared to the inner shelf. Currents at SH15 and LB15 are polarized in the along-shelf direction, in agreement with the 15-m isobath and the mean wind direction.

In the vertical, mean southward and offshore surface flow and onshore return flow in the interior is expected [*Winant et al.,* 1987; *Smith et. al.,* 1981; *Huyer et al,* 1979]. Mean vertical profiles from the inner shelf (SH15, LB15) show southward along-shelf and near-zero depth-integrated cross-shelf flow (Fig 2.4). The mid shelf is anomalous with a cross-shelf mean directed onshore and weakly northward. Along-shelf vertical shear suggests subsurface, poleward pressure-driven flow opposing the direction of the wind-driven currents. The uniform onshore flow at SH70 indicates a deviation from wind-driven Ekman surface transport over the bank due to flow-topography interaction.

Vertical density profiles show the structure of stratification during upwelling at SH15, LB15 and SH70 (Fig 2.4c). Qualitatively similar, the inner shelf sites have weaker stratification and a relatively thicker upper mixed layer (~40% vs ~10%) than the mid shelf site. This indicates vertical, diapycnal advection and mixing

processes are more restricted on the mid shelf. During downwelling, a lighter and well-mixed water column is observed on the inner shelf, whereas only the thicknesses of the boundary layers of the mid shelf density structure change (not shown). The thickness of the bottom mixed layer at SH70 (~20%, or 14 m) yields an estimate for the vertical extent of near-bottom low-oxygen waters for the mid shelf.

2.4.2. Subtidal variability

Low-pass filtered (> 40 hrs, < seasonal) time series of wind stress and moored near-bottom temperature, salinity, dissolved oxygen, and cross- and along-shelf velocities at inner shelf sites SH15 and LB15 and the mid shelf site SH70 during the upwelling season of 2009, reveal differences in low-frequency variability across the shelf (Fig 2.5). With a higher dynamic range than the mid shelf, the inner-shelf records cycle from high to low oxygen at a period of ~30 days that is significantly correlated with along-shelf wind stress (Table 2.3). This cycle can be explained by wind-driven coastal upwelling circulation. During upwelling-favorable wind events, low-oxygen bottom waters are transported to the inner shelf, decreasing the cross-shelf gradient in DO (Fig 2.5; SH15 and SH70). The opposite is observed during downwelling-favorable wind events, when the cross-shelf difference in DO exceeds 6 ml l^{-1} (SH15 – SH70). A similar cycle is evident in temperature and salinity (Fig 2.5), suggesting that low-frequency variability of DO is driven by a physical mechanism: advection via wind-driven upwelling currents. A ~30 day cycle observed in the inner-shelf indicates intraseasonal oscillations, previously found to be due to fluctuations in the location of the Jet Stream [Bane et al., 2007]. Air-sea oxygen fluxes could also cause an increase in near-bottom DO on the inner shelf during times of low stratification, however the event-scale DO cycles observed in 2009 are strongly related to changes in density most likely due to upwelling and downwelling currents.

Near-bottom current records (Fig 2.5e-f), however, have a higher frequency variability, ~2-5 days, similar to the wind record. On day 180 of 2009, during an upwelling-favorable wind event, southward and onshore near-bottom currents at SH15, LB15 and SH70 were observed. Current response to downwelling-favorable wind events is more complicated. On day 245, during a downwelling-favorable event, offshore near-bottom currents are observed on the inner shelf and a response in the mid-shelf record occurs a few days later. Correlation analysis results quantify the relationships between the wind record and moored observations (Table 2.3). Although wind-current correlations are similar across the shelf, wind-DO correlations are larger on the inner shelf due to the strong, cross-shelf gradients advected on the inner shelf between upwelling and downwelling. Furthermore, a positive correlation of wind and near-bottom along-shelf currents at SH70 indicates the strong effect of an along-shelf pressure gradient when upwelling-favorable winds weaken or reverse [*Barth et al.*, 2005].

To quantify the variation of currents across the Bank, cumulative displacements, or time integrated currents, [*Kirincich and Barth*, 2009; *Send and Nam*, 2012] are calculated for the 2009 near-bottom current records. Cumulative displacement (CD) represents the total distance a water parcel travels over time. Along-shelf CDs at the two inner-shelf sites agree well with each other and with the cumulative along-shelf wind stress (Fig 2.6), however, cross-shelf CDs are weak and slightly offshore. North of the Bank, the along-shelf CD for the NH10 mooring agrees with the wind record, but is larger in magnitude than on the inner-shelf, indicating stronger or more persistent southward currents. Cross-shelf CD at NH10 is offshelf, indicating that the onshore compensatory flow balancing the offshore surface Ekman transport is in the interior. The SH70 site is anomalous with onshore and northward along-shelf CD over the season, indicating a recirculation pathway on shore of the Bank and a more retentive, less wind-driven location.

Cumulative hypoxia, or the total time DO < 1.4 ml l^{-1} is observed throughout a season, is an indicator of the frequency of low-oxygen events for each location. Based on the overlapping data records of 2009 (Fig 2.5), cumulative hypoxia results are 3 days (4% of record) at LB15, 12 days (12%) at SH15 and 104 days (73%) at SH70, indicating a large cross-shelf gradient in hypoxic measurements from 15-m to 70-m water depth (10 km cross-shelf distance) and a slight along-shelf gradient between the two inner shelf moorings (60 km alongshelf distance). The mid-shelf site (SH70) located over Stonewall Bank measures hypoxic water for the majority of the observed season.

2.4.3. High-frequency variability

High-pass filtered (< 40 hr) DO records from the three moorings SH15, LB15 and SH70 show a high-frequency range of +/- 2 ml l^{-1} on the inner shelf (Fig 2.7b). The high-frequency variability of DO on the mid shelf is low (< 0.5 ml l^{-1}) yielding two possible scenarios: high-frequency currents differ greatly from the inner shelf or the gradient of mid-shelf DO is low over the length scales affected by the high-frequency currents.

High-pass filtered, depth-averaged currents at SH15, LB15 and SH70 (Fig 2.7d-e) were analyzed using T_Tide [*Pawlowicz et al.*, 2002], a harmonic regression analysis tool. The diurnal (K1) and semidiurnal (M2) amplitudes (m s^{-1}) for along- and cross-shelf current variability are shown in Table 2.4. At the northern site (LB15), a mixed, semidiurnal tide with M2 along-shelf amplitude greater than K1 is found. Since the barotropic tidal velocities are similar between the inner (SH15) and mid shelf (SH70) along 44.25°N, we conclude that the presence of tidal-band variations in dissolved oxygen on the inner shelf are a result of advection of horizontal gradients – higher oxygen present shoreward of the 15-m inner shelf mooring – and their absence at the mid shelf is because horizontal gradients of dissolved oxygen are low there.

Note that the diurnal (K1) tidal constituent is dominant at SH15 and SH70, indicating agreement in tidal velocity variability across the shelf along 44.25°N and a variation in the along-shelf direction. The along-shelf current variability amplitudes explained by the K1 and M2 constituents are 4 times greater at SH15 and SH70 than at LB15. This result is supported by previous modeling work [*Erofeeva et al.*, 2003; *Osborne et al.*, 2011] and verification of model results with COAST mooring data (Fig 2.1) [*J. Osborne*, personal communication] which show a resonance of coastal shelf waves at tidal frequencies (K1, M2) due to the geometry of the Bank.

Mechanisms other than advection of horizontal oxygen gradients by the barotropic tide may contribute to the high-frequency variability of oxygen on the inner shelf (+/- 2 ml l^{-1}). Off Southern California, nonlinear internal waves observed on the inner shelf result in cold water intrusions and enhanced near-bottom mixing [*Nam and Send*, 2011], both of which may impact near-bottom oxygen variability. Nonlinear internal tides are frequently observed in the SH15 and LB15 temperature and velocity records [*Suanda and Barth*, 2012].

Tidal excursion estimates for the K1 and M2 are calculated by integrating over half of a tidal cycle

$$TE = A_{K1} \int_{0}^{0.5 \cdot T_{K1}} \sin\left(\frac{2\pi}{T_{K1}} t\right) dt$$

where A_{K1} is the amplitude of current variability (m s^{-1}) and T_{K1} is the K1 tidal period (23.93 hours). Along-shelf and cross-shelf tidal excursion estimates for the K1 and M2 (Table 2.4) give a spatial bound of the region over the Bank vulnerable to hypoxia: 4.4 km (1.42 km) in the along-shelf (cross-shelf).

2.4.4. Interannual Variability

2.4.4.1. Density and oxygen

Time series of near-bottom density anomaly (σ_t) and dissolved oxygen (DO) observations from three upwelling seasons (2009 – 2011) from the mid-shelf mooring site (SH70; 70-m water depth) are presented in Figure 2.8a. A clear spring transition from wintertime (relatively warm, fresh and high-oxygen water) to summertime values on the mid shelf is evident in early April, 2009 (day 96), mid June, 2010 (day 167), and early May, 2011 (day 128) (Fig 2.8a). The fall transition is most evident in mid-September 2011 (day 236) with a sharp transition due to a storm event, characterized by positive wind stress (not shown) when oxygen increased 1 ml l^{-1} day^{-1} for 4 days.

As each upwelling season progresses, density values approach ~26.5 kg m^{-3}. Dissolved oxygen time series, however, decline at a near-linear rate, quantified and discussed further below. Hypoxia (DO < 1.4 ml l^{-1}) is observed at this location for 104 d (2009), 81 d (2010) and 110 d (2011).

Re-aligning the mid shelf DO time series of each year to start on the respective spring transition date allows for a comparison based on the start of the upwelling season rather than calendar date (Fig 2.8a-c). The time evolution of the shifted time series has a few key differences. First, the values of density and dissolved oxygen at the beginning of upwelling (day 0) are different between the years. Second, the 2009 DO time series now begins at a near-hypoxic value and hypoxic measurements were made ~12-18 days before the start date to the upwelling season (day 134) indicating that the transition to summertime conditions (colder, saltier, lower in oxygen) occurred prior to day 134. Third, shifted density measurements reach a "steady-state" σ_t value (26.5 kg m^{-3}) between days 60 and 80 of each upwelling season. During this time period, while waters of nearly

equal density are measured each year, DO content in 2009 is on the order of 0.5 ml l^{-1} lower than in 2010 and 2011 (Fig 2.8b).

As established above, the spring transition dates as determined by wind alone [*Pierce et al.,* 2006] do not fully capture the low-oxygen season observed on the shelf each year (Fig 2.8a-b). A disconnect between spring transition dates based on wind forcing and *in situ* measurements has been previously observed [*Kosro et* al., 2006]. Hence, we define an alternative spring transition date, based on *in situ* data (see Section 2.3). Shifting density and dissolved oxygen time series by these new dates (Fig 2.8c) reveal remarkable similarity between years, with the exceptions of the two distinct high-oxygen events in 2009 near days 30 and 75. With this new shifting, values of dissolved oxygen and density are similar at the beginning of each upwelling season (day 0), the time series agree throughout most of the upwelling season and a near-linear decline in oxygen is evident. Furthermore, with the new shifting, the variability between years is controlled principally by the slope of the decline and the length of each season (Fig 2.8c). Each upwelling season begins with approximately equal DO concentrations, which are lower than glider-measured source water DO concentrations. The absolute minimum oxygen value observed each year occurs within a week or two of the fall transition. The time separating the spring and fall transition dates yields upwelling season lengths of 121, 92 and 109 days for 2009-2011.

2.4.4.2. Currents

Mean depth-profiles of SH70 current records are very similar between years (Fig 2.4), indicating no significant change of currents averaged over each upwelling season. Time series of cumulative displacements (CD) are calculated, following *Kirincich and Barth* [2009], for the mid-shelf (SH70), near-bottom (~65-m) cross-shelf and along-shelf components of velocity (Fig 2.9b). The CDs on the mid shelf over the Bank are poleward and onshore. Poleward displacement at the SH70 location is opposing the direction of the local wind forcing and further

supports the influence of a poleward along-shelf pressure gradient [*Barth et al.*, 2005]. Changes in cross-shelf displacement on the order of the mid-shelf width (30 km at SH70) occur over 10-30 day periods (Fig 2.9b). These estimated residence times suggest it can take up to one month for water to move on or off the shelf at this location. The stretches of time when cross-shelf CD does not change are periods when flushing rates are lowest on the shelf and biological processes are expected to have an increased effect on oxygen decline.

In 2010 a persistent (~20 day) positive (onshore) near-bottom flow is observed (days 190 – 210, Fig 2.9b) during a strong upwelling-favorable period in the wind record (Fig 2.9a). The strong, uninterrupted near-bottom return flow during 2010 is expected to have a flushing effect on shelf waters to replenish near-bottom oxygen levels to source water concentrations as discussed in Section 2.4.4.5.

2.4.4.3. Winds

Analysis of off-shore wind stress for each upwelling season (as defined in Section 2.3.2 based on *in situ* source water temperature) indicate interannual variability in the cumulative along-shelf wind stress and the occurrence of wind reversals. Cumulative along-shelf wind stress, used as a proxy for upwelling intensity, varies between years (yearday: stress in N m^{-2} day^{-1}: 2009: -2.57; 2010: -3.26; 2011: -1.57) (Table 2.5; Figure 2.9a). This metric shows that stronger upwelling occurred in 2010 than in other years. Stronger winds suggest stronger advective currents, as evident in Figure 2.9c. The ratio of upwelling favorable wind events to downwelling favorable wind events, defined by the cumulative time negative:positive along-shelf wind stress was measured, also differs significantly (Table 2.5). Downwelling relative to upwelling was higher in 2009 and 2011 than in 2010. Furthermore, in 2009 (2010) (2011), upwelling favorable winds were observed 2.1 (5.4) (2.3) times more than downwelling favorable winds. This ratio is indicative of the distribution of upwelling over a season rather than the total

amount which may be of first order importance to biological communities and biogeochemical cycles on the shelf [*A. Galan*, personal communication].

2.4.4.4. Source water

Coastal upwelling brings cold, salty, oxygen-poor and nutrient-rich water, here called source water, onto the central-Oregon shelf each year. Source water dissolved oxygen concentrations are low, but are above the hypoxic threshold of 1.4 ml l^{-1}. While the exact source water pathway over the Bank is not known in detail, earlier work suggests that source water may originate from the slope southwest of the Bank [*Castelao and Barth*, 2005]. In the absence of data from this part of the slope, glider data (30-day averages, σ_t of 26.5±0.01 kg m^{-3}) of waters from NH25 (Fig 2.1), along the Newport-hydrograph line are used as a proxy for source water over the Bank due to its location over the slope. DO values at σ_t of 26.5 kg m^{-3} are higher (> 2 ml l^{-1}) at NH25 than measurements on the shelf (< 1.4 ml l^{-1}) (Fig 2.8). A strong correlation between glider-measured source water DO and density is calculated for 2009 - 2011 (Figure 2.10). For a 0.1 kg m^{-3} change in density, a ~0.32 ml l^{-1} change in oxygen is observed at NH25. The interannual variability of average source water DO concentration at σ_t of 26.5 kg m^{-3} is O(0.1 ml l^{-1}). Source water concentrations are above the hypoxic threshold indicating hypoxic waters are not advecting onto the shelf from offshore.

Differences between 30-day averaged source water (glider; NH25) and shelf (SH70) dissolved oxygen measurements reveal a seasonal cycle (Fig. 2.11). During wintertime, the shelf is ventilated due to strong mixing and advection yielding higher DO concentration over the slope. During the upwelling season, the DO levels on the shelf decrease 1.5 ml l^{-1} below source water concentrations, due to shelf processes such as microbial respiration. Interannual variability in the phase and amplitude of this cycle is observed. If source water concentrations controlled DO levels on the shelf, this annual cycle would level off near zero after the spring transition assuming the DO concentration of source water is constant.

The fall transition marks the end of the upwelling season as shelf DO increases due to the increased mixing associated with strong winter storms.

2.4.4.5. Net Dissolved Oxygen Decline

At the beginning of the upwelling season, dissolved oxygen concentrations on the shelf sharply decrease to source water levels (> 2 ml l^{-1}) and continue to decline due to biogeochemical consumption. A low-frequency, near-linear decline is apparent in the shifted SH70 DO time series (Fig 2.8c). This observed decline during the upwelling season is modulated by respiration, advection, and mixing. To determine and quantify which processes control the rate of oxygen decline on the shelf, linear regression lines are fitted to DO and density time series at LB15, SH15 and SH70 (2009 – 2011). Mid-shelf SH70 net DO decline rates of -1.0 ± 0.1 x 10^{-2} (-0.5 ± 0.2 x 10^{-2}) (-1.0 ± 0.2 x 10^{-2}) ml l^{-1} day^{-1} result in a decrease of ~0.3 ml l^{-1} per 30 days (Fig 2.12a). The lower rate of decline in 2010 agrees well with the onshore near-bottom transport of source water and prolonged upwelling-favorable winds (Fig 2.9a) (Sections 2.4.4.1 & 2.4.4.2). The inner-shelf sites (LB15 and SH15) experience high-oxygen events the majority of the upwelling season. A linear decline of low-oxygen events is observed at SH15 but not at LB15 (not shown). The net observed decline of DO along 44.25°N (SH15 and SH70) suggests a pathway of onshore flow from SH70 (cumulative hypoxia ~ 90 days) to SH15 (cumulative hypoxia ~ 12 days) and is important for nearshore biological communities, especially during years of severe hypoxia [*Chan et al.,* 2008].

Comparing the mid shelf net DO decline rates to the pelagic respiration rates measured at SH70 during 2009 (Table 2.2), we find that the observed seasonal rates of decline are less than that expected due to respiration alone. Interpolating respiration rates between samples yields a biologically-induced DO decrease of ~3 ml l^{-1} over an upwelling season. An oxygen sink of this magnitude would result in anoxia approximately 95 days into the 2009 upwelling season (Fig

2.12a); however, anoxia was not observed. This result indicates that the rate of DO decline on the shelf is restricted due to the physical (advection, mixing) processes, not the availability of organic matter. Rates of change on shorter time scales (2-5 days) are much higher than respiration rates (Fig 2.12a). These sharp changes in oxygen concentration can be explained by advection of gradients, not local biogeochemical properties.

As presented in Figure 2.10, an oxygen decline of 0.32 ml l^{-1} is expected for a 0.1 kg m^{-3} decrease in source water density. The contribution of density changes to the observed oxygen decline at SH70 (Fig 2.12a), is calculated by fitting linear regression lines to the density time series (Fig 2.12b) at measurements used in the DO regression analysis. There is no significant change in density over the 2009 upwelling season and a decrease of 0.2 kg m^{-3} in 2010 and an increase of 0.1 kg m^{-3} in 2011 (Fig 2.12b). Applying the source water DO-density relationship (Fig 2.10), no significant change in oxygen is expected in 2009 and a change of 0.65 (-0.31) ml l^{-1} is expected in 2010 (2011). The DO variability associated with density changes is due to advection and mixing processes acting across isopycnals.

The relationship of physical:biological mechanisms driving oxygen decline varies between years. To quantify the contribution of the drivers of DO variability at SH70 each year, the effect of respiration (assuming the average rate from 2009 of -2.6×10^{-2} ml l^{-1} day^{-1} x days of upwelling) and density (slopes from Figure 2.2.12b x days of upwelling) are subtracted from the observed net oxygen decline rates (slopes from Figure 2.12a times days of upwelling) revealing a residual which we attribute to advection and mixing processes along the 26.5 kg m^{-3} isopycnal (Figure 2.13). Positive residuals signify that physical processes (advection and mixing) are responsible for oxygen concentrations on the shelf from reaching the anoxic levels that are anticipated from respiration rates alone. The relative contribution from physical (density + residual) versus biological

mechanisms is calculated as (density + residual)/respiration. The three-year average is (1.7 + 0.1)/ 2.8, or 64%, contribution by physical processes. Alternatively, the net observed decrease is 36% of the potential draw down expected from microbial respiration. Variations in source water DO concentrations (not presented here) are small in comparison to the net observed rates of the decline (Fig 2.12a) and the calculated change in DO due to density (Fig 2.12b). In 2010, hypoxia was less severe than in other years. We attribute this to the shorter season length (Fig 2.8, Table 2.5) and to the decrease in source water density throughout the season (Fig 2.12b, Fig 2.13).

2.5. Discussion & Summary

Dissolved oxygen measurements of near-bottom central-Oregon shelf waters are compared across time bands and across the shelf to investigate driving mechanisms of variability. The analysis of continuous time series of DO reveals event-scale, high frequency (tidal) and seasonal variability not previously resolved with conventional ship-based sampling conducted on the Oregon shelf. The inner shelf (15 m) is well-ventilated during reversals or downwelling-favorable wind events and has a low incident rate of low-oxygen, or hypoxic (DO < 1.4 ml l^{-1}), events. The mid shelf location (70 m) in the lee of the Heceta and Stonewall Bank complex, however is less correlated with wind forcing and experiences 98 ±15 days of hypoxia annually. The Bank is especially vulnerable to low-oxygen events due to the large shelf width, as well as weak currents and high productivity [*Barth et al.,* 2005]. Previous ship-based measurements from the 2002 upwelling season indicate hypoxia on the central-Oregon shelf (~50-m water depths) from July to September (~90 days) [*Grantham et al.,* 2004]. Our results corroborate their finding and paint a clearer picture for ecological implications; hypoxia on the mid shelf over the Bank is recurring annually and is present for the majority of each upwelling season.

High-frequency, or tidal band, analysis shows an amplification of K1 tidal currents at the inner and mid shelf locations along 44.25°N due to the bank geometry. Near-bottom DO tidal fluctuations are $O(2\ \text{ml}\ \text{l}^{-1})$ on the inner shelf and are much less on the mid shelf. Variability of this magnitude is an important consideration for ship-based observational studies with duration longer than half an M2 tidal period. Tidal excursion calculations (Table 2.4) yield spatial estimates for the mid shelf low-oxygen zone of 2.2 and 0.27 km in the along- and cross-shelf directions, respectively. The M2 internal tide may also contribute to inner-shelf, near-bottom DO fluctuations but is not explicitly studied here.

On seasonal timescales, variability of DO over the Oregon shelf is controlled by physical and biological processes in concert. Wind-driven coastal upwelling initiates low-oxygen events on the shelf via the transport of source water which, off Oregon, has DO concentrations above the hypoxic threshold ($1.4\ \text{ml}\ \text{l}^{-1}$). Biological and biogeochemical processes take effect in the productive spring and summer, and the balance of respiration and advection/mixing along with the season length determine the duration of low-oxygen events on the shelf each year. Seasonal decreases in shelf oxygen below source water concentrations range from $0.4 – 1.2\ \text{ml}\ \text{l}^{-1}$, similar to findings on the Washington shelf ($0.5 – 2.5\ \text{ml}\ \text{l}^{-1}$) [*Connolly et al*., 2010]. DO decline rates are linear for the 2009 – 2011 upwelling seasons. One of the determining factors of how low near-bottom DO concentrations drop, therefore, is the season length. This fits with the 2006 upwelling season, almost 200 days in duration, when anoxia was first observed on the Oregon inner shelf. The average net observed DO decline rate for 2009-2011 ($-0.9 \times 10^{-2}\ \text{ml}\ \text{l}^{-1}\ \text{day}^{-1}$) is only 32% of the expected decline due to the average water column respiration rate from 2009 ($-2.6 \times 10^{-2}\ \text{ml}\ \text{l}^{-1}\ \text{day}^{-1}$). This indicates physical processes such as advection and mixing are “flushing” or entraining higher DO water into the near-bottom environment. In fact, stronger onshore flow supports the less severe hypoxia observed in 2010. Without the contribution from

physical processes, anoxia is expected about 90 days into the upwelling season (Fig 2.12).

Since upwelling source water DO concentrations are above the hypoxic threshold, hypoxia cannot occur on the Oregon shelf without the presence of biological processes (e.g. microbial respiration) (Fig 2.11); nor on the Washington shelf [*Connolly et al.,* 2010]. In addition to the water-column respiration rates presented here, benthic oxygen fluxes into the sediment also contribute to near-bottom hypoxia. *Reimers et al*., [2012], based on a single realization, find Oregon mid shelf benthic oxygen consumption (~ 1 μM d^{-1} or 2.3 x 10^{-2} ml l^{-1} d^{-1}) in the sediment surface to contribute to hypoxia. This benthic respiration rate is nearly equal to the pelagic average from 2009 (2.6 x 10^{-2} ml l^{-1} d^{-1}). Similarly, on the Washington shelf, *Connolly et al.* [2010] found water column respiration rates within the range reported here. Accounting for benthic oxygen flux, the average observed DO decline of 0.9 ml l^{-1} (Fig 2.13) would change from 32% (pelagic only) to 16% of the expected DO decline due to pelagic and benthic respiration.

By understanding how physical and biological processes affect DO on the shelf, we can project how predicted climate change effects will alter shelf DO concentrations. Based on our analysis, conditions conducive to more severe shelf hypoxia include longer upwelling seasons, denser source water, lower DO source water concentrations, and lower advection and mixing rates. If the effectiveness of physical processes, presently keeping biological processes in check, is diminished, then severe hypoxia or anoxia is expected on the Oregon shelf. Although changes in advection and mixing rates due to climate change are uncertain, source water DO concentrations may decline [*Keeling et al.*, 2010].

The source water DO concentration difference between years of O(0.1 ml l^{-1}) does not account for the ~1 ml l^{-1} difference in observed oxygen decline over the 2010 season (Fig 2.13) or the slower seasonal rate of decline (Fig 2.12a) compared to

other years. Monthly source water averages of temperature, salinity and oxygen are similar between years unlike the southern California shelf where interannual DO variability, O(~2 ml l-1) is attributed to El Niño/Southern Oscillation (ENSO) [Nam et al., 2011]. Large-scale circulation differences between Oregon and California explain this difference. First, the California shelf is impacted greater by events originating at the equator. Only 30% of the Pacific Equatorial water signal makes it up to Oregon via the CU [*Thomson and Krassovski*, 2010]. Second, the northern part of the CCS is greatly influenced by subarctic water masses [*Whitney et al.*, 2007] which may dampen the ENSO signal off the Oregon shelf. Although interannual variability of source water characteristics is small during the three years of this study, long-term variability and driving mechanisms of the source water composition upwelling on the Oregon shelf are largely unknown. Understanding source water origins is a future research direction that has important implications for shelf processes during the upwelling season.

The near-bottom time series presented here do not address questions about the vertical structure of hypoxia. Data from the proposed instruments on the National Science Foundation's Ocean Observatories Initiative Endurance line, off Newport, Oregon, will be able to address vertical gradients in physical water properties and oxygen. Vertical resolution is key to understanding the stress exposure to biological communities in the water column as well as to parameterize vertical mixing rates. Biophysical models could be used to address questions left unanswered here regarding the relative importance of benthic versus pelagic respiration or cross-shelf versus along-shelf advective fluxes on near-bottom oxygen dynamics.

2.6. Acknowledgments

The authors would like to acknowledge the Gordon and Betty Moore Foundation for the support of the MI_LOCO program (Grant # 1661). This is contribution 440 from PISCO, the Partnership for Interdisciplinary Studies of Coastal Oceans

funded primarily by the David and Lucile Packard Foundation and the Gordon and Betty Moore Foundation. We thank our OSU glider group colleagues, specifically K. Shearman, A. Erofeev, Z. Kurokawa and P. Mazzini, for glider data collection along the Newport Hydrographic line supported by National Science Foundation (NSF) Grants OCE-0527168 and OCE-0961999. M. Levine provided the COAST and NH10 mooring data. Instruments were borrowed from E. Dever, C. Wingard and R. Letelier for the SH70 mooring. We thank SungHyun Nam for his thoughtful review. Special thanks to W. Waldorf, C. Risien and A. Suanda for invaluable guidance with programming instruments, processing data and assistance in the field. We thank the marine technicians who assisted with mooring operations: J. Brodersen, K. Page-Albins, B. Focht, T. Rohrer, D. Swensen, D. O'Gorman, and E. Arnesen as well as Captain Mike Kriz and the crew of the R/V Elakha for their data collection efforts.

REFERENCES

[1] Bane, J.M., Y. H. Spitz,, R. M. Letelier, and W. T. Peterson (2007), Intraseasonal oscillations in Oregon's coastal upwelling system: from the jet stream to zooplankton. *Proceedings of the National Academy of Sciences*, USA 104, 13262–13267.

[2] Barth, J. A., S. D. Pierce, and R. M. Castelao (2005), Time dependent, wind-driven flow over a shallow mid shelf submarine bank. *J. Geophys. Res*., 110, C10S05, doi:10.1029/2004JC002761.

[3] Bograd, S. J., C. G. Castro, E. Di Lorenzo, D. M. Palacios, H. Bailey, W. Gilly, and F. P. Chavez (2008), Oxygen declines and the shoaling of the hypoxic boundary in the California Current, *Geophys. Res. Lett., 35,* L12607, doi:10.1029/2008GL034185.

[4] Boyd, T., M.D. Levine, P.M. Kosro, S.R. Gard, and W. Waldorf (2002), Observations from Moorings on the Oregon Continental Shelf (May-August 2001), COAS Data Report 190, Reference 2002-6.

[5] Castelao, R. M., and J. A. Barth (2005), Coastal ocean response to summer upwelling favorable winds in a region of alongshore bottom topography variations off Oregon, *J. Geophys. Res*., 110, C10S04, doi:10.1029/2004JC002409.

[6] Chan, F., J. A. Barth, J. Lubchenco, A. Kirincich, H. Weeks, W. T. Peterson, B. A. Menge (2008), Emergence of anoxia in the California Current large marine ecosystem, *Science*, 319, doi:10.1126/science.1149016.

[7] Connolly, T. P., B. M. Hickey, S. L. Geier, and W. P. Cochlan (2010), Processes influencing seasonal hypoxia in the northern California Current system, *J. Geophys. Res.*,115, C03021, doi:10.1029/2009JC005283.

[8] D'Errico, J. (2004), Inpaint_nans, (http://www.mathworks.com/matlabcentral/fileexchange/4551), MATLAB Central File Exchange. Retrieved 24 June 2012.

[9] Diaz, R. J., and J. Rosenberg (1995), Marine benthic hypoxia: A review of its ecological effects and the behavioural responses of benthic macrofauna, Oceanogr. Mar. Biol., 33, 245–303.

[10] Erofeeva, S. Y., G. D. Egbert, and P. M. Kosro (2003), Tidal currents on the central Oregon shelf: Models, data, and assimilation, J. Geophys. Res., 108, 3148, doi:10.1029/2002JC001615.

[11] Grantham, B. A., F. Chan, K. J. Nielsen, D. S. Fox, J. A. Barth, A. Huyer, J. Lubchenco, and B. A. Menge (2004), Upwelling-driven nearshore hypoxia signals ecosystem and oceanographic changes in the Northeast Pacific, Nature, 429, 749-754.

[12] Gray, J. S., R. S. Wu, and Y. Y. Or (2002), Effects of hypoxia and organic enrichment on the marine environment, Mar. Ecol. Prog. Ser., 238, 249–279, doi:10.3354/meps238249.

[13] Huyer, A., E. J. C. Sobey, R. L. Smith (1979), The spring transition in currents over the Oregon continental shelf. J. Geophys. Res., 84, 6995–7011.

[14] Keeling, R. F., A. Kortzinger, and N. Gruber (2010), Ocean deoxygenation in a warming world, Annu. Rev. Mar. Sci., 2, 199-229.

[15] Kirincich, A. R., J. A. Barth, B. A. Grantham, B. A. Menge, and J. Lubchenco (2005), Wind-driven inner-shelf circulation off central Oregon during summer, *J. Geophys. Res*., 110, C10S03, doi:10.1029/2004JC002611.

[16] Kirincich, A. R., and J. A. Barth (2009), Alongshelf Variability of Inner-Shelf Circulation along the Central Oregon Coast during Summer, *J. Phys. Oceanogr*., 35, 1380 – 1398, doi: 10.1175/2008JPO3760.1.

[17] Kosro, P. M., W. T. Peterson, B. M. Hickey, R. K. Shearman, and S. D. Pierce (2006), Physical versus biological spring transition: 2005, *Geophys. Res. Lett*., 33, L22S03, doi:10.1029/2006GL027072.

[18] Large, W. G., J. C. McWilliams, and S. C. Doney (1994), Oceanic vertical mixing: A review and a model with a nonlocal boundary layer parameterization, *Rev. Geophys*., 32, 363-403.

[19] Nam, S. H., and U. Send (2011), Direct evidence of deep water intrusions onto the continental shelf via surging internal tides, *J. Geophys. Res.*, 116, C05004, doi:10.1029/2010JC006692.

[20] Nam, S. H., H. J. Kim, and U. Send (2011), Amplification of hypoxic and acidic events by La Niña conditions on the continental shelf off California, *Geophys. Res. Lett*., 38, L22602, doi:10.1029/2011GL049549.

[21] Osborne, J. J., A. L. Kurapov, G. D. Egbert, and P. M. Kosro (2011), Spatial and Temporal Variability of the M2 Internal Tide Generation and Propagation on the Oregon Shelf, *J. Phys. Oceanogr.*, 41, 2037–2062. doi:10.1175/JPO-D-11-02.1.

[22] Pawlowicz, R., B. Beardsley, and S. Lentz (2002), Classical tidal harmonic analysis including error estimates in MATLAB using T_TIDE, *Comput. Geosci*., 28, 929–937.

[23] Pierce, S. P., J. A. Barth, R. E. Thomas, and G. W. Fleischer (2006), Anomalously warm July 2005 in the northern California Current: Historical context and significance of cumulative wind stress. *Geophys. Res. Lett*., 33, L22S04, doi:10.1029/2006GL027149.

[24] Pierce, S. D., J. A. Barth, R. K. Shearman, A. Y. Erofeev (2012), Declining Oxygen in the Northeast Pacific, *J. Phys. Oceanogr.*, 42, 495–501. doi:10.1175/JPO-D-11-0170.1.

[25] Reimers, C.E., H. T. Özkan-Haller, P. Berg, A. Devol, K. McCann-Grosvenor, and R. D. Sanders (2012), Benthic Oxygen Consumption Rates during Hypoxic Conditions on the Oregon Continental Shelf: Evaluation of the Eddy Correlation Method. *J. Geophys. Res.* 117, C02021, doi:10.1029/2011JC007564.

[26] Send, U. and S. H. Nam (2012), Relaxation from upwelling: The effect on dissolved oxygen on the continental shelf. *J. Geophys. Res.* 117, C04024, doi:10.1029/2011JC007517.

[27] Schlax, M. G., and D. B. Chelton (1992), Frequency domain diagnostics for linear smoothers. *J. Amer. Stat. Assoc.*, 87, 1070-1081.

[28] Smith, R. L. (1981), A comparison of the structure and variability of the flow field in three coastal upwelling regions: Oregon, northwest Africa, and Peru, in *Coastal Upwelling, Coastal Estuarine Ser*., vol. 1, edited by F. A. Richards, pp. 107– 118, AGU, Washington, D. C.

[29] Steindler L., M. S. Schwalbach, D. P. Smith, F. Chan, and S. J. Giovannoni (2011), Energy Starved Candidatus Pelagibacter Ubique Substitutes Light-Mediated ATP Production for Endogenous Carbon Respiration. *PLOS ONE* 6(5): e19725. doi:10.1371/journal.pone.0019725.

[30] Suanda, A. and J. A. Barth (2012), Observations of High-Frequency Internal Waves across the Oregon Inner Shelf, paper presented at 2012 Ocean Sciences Meeting, ASLO and AGU, Salt Lake City, Utah. http://www.sgmeet.com/osm2012/viewabstract2.asp?AbstractID=10085

[31] Tengberg A., J. Hovdenes, H. Andersson, O. Brocandel, R. Diaz, D. Hebert, T. Arnerich, C. Huber, A. Kortzinger, A. Khripounoff, F. Rey, C. Ronning, J. Schimanski, S. Sommer, A. Stangelmayer (2006), Evaluation of a lifetime-

based optode to measure oxygen in aquatic systems. *Limnology and Oceanography methods*, 4, 7-17.

[32] Thomson, R. E., and M. V. Krassovski (2010), Poleward reach of the California undercurrent extension. *J. Geophys. Res.*, 115, C09027, doi:10.1029/2010JC006280.

[33] Whitney, F. A., H. J. Freeland, and M. Robert (2007), Persistently declining oxygen levels in the interior waters of the eastern subarctic Pacific, *Prog. Oceanogr.*, 75, 179-199, doi:10.1016/j.pocean.2007.08.007.

[34] Winant, C. D., R. C. Beardsley, R. E. Davis, (1987), Moored Wind, Temperature,and Current Observations Made During Coastal Ocean Dynamics Experiments 1 and 2 Over the Northern California Continental Shelf and Upper Slope. *J. Geophys. Res., 92, C2,* 1569-1604.

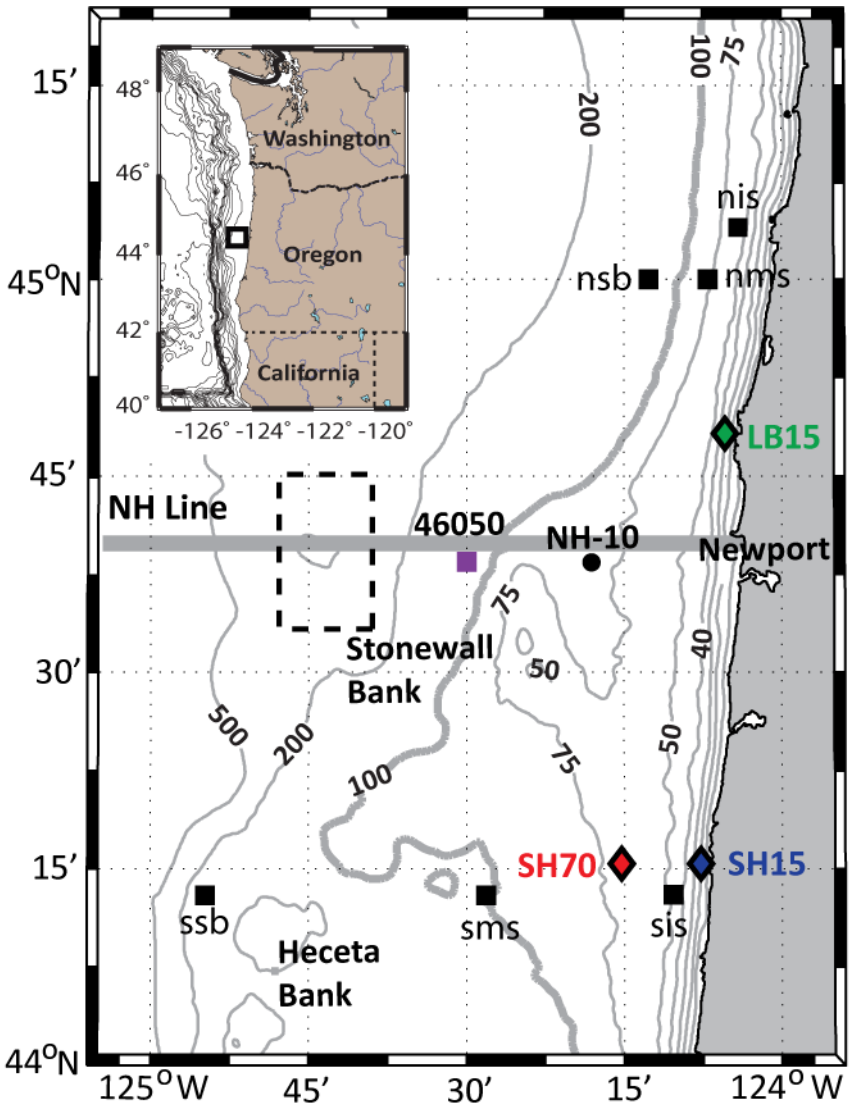

Figure 2.1: Central-Oregon shelf study area with Pacific northwestern U.S. inset. Mooring locations from COAST (2001; black squares), NH-10 (2009), PISCO (2009 – 2011; SH15 and LB15) and MI_LOCO (2009 – 2011; SH70). Wind measurements from NDBC 46050 and NWP03, as well as glider measurements from Newport-hydrographic line (NH) station NH-25 (dashed box) are also shown.

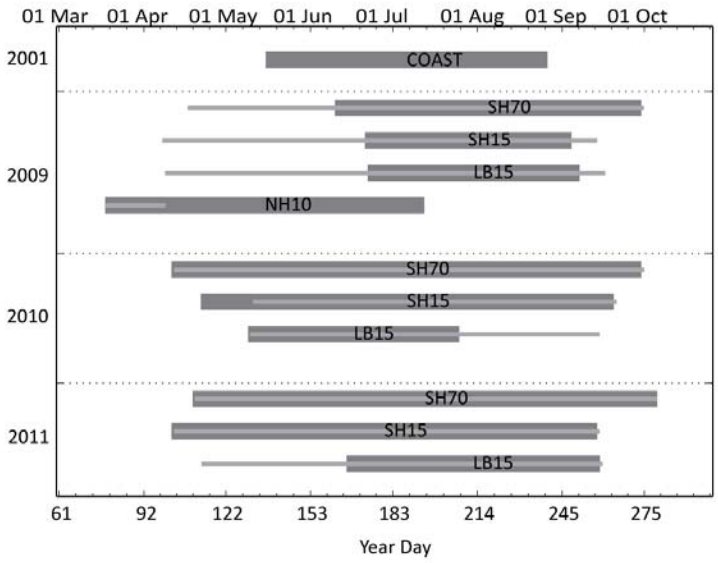

Figure 2.2: Timeline of CTD (thin) and ADCP (thick) measurements from COAST, SH15, LB15, SH70 and NH-10 mooring programs for indicated years.

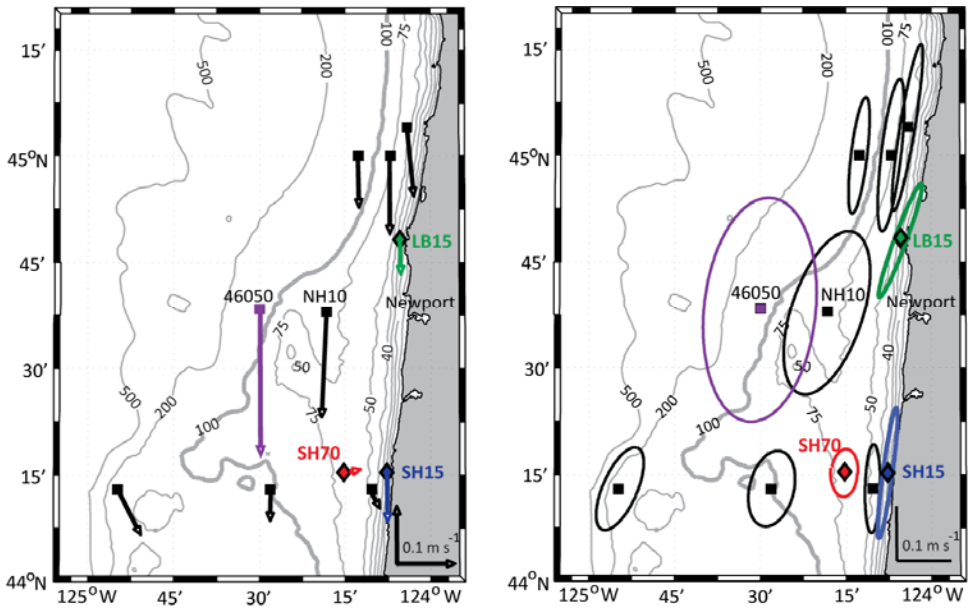

Figure 2.3: Depth-averaged velocity vectors (left) and variability ellipses (right) for mooring locations described in Section 2.1. Wind velocity data from NDBC 46050 are scaled down to 1/10 original magnitude. Semi-major (-minor) axis lengths of ellipses are equivalent to the standard deviation of depth-averaged along-shelf (cross-shelf) velocities at each location: black (COAST 2001 and NH-10 2009); green (Lincoln Beach 15-m water depth 2009 - LB15); blue (Strawberry Hill 15-m water depth 2009 - SH15); and red (Strawberry Hill 70-m water depth 2009 - SH70).

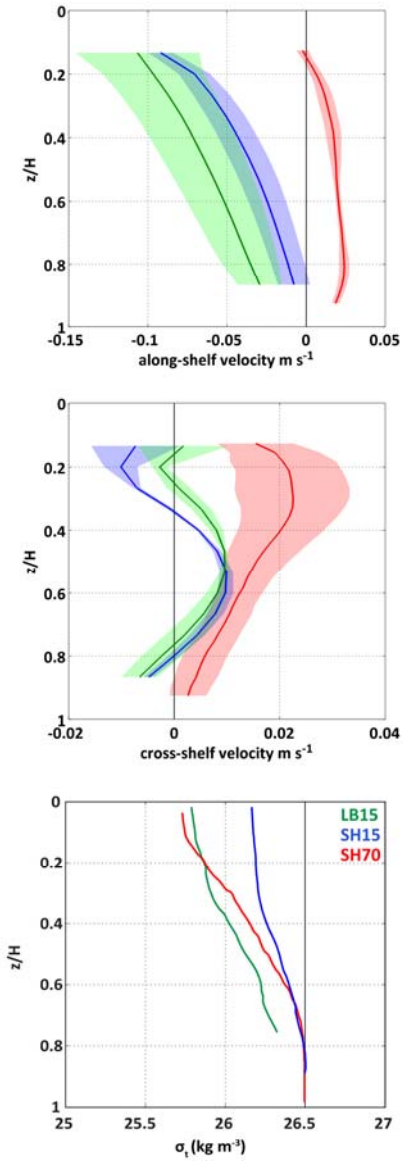

Figure 2.4: Depth profiles of along-shelf (a) and cross-shelf (b) velocities averaged over three field seasons (2009 – 2011), with standard deviation shaded, at SH15 (blue), LB15 (green) and SH70 (red). Positive velocities represent northward and onshore flows. (c) Ship-cast density data show typical vertical structure during upwelling. The vertical axis, z/H, is measurement depth normalized by water depth where 0 is the surface and 1 is the bottom.

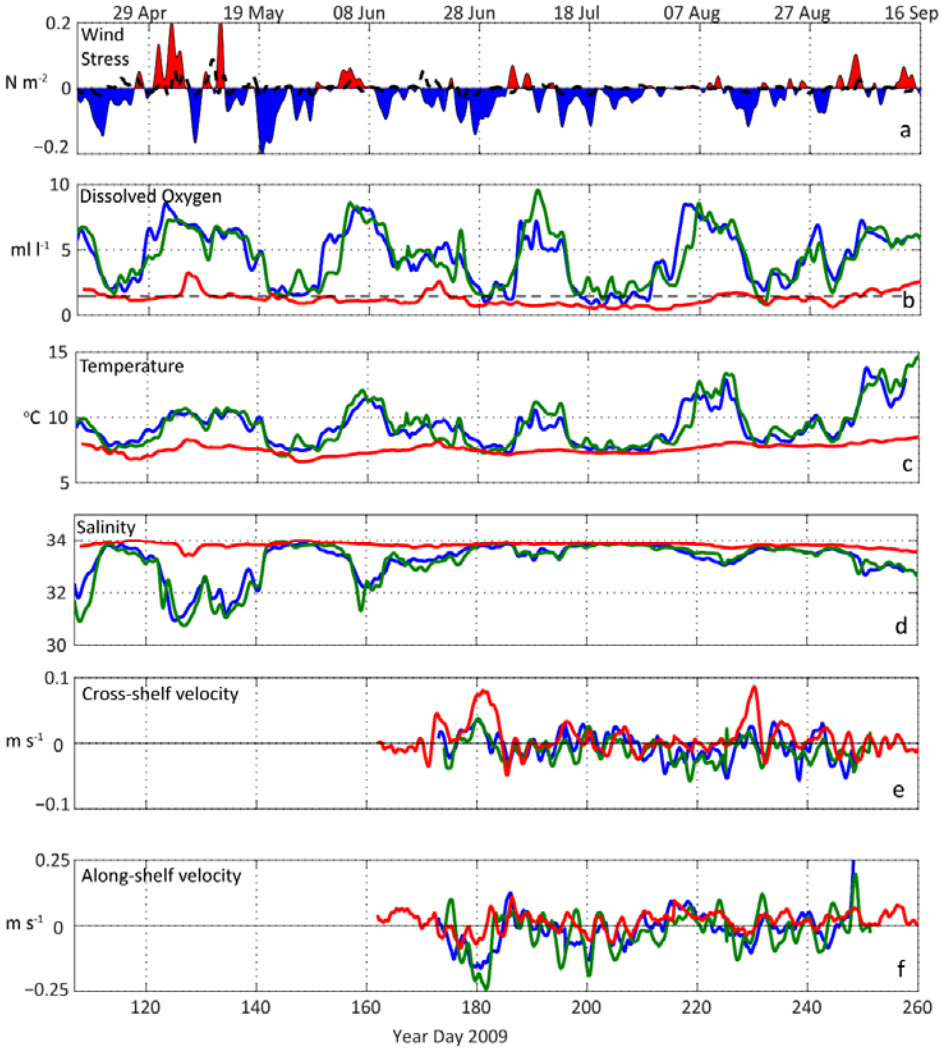

Figure 2.5:(a) Low-pass filtered time series (2009) of north-south wind stress component from NDBC Buoy 46050 with positive (red) and negative (blue) values corresponding to downwelling-favorable and upwelling-favorable conditions, respectively. (b-f) Low-pass filtered near-bottom dissolved oxygen, temperature, and salinity, cross-shelf velocity and along-shelf velocity observations from inner-shelf (13-m depth in 15 m of water) SH15 (blue) and LB15 (green), and mid-shelf (68-m depth in 70 m of water) SH70 (red) moorings indicate stronger cross-shelf variability than along-shelf variability for the 150-day overlapping time record. The hypoxic threshold, or dissolved oxygen concentrations below 1.4 ml l^{-1}, is plotted as a dashed line in (b), the dissolved oxygen panel.

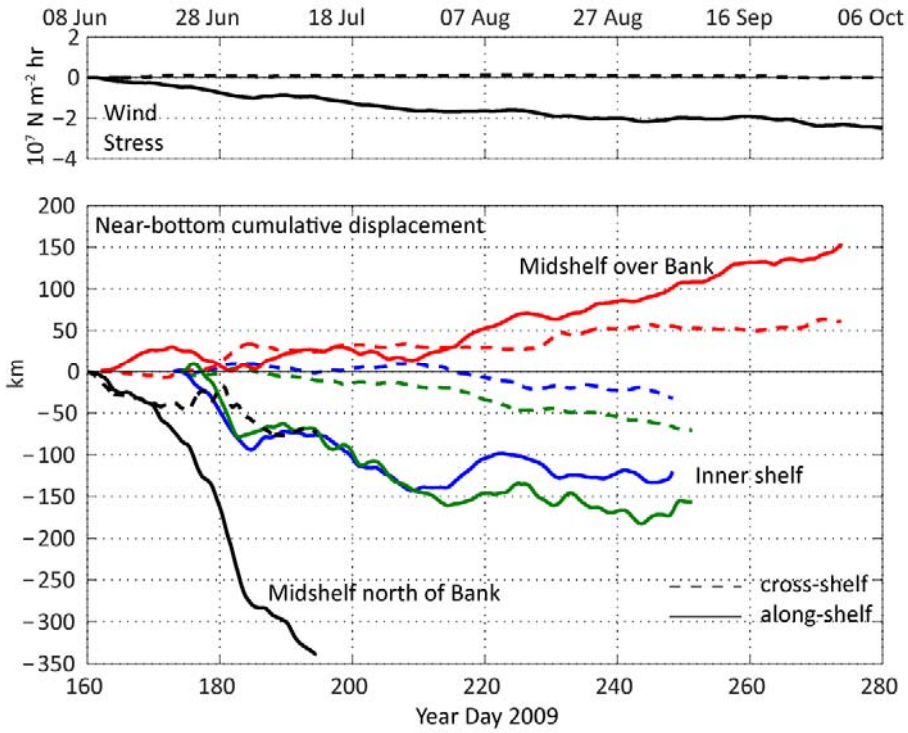

Figure 2.6: Cross-shelf (dashed) and along-shelf (solid) wind stress (NDBC 46050) and cumulative displacements at inner-shelf [SH15 (blue) and LB15 (green)] and mid-shelf [SH70 (red) NH10 (black)] mooring locations based on low-pass filtered, near-bottom current velocities. Near-bottom sampling depths are 65 m for SH70, 75 m for NH10, and 12 m for inner shelf moorings. Positive values represent northward and onshore flows.

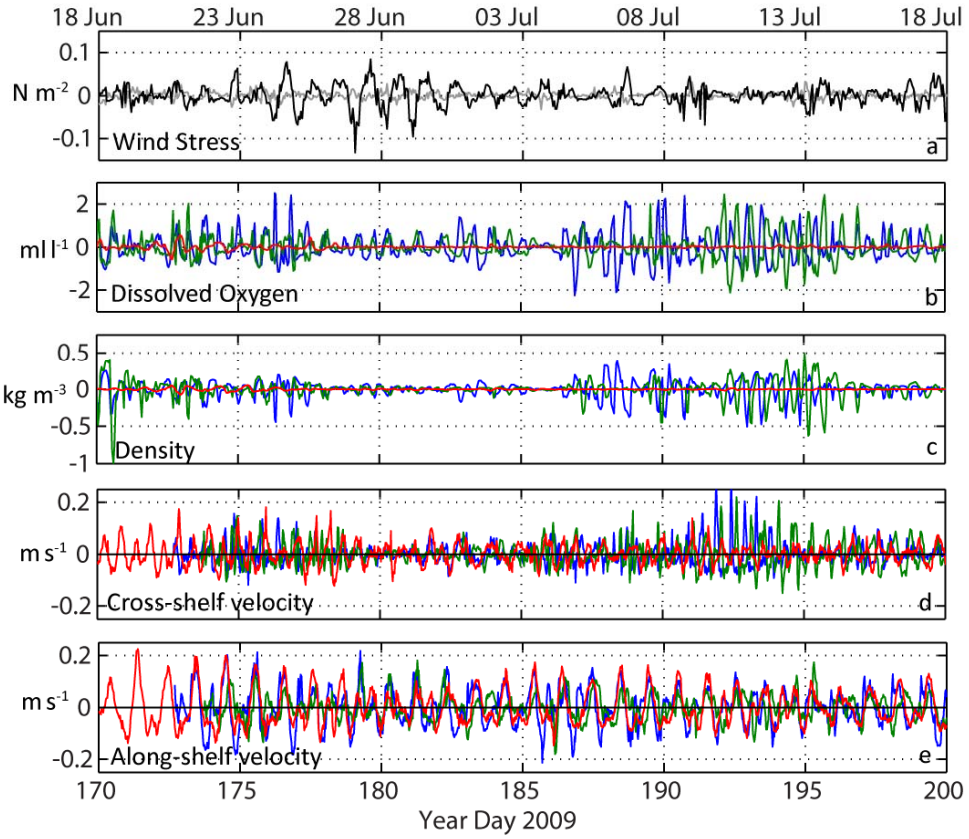

Figure 2.7: High-pass filtered (a) along-shelf (black) and cross-shelf (grey) wind stress (NDBC 46050), (b) DO, (c) temperature, (d) salinity, (e) cross-shelf and (f) along-shelf depth-averaged velocity time series from LB15 (green), SH15 (blue) and SH70 (red) mooring locations from 2009.

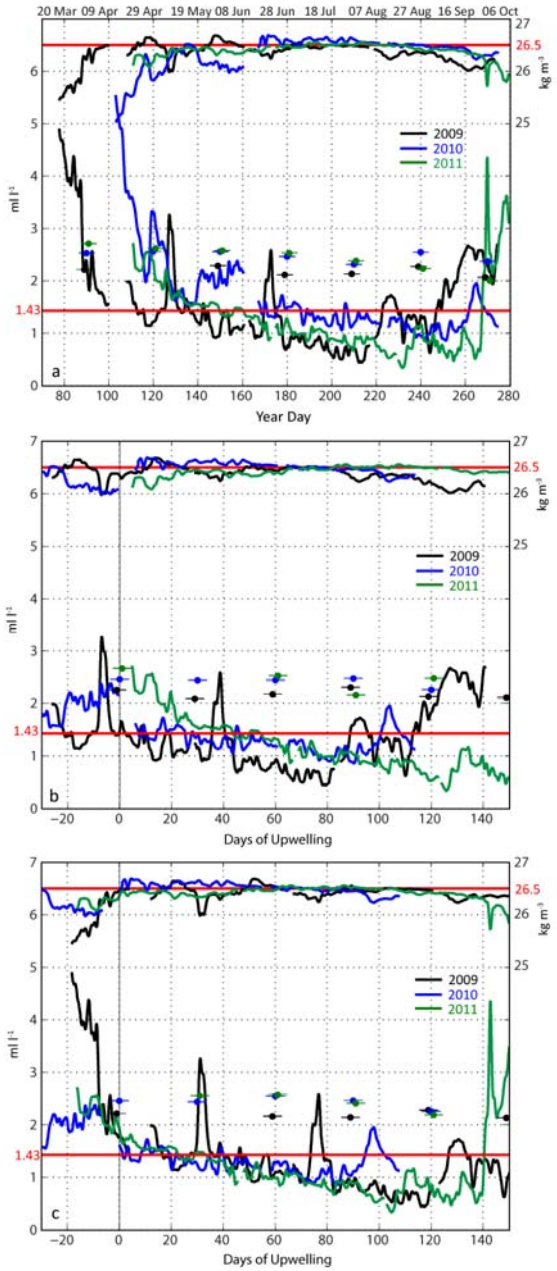

Figure 2.8: (a) Dissolved oxygen and σ_t (density – 1000 kg m^{-3}) time series at SH70 for the 2009 (black), 2010 (blue) and 2011 (green) upwelling seasons with the 30-day average glider data from NH25 (σ_t 26.5 kg m^{-3}) (filled circles). (b) Shifting by the respective start day of upwelling (2009:134, 2010:161, 2011:106) based on wind forcing shows water with equal density (26.5 kg m^{-3}) and differing oxygen concentrations around 75 days into the upwelling season. (c) Shifting by the spring transition date based on source water data (2009: 96, 2010: 167, 2011: 127) shows strong agreement throughout each respective season.

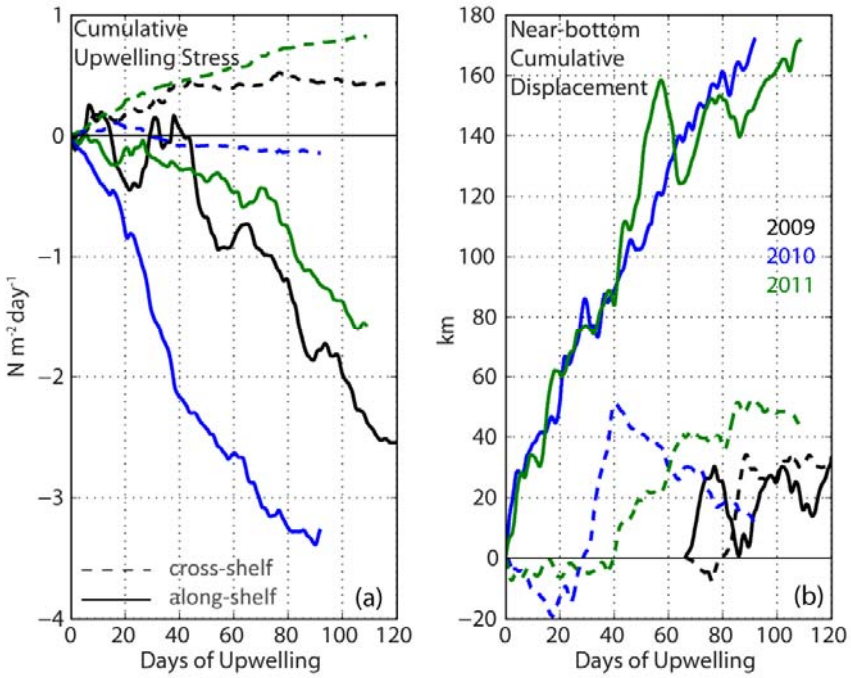

Figure 2.9: Interannual comparison of (a) cumulative wind stress (NDBC 46050) and (b) near-bottom (~65-m) cumulative displacements (SH70) for the 2009 (black), 2010 (blue) and 2011 (green) upwelling seasons. Positive values indicate northward or eastward (onshore) directions.

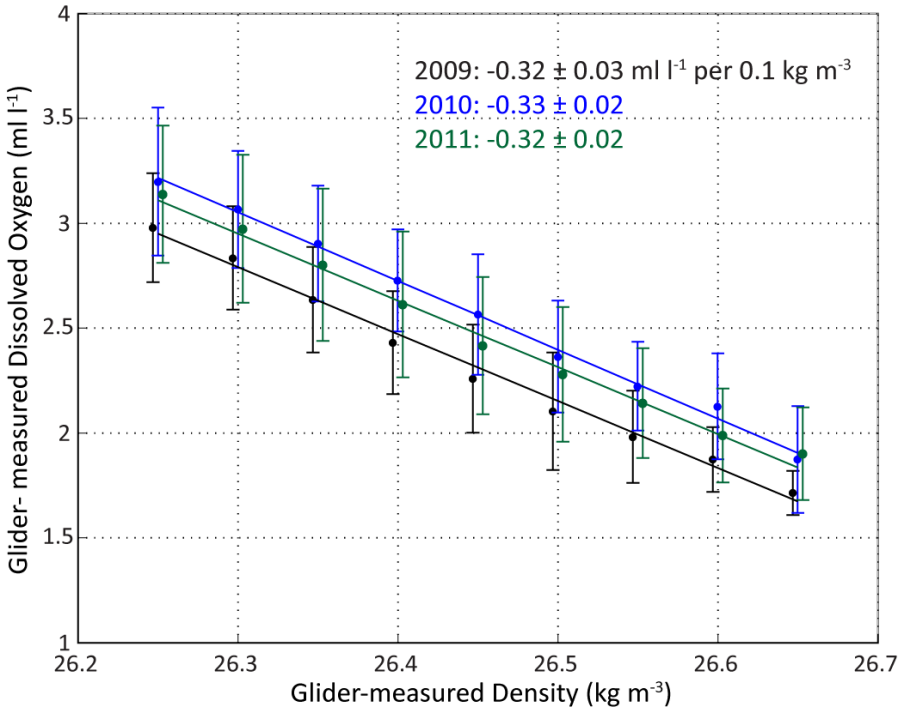

Figure 2.10: Source water DO-density relationship from glider-measured data at NH25 for 2009 – 2011 averaged over each respective upwelling season, indicating ~ 0.32 ml l^{-1} change in DO per 0.1 kg m^{-3}.

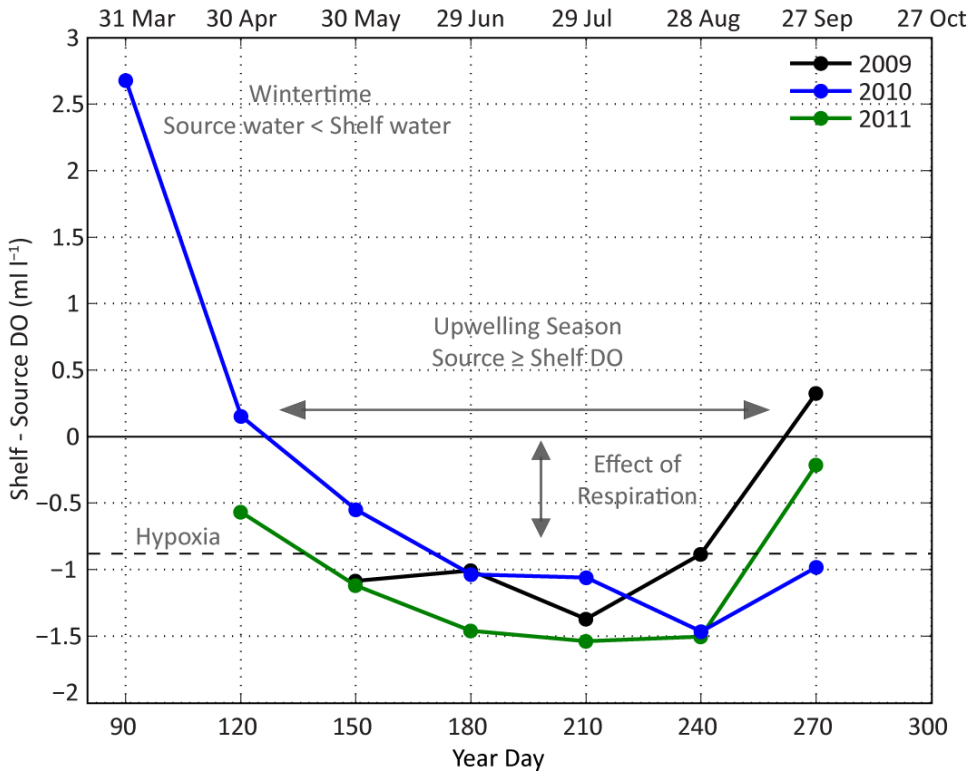

Figure 2.11: Difference between 30-day average of dissolved oxygen measurements from NH25 (glider, 26.5±0.01 σ-t) and SH70 (near-bottom) for the three years of the study. A negative (positive) value indicates higher dissolved oxygen over the shelf (shelf break). Hypoxia is indicated by the dashed line with a value of 0.87 ml l^{-1}, the difference between average source water DO concentration (~2.3 ml l^{-1} for 26.5 kg m^{-3} σ_t) and the hypoxic threshold (1.4 ml l^{-1}).

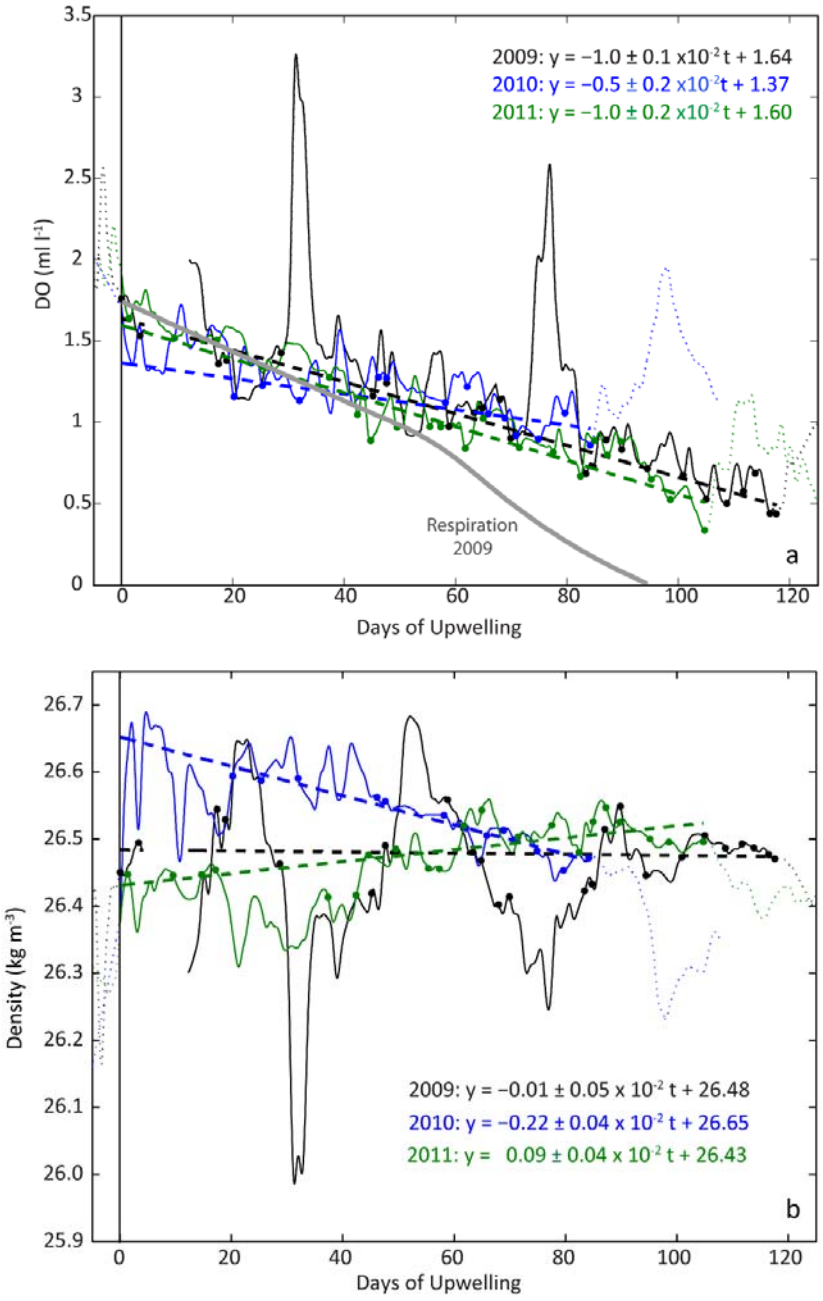

Figure 2.12: (a) Near-bottom oxygen and (b) density measurements at SH70, shifted by start of upwelling season date based on *in situ* source water data (described in Section 2.2). Linear regression lines (dashed) are fitted to minimum oxygen measurements less than source water concentrations (2.2 ml l^{-1}) corresponding to density 26.5 ± 0.1 kg m^{-3} (filled circles). Net oxygen decline rates, or regression line slopes, are less than the decline expected from near-bottom bottle respiration rates (grey) from 2009 (Table 2.2). Regression line slopes and offsets are above 95% significance level.

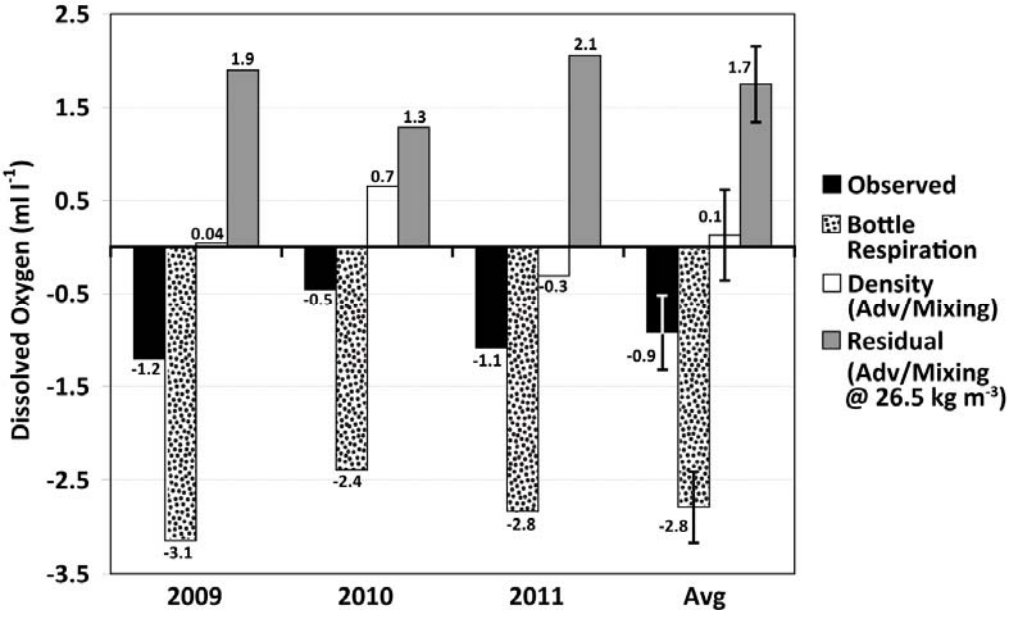

Figure 2.13: Contributions to oxygen decline (ml l^{-1}) on the mid shelf (SH70) from physical and biological processes over each upwelling season, as defined in Section 2.2. The observed decrease is calculated from slopes of linear regression lines in Figure 2.2.14. Respiration rates are calculated using the average from Table 2.2: -2.6 x 10^{-2} ml l^{-1} day^{-1}. Contribution from the change of density is derived from the slopes of linear regression lines of density at SH70 (Fig 2.12b) and the density-dissolved oxygen relationship calculated for source water (Fig 2.10). The advection/mixing term is the residual.

Table 2.1: Data source locations and principal axes rotation angles for individual deployments.

			Latitude (°N)	Longitude (°E)	θ (° from N)
SH15	2009	a,b			7.7, 6.6
	2010	a,b	44.25	-124.13	5.3, 8.1
	2011	a,b,c			4.9, 2.3, 9.3
LB15	2009	a,b			20.4, 21.4
	2010	a,b	44.80	-124.09	18.8, 14.8
	2011	a,b			25.0, 16.5
SH70	2009	a,b			5.0, -10.1
	2010	a,b,c	44.25	-124.25	-3.4, -7.6, 9.9
	2011				1.5, -8.0, -5.9
NH10	2009		44.63	-124.30	18.3
	2010				21.4
46050 τ_y	2009				5.1
	2010		44.64	-124.50	2.1
	2011				7.7
COAST	2001	nis	45.07	-124.07	9.4
		nms	45.00	-124.12	6.8
		nsb	45.00	-124.21	6.9
		sis	44.27	-124.17	1.4
		sms	44.22	-124.47	13.8
		ssb	44.22	-124.91	23.7

Table 2.2: Water column respiration rates measured from near-bottom samples taken at SH70 in 2009 are shown along with expected DO (ml l^{-1}) due to respiration, assuming a constant average rate between samples and an initial DO value of 1.75 ml l^{-1} from 2009 SH70 oxygen time series at year day 0 (Fig 2.8c,12a). Since the first bottle sample was taken at day 105, a constant respiration rate is assumed for the first nine days of the upwelling season (row 1).

Year Day 2009	Days of Upwelling	Bottle Respiration Rate 10^{-2} (ml $l^{-1}day^{-1}$)	# days	Average Respiration Rate 10^{-2} (ml $l^{-1}day^{-1}$)	Expected Oxygen due to Respiration (ml l^{-1})
96	0	-1.55[a]			1.75
			9	-1.55	1.61
105	9	-1.55			
			41	-1.52	0.99
146	50	-1.48			
			14	-2.21	0.68
160	64	-2.93			
			28	-2.23	0.05
188	92	-1.54			
			22	-2.82	-0.57
210	114	-4.09			
			6	-4.53	-0.84
216	120	-4.97			
			9	-3.85	-1.18
225	129	-2.73			
			10	-3.37	-1.52
235	139	-4.02			
			28	-2.80	-2.31
263	167	-1.58			
			72	-1.36	-3.28
335	239	-1.14			

[a] A constant respiration rate value is used prior to data collection.

Table 2.3: Maximum, time-lagged, cross-correlation coefficients calculated between along-shelf wind stress and observed variables. Corresponding lags (hours) are in parentheses. Wind leads observed variables for positive lags.

	SH15	LB15	SH70
Oxygen	0.63 (46)	0.65 (53)	0.24[a] (82)
Temperature	0.53 (53)	0.54 (54)	0.37 (197)
Salinity	-0.56 (54)	-0.53 (57)	-0.37 (216)
$u_{depth\text{-}avg}$	0.42 (225)	-0.28 (312)	-0.57 (27)
$u_{near\text{-}bottom}$	-0.80 (3)	-0.70 (5)	-0.69 (10)
$u_{near\text{-}surface}$	0.56 (-1)	0.52 (-2)	0.37 (3)
$v_{depth\text{-}avg}$	0.75 (7)	0.82 (7)	0.64 (4)
$v_{near\text{-}bottom}$	0.71 (4)	0.82 (7)	0.55 (-2)
$v_{near\text{-}surface}$	0.78 (5)	0.82 (5)	0.54 (10)

[a]Not within 95% confidence interval.

Table 2.4: Tidal current amplitudes and tidal excursion estimates due to K1 and M2 tidal constituents based on depth-averaged 2009 data records.

	K1 Amplitude ($m\ s^{-1}$)	K1 Tidal Excursion (km)	M2 Amplitude ($m\ s^{-1}$)	M2 Tidal Excursion (km)
		Along-shelf		
LB15	0.02	0.55	0.03	0.43
SH15	0.07	1.9	0.06	0.85
SH70	0.08	2.2	0.05	0.71
		Cross-Shelf		
LB15	2.6×10^{-3}	0.07	6.8×10^{-3}	0.10
SH15	1.3×10^{-3}	0.04	8.4×10^{-3}	0.12
SH70	0.01	0.27	0.02	0.28

Table 2.5: Interannual wind statistics for NDBC 46050 north-south (along-shelf) wind stress, derived using *Large & Pond* [1994] drag coefficients during the upwelling season, as defined in Section 2.2. Upwelling-favorable wind events are defined by negative wind stress.

	Length of season (days)	Cumulative Wind Stress ($N\ m^{-2}$ day)	% Upwelling Favorable Events	Upwelling- : Downwelling-Favorable Events
2009	121	-2.57	67.9	2.1
2010	92	-3.26	84.3	5.4
2011	109	-1.57	70.1	2.3

3. Cross-shelf variability of hypoxia along the Newport, Oregon, Hydrographic line

Katherine Adams, John A. Barth, and R. Kipp Shearman

Journal of Physical Oceanography
45 Beacon Street, Boston, MA 02108-3693
To be submitted

3.1. Abstract

Hypoxia, dissolved oxygen < 1.4 ml l^{-1}, observed off the central Oregon coast varies in duration and spatial extent during each upwelling season due to the combined influence of physical and biological shelf and slope processes. Hypoxia has been observed in over 100 underwater glider cross-shelf transects along the Newport-Hydrographic (NH) line since April 2006. Two distinct cross-shelf locations with prevalent hypoxia along the NH line are identified, as is a mid-shelf region with less severe hypoxia directly north of Stonewall Bank, a location of enhanced mixing. Intraseasonal cross-shelf variability is investigated with data from 10 sequential glider lines during the 2011 upwelling season. Cross-sectional hypoxic area ranges from 0 to 1.41 km^2. The vertical extent of hypoxia generally falls within the bottom mixed layer. Mid-shelf mooring (80-m water depth) water velocities show that cross-shelf advection cannot account for the large decrease in outer-shelf DO observed in the glider sequence. This decrease is attributed to a northern along-shelf DO gradient of -0.72 ml l^{-1} over 2.58 km, or 0.28 ml l^{-1} per km. In early July of the 2011 upwelling season, time-integrated near-bottom cross-shelf currents change sign from onshore to offshore as an increase of onshore flow at 30-m depth is observed. This indicates that the return flow depth shoals throughout the season, after the coastal jet moves offshore. Slope-Burger numbers calculated through the season do not explain this return flow depth change, providing evidence that simplified 2-dimensional upwelling model assumptions do not hold in this location.

3.2. Introduction

Subsurface waters low in dissolved oxygen (DO) upwell onto the continental shelf along the U. S. west coast each spring and summer. As wind-driven coastal upwelling seasons progress, near-bottom DO concentrations below the hypoxic threshold (1.4 ml l^{-1}) are observed off Washington, Oregon and California. These so-called 'dead zones' (Diaz and Rosenberg et al., 2008) are not linked to anthropogenic eutrophication like the majority of coastal and estuarine low-DO environments on the U.S. south and east coasts, but have similar detrimental effects on marine organisms (Diaz and Rosenberg, 1995; Gray et al., 2002; Keller et al., 2010). Off central-Oregon, hypoxia has been observed across the shelf and throughout the upwelling season, with ~ 3 months of persistent, seasonal hypoxia in one location (Adams et al., 2013), yet invertebrate and fish kills are only occasionally observed (Grantham et al., 2004; Chan et al., 2008). The severity and duration of hypoxic events vary in both space and time, yet extant data sets have not resolved cross-shelf and along-shelf gradients $O(< 10$ km) on intraseasonal time scales.

Spatial and temporal variability of hypoxia has been observed on decadal, interannual, intraseasonal, event and tidal scales (Adams et al., 2013; Peterson et al., 2013; Pierce et al., 2012, Chan et al., 2008; Hales et al., 2006; Grantham et al., 2004), however previous studies consisted of few high-resolution or several low-resolution realizations forsaking either temporal or spatial resolution for the other. Underwater gliders with non-stop data collection at ~0.2 knots, allow finer-scale investigations of cross-shelf variability on finer time scales than ever before (event, intraseasonal, interannual).

Seasonal DO decline on the central-Oregon mid shelf, 70 to 80-m isobaths, has been calculated from ship-based observations (Hales et al., 2006) and from moored continuous time series (Adams et al., 2013). Both studies have reported a

local seasonal decline rate of ~ 0.01 ml l^{-1} day. This decline is the result of local respiration balanced by physical advection and mixing processes. Adams et al., 2013 calculate the local rate of change as only 1/3 of the expected local respiration draw down on the shelf and find physical processes keep the system from reaching anoxia. In a shelf DO-flux budget, Hales et al., 2006 find physical advection mechanisms to be the same magnitude as the local rate of change. However, this budget was calculated from 4 cross-shelf sections spaced over 2 months in time and ~40 km in along-shelf separation. This yields an early and late season snap shot but does not resolve intraseasonal variability. Hypoxic waters off central-Oregon develop and evolve throughout each season influenced by physical and biological processes in concert, all with along-shelf and cross-shelf gradients that haven't been well resolved to date.

An important detail not addressed in the current California Current System near-bottom DO variability literature is the intraseasonal variability of near-bottom flow. The onshore return flow depth during upwelling can occur in the bottom boundary layer (BBL) or in the interior of the water column (Smith, 1981). The return flow depth has previously been related to the Slope-Burger number, *S*, which depends on the water-column stratification, Coriolis parameter and bottom slope. *S* values ~ 1 indicate a return flow in the interior for the Oregon coast (Huyer et al., 1976; Smith, 1981; Lentz and Chapman 2004). The BBL flow may also diminish from buoyancy arrest (Garrett et al., 1993) where onshore transport in the bottom stalls. Regardless of the mechanism, return flow depth is important to DO dynamics since near-bottom waters rely on cross-shelf currents for flushing and replenishment with source water. As hypoxic observations are at near-bottom depths, BBL flows are paramount to identifying the affect of physical advection mechanisms on near-bottom DO dynamics.

Here, we first use a combination of mooring and glider data to resolve fine-scale DO variability spatially (<1 km) and temporally (days – months) and then test

hypothetical mechanisms responsible for the observed variability. Data sources and processing methods are detailed in Section 3.3. Mid-shelf mooring and glider data are presented for the 2011 upwelling season in Section 3.4.1. Spatial patterns of glider-measured hypoxia are determined in Section 3.4.2. The importance of cross-shelf and along-shelf circulation and return flow depth on hypoxia is discussed in Section 3.5. Finally, we summarize and conclude our findings in Section 3.6.

3.3. Data & Methods

3.3.1.Data

Newport-Hydrographic (NH) line glider data 2006 - 2012

The continental shelf and slope waters along the historic Newport Hydrographic line (NH line; 44.65°N) were sampled by Teledyne Webb Electric G1 Slocum gliders (0 to 200-m water depth; 124.1°W to 125.1°W; 2006 to 2012) operated by the Oregon State University (OSU) glider group. The Slocum gliders sampled from 2-90 km offshore with cross-shelf transects taking an average of 3.8±1.1 days. With a pitch angle of approximately 26°, the horizontal separation of Slocum glider vertical dive and climb pairs ranges from 62 m to 410 m for 30-m and 200-m water depths, respectively. Variability in the glider's location during cross-shelf transects arises from the slow horizontal vehicle speed, 0.25 m s^{-1}, compared with the strong along-shelf coastal currents, 0.5 – 1 m s^{-1} coastal upwelling jet and 1 – 2 m s^{-1} wintertime Davidson current.

Slocum gliders collected data via a Sea-bird Electronics, Inc. (SBE) 41CP unpumped CTD (conductivity, temperature and pressure) and an Aanderaa 3835 optode measuring dissolved oxygen. Thermal-mass corrections to the conductivity cell have been applied for the Slocum glider data set prior to oxygen concentration calculations (Garau et al., 2001). The dissolved oxygen data set is shifted by the reported 24-second response time of the optode.

Optode Calibration Procedure

Dissolved oxygen optode sensors aboard the Slocum gliders were calibrated in the laboratory several times each year of operation. The two-point linear calibration procedure consisted of triplicate Winkler titration samples taken at a mid-range (5-6 ml l^{-1}) concentration followed by the addition of sodium sulfite to a well-stirred glass container until a zero-point for each sensor is reached. The slopes and offsets calculated after each in-lab calibration are applied to the measured DO values. In-lab calibrations were conducted approximately quarterly and after each manufacturer factory service.

Glider-calculated depth-average currents

Depth-averaged currents are inferred by Slocum gliders by dead-reckoning (e.g., Merkelbach et al., 2008). Using the glider vehicle flight model, the glider's target location in still water is calculated. The difference between the target location and the actual location during the next GPS reading per travel time is the depth-average current for the top 200 m of the water column, which has a N-S component, v_{avg}. Glider v_{avg} values are calculated between glider GPS readings. The time between GPS readings, 1 to 6 hours, is user-defined and varies with distance offshore. Around the mid shelf (80-m isobath) one dive-pair climb takes approximately one hour and the 'callback interval' is typically set to 3 hours. Thus each mid-shelf v_{avg} calculation applies to 6 vertical profiles.

Reported accuracies of glider-calculated depth-average currents are $O(0.01\ m\ s^{-1})$ in glider studies in deeper waters using the Seaglider and Spray gliders (Eriksen *et al.,* 2001; Todd *et al.,* 2011) which calculate the depth-average current after each dive-climb pair. Inaccuracies $O(10\%)$ have been reported for Slocum-measured v_{avg} values due to compass calibration error and from the exclusion of attack angle in the Slocum flight model (Merkelbach et al., 2008). This error should also be attributed to the dynamic environments Slocum gliders are used in and the length of time between the v_{avg} calculations. A comparison of moored and glider-derived N-S velocities over the mid shelf is presented in Appendix 3.7.

NH-line mid-shelf mooring (NH10)

Horizontal water velocity, temperature, conductivity and dissolved oxygen data from the 2011 upwelling season are analyzed from the NH-10 buoy (44.65°N, 124.30°W, 80-m water depth, 18-km offshore) along the NH-line. A downward-looking Teledyne RD Instruments 300 kHz Workhorse Sentinel measured horizontal water-column velocities at 7 – 73 m depths in 2-min intervals and 2-m bins. N-S and E-W velocities are corrected for magnetic declination and subsequently rotated into principal axes, 22.3° true, based on depth average velocities from the 2011 upwelling season deployment. This rotation minimizes variability in the cross-shelf direction and is similar to the orientation of local isobaths. Rotated E-W and N-S velocities are referred to hereafter as cross-shelf and along-shelf velocities, respectively.

Temperature and conductivity data were measured by a SBE16plus at 73-m and a SBE16 at 60-m depths. SBE reported accuracies for the temperature and conductivity sensors are 0.002°C and 0.002 (equivalent salinity), respectively. A Clark electrode-type SBE43 was installed on both instruments for dissolved oxygen measurements. Temperature, salinity and dissolved oxygen data, recorded at 2-hr intervals, were 40-hr low-pass filtered. The 73-m time series is incomplete due to instrument failure. Sensors on the 73-m and 60-m instruments were factory calibrated prior to the April 2011 and 2010 deployments, respectively.

Strawberry Hill mid-shelf mooring (SH70)

In 2011, near-bottom temperature, conductivity, dissolved oxygen (DO), and current data were collected on the 70-m isobath approximately 40 km to the south of the NH-line (Figure 1) off Strawberry Hill (SH70; 44.25°N, 124.25°W), previously presented in Adams et al. (2013). SBE16plus CTD (conductivity, temperature, depth) and SBE43 (DO) sensors collected measurements on 30-min intervals. Current measurements made using a Teledyne RD Instruments 300-kHz

Workhorse Sentinel ADCP were filtered and rotated similar to NH10 currents described above. CTD and DO sensors were factory calibrated before and after each field season. Several in-lab and calibration casts were taken throughout the season to verify the CTD and DO data quality.

Wind stress

Wind speed and direction were measured at 10-minute intervals at National Data Buoy Center (NDBC) station 46050 (44.64°N, 124.53°W, 35-km offshore). Wind measurements at 46050 correlate strongly with those from the coastal meteorological station (NWP03; 44.61°N, 124.07°W), correlation coefficient of 0.76 at zero lag. Gaps in the 2011 46050 record were filled with NWP03 winds using the regression coefficients: slope 0.90, offset 0.34 m s^{-1}. N-S wind stress was derived (Large *et al.,* 2004) from hourly-averaged wind speed and direction prior to 40-hr low-pass filtering to remove high-frequency variability, e.g., diurnal seabreeze, which is not a focus of this study.

3.3.2. Derived data products and methods

Glider data gridding and filtering

The Slocum data sets were binned by depth (2 m) and gridded using two methods. Linear interpolation resulted in unfiltered gridded glider lines on a desired grid. Filtered, gridded glider lines were processed using an iterative 2-dimensional Gaussian function (Barnes 1964) with decorrelation radii of 10-km in the horizontal and 5-m in the vertical. These smoothing length scales were determined from spatial autocorrelations and power spectral density behavior of isopycnal depths along each cross-shelf transect. Other glider studies found horizontal smoothing scales of 25 – 30 km were necessary to remove high-frequency signals such as internal waves (UW Seagliders, Pelland *et al.* 2013; Spray gliders, Todd *et al.,* 2011 and Rudnick and Cole 2011). The specified grid is the same for both methods and telescopes horizontally and vertically based on the depth-dependent separation distances of glider dive and climb pairs, < 500 m

and 5 m over the shelf. Unfiltered glider lines are used to analyze scalars like DO. Filtered glider lines are used prior to calculations such as geostrophic velocity (see below). Barnes filtering of glider-calculated v_{avg} was necessary to remove tidal frequency aliasing.

Glider-derived geostrophic and absolute N-S velocities

N-S geostrophic velocities are calculated from gridded and filtered cross-shelf glider temperature and salinity sections (not shown). Each horizontal grid space represents a different sampling station, analogous to tightly-spaced, ship-based CTD observations. The reference level, or level-of-no-motion, is set to 190 m. Geopotential anomaly is calculated by vertically integrating specific anomaly changes with depth, starting from zero at the reference level for each horizontal station. For stations where the bottom depth is less than the reference level, geopotential anomaly at the deepest data point for each station is linearly extrapolated from the two nearest offshore stations following Reid & Mantyla (1976). Specific volume anomaly is then vertically integrated from this extrapolated value, rather than from zero at the reference level. This method assumes zero horizontal shear in geostrophic velocity between the stations at their deepest common depth.

Cross-path geostrophic velocities are then calculated by taking the horizontal difference between geopotential anomalies of two adjacent horizontal stations and dividing by the Coriolis parameter and the horizontal distance between stations. Geostrophic velocity vectors are orthogonal to glider paths which deviate from a line of constant latitude. Hence, only the North-South (N-S) component of the calculated geostrophic velocity vector is retained, v_{geo}.

An absolute N-S velocity can be obtained from v_{geo} by adding the N-S component of glider-calculated depth-averaged velocity, v_{avg}, to v_{geo}, similar to Todd *et al.*, (2009). Comparison of depth-averaged and 70-m depth moored N-S velocities in

Appendix A shows a + 0.05 m s^{-1} offset of v_{abs} over the 80-m isobath. Corrections of N-S depth-averaged velocities calculated from measured compass inaccuracies after the 2011 Slocum glider deployments are on the order of 0.03 m s^{-1}.

3.4. Results

Variability of cross-shelf, near-bottom dissolved oxygen (DO) concentrations on intraseasonal time scales (weekly – monthly) are investigated using 10 sequential Slocum cross-shelf sections of the Newport-Hydrographic (NH) line (44.65°N) sampled over 50 days, 08 August – 27 September 2011 (Figure 1). Glider lines took 3 – 7.5 days to sample from 124.1°W – 125.1°W (2 - 90 km from shore), spanning from the 30-m to the 1500-m isobath (Table 3.1). The duration of each line depended on the strength and directionality of coastal water velocities. Moored current data at two mid-shelf moorings, NH10 and SH70 (Figure 3.1), are included in the analysis to provide water velocities during the glider sequence and to investigate the intraseasonal variability of near-bottom currents in 2011.

3.4.1. 2011 Mid-shelf mooring and glider time series

Central-Oregon coastal winds shifted to upwelling-favorable around year day 106 (15 April) (Pierce *et al.,* 2006; damp.coas.oregonstate.edu), although the cold, salty and low-DO signature of upwelling source water was not observed until early May (year day 128; 07 May, Adams *et al*., 2013). Cumulative N-S wind stress (Figure 3.2a) shows predominantly upwelling-favorable wind forcing until mid September when a strong poleward wind event was observed.

Continuous time series of near-bottom density (σ_θ) and DO from the mid-shelf moorings NH10 (73-m measurements in 80-m water depth) and SH70 (70-m water depth), are presented in Figure 2b-c. Data from the NH10 60-m DO sensor are also included since the 73-m DO sensor failed during the deployment. The time series show a density increase to 26.5 kg m^{-3} and a gradual DO decrease throughout the upwelling season. Moored DO at NH10 (73-m and 60-m)

approaches the hypoxic threshold (1.4 ml l^{-1}) several times throughout the time series but persistent hypoxia is not observed until early August (Figure 3.2c). The SH70 DO record, however, is persistently hypoxic for over 100 days. This location has previously been identified as vulnerable to hypoxia due to high productivity, recirculation of currents and low flushing rates over the bank (Barth et al., 2005; Castelao and Barth 2005; Adams et al., 2013). A similar seasonal DO decline rate is observed in both the NH10 and SH70 near-bottom DO time series, ~1 ml l^{-1} per 100 days (Adams et al., (2013).

Unfiltered gridded glider data from the 10 sequential glider lines (Figure 3.1) from 60-m and 70-m water depths at each 80-m isobath crossing are plotted alongside the moored density and DO time series (Figures 3.2b-c). During the short overlapping section with the moored continuous time series, there is good agreement between glider and mooring data (Figure 3.2a-b). Late-season glider-measured density steadily decreases from 26.5 to 26.25 kg m^{-3} at 70-m (Figure 3.2a), while a trend in near-bottom DO is less clear. The scatter of glider-measured DO (Figure 3.2b) is expected since the separation of measurements at the 80-m isobath ranges from 2.6 – 9.8 days (Table 3.2). There is also latitudinal variability in the 80-m isobath crossings (Fig. 3.1).

Cross-shelf cumulative displacements (CD), or time integrated currents, from the 31, 61 and 73 m ADCP depth bins from the NH10 mooring are included in Figure 3.2c. A large, positive CD slope in the 73-m record early in the season (days 120-200) indicates strong onshore flow near bottom. A transition to a negative slope around day 210 is observed indicating weak and offshore currents in the near-bottom at the 80-m isobath. At SH70, onshore currents are near-zero until mid season. Equatorward along-shelf velocities at NH10 (Figure 3.2e) also decrease sharply around day 200 (Fig. 3.2.e). This is consistent with the upwelling-coastal jet moving farther off shore during the upwelling season (Barth *et al.,* 2005). These mid-season changes in cumulative displacements equate to diminished

along-shelf and cross-shelf advection, or flushing, of near-bottom waters at NH10 which increases the risk for hypoxia.

Low CD values at the 61-m depth bin indicate overall weak cross-shelf flow at this depth. This weak flow suggests 60 m is the transition from interior to BBL flow. This is consistent with ~20 m bottom mixed layer (BML) heights from the glider 80-m isobath crossings (Table 3.1, Figure 3.4). BML height is defined as the first vertical grid cell from the bottom of each horizontal grid column with a density difference greater than 0.2 kg m^{-3}.

At the shallower 31-m depth bin, cross-shelf currents are strongly onshore after day 190 (positive CD slope) as the near-bottom currents switch to weak and offshore flow (Figure 3.2d). This is indicative of a change of return flow depth from near-bottom to just below the surface boundary layer. Late-season return flow in the interior was observed previously off Oregon (Huyer et al., 1976). The change in return flow depth has implications for near-bottom flushing rates late in the season and is investigated further in Section 3.4.3. A shallow return flow depth below the surface Ekman layer has been shown using a 2-dimensional upwelling model with Slope-Burger number, *S*, ~1 (Lentz and Chapman, 2004). We investigate the relationship between *S* and return flow depth in Section 3.5. The temporary sharp change in the 31-m cross-shelf CD slope between days 170 - 190 is due to a deepening of the surface layer offshore flow.

The apparent weakening of the cross-shelf near-bottom flow during the 2011 upwelling season is investigated further. Cross-shelf Ekman BBL transport is calculated using overlying interior water velocities from the formulation,

$$U_b^{Ek} = \frac{\tau_b^y}{\rho_o f} = -\frac{\delta}{2}\left(u_i + v_i\right) \tag{3.1}$$

where the along-shelf bottom stress, τ_b^y, is related to the cross-shelf and along-shelf interior flows just above the Ekman BBL height, δ, here assumed to be 20

mab and 10 mab. Using a density of 1026 kg m^{-3} and the time series of moored NH10 ADCP currents at the 61-m and 71-m depth bins, U_b^{Ek} is calculated (Figure 3.3). Onshore transport in the BBL is much stronger and persistent at the beginning of the 2011 upwelling season at both depths. Towards the end of the season, when the 10 glider lines were collected, U_b^{Ek} alternates from onshore and offshore but is overall much weaker than early-season transport magnitudes. A seasonal decline in U_b^{Ek} is also evident from monthly averages of 2006 – 2012 NH10 ADCP currents, changing from 15 m^2 s^{-1} to 0 m^2 s^{-1} from April to September at 20 mab (Figure 3.3). This is further evidence that late-season flow in the BBL is weak or arrested.

3.4.2. 2011 NH-line Glider sequence (08 Aug – 27 Sep)

Unfiltered Dissolved oxygen and Density

Dissolved oxygen (DO) and potential density anomaly (σ_θ) cross-shelf (NH line) sections for the 10 sequential glider lines in late summer 2011 are shown in Figure 3.4. The direction of the glider path (onshore or offshore) is indicated by arrows, alternating direction every other line. The shelf bottom topography in line 6 is steeper and narrower than in other sections. As shown in Figure 3.1, the glider path during line 6 deviated to the north of the NH line (14 km at maximum separation). Tidal-band frequency undulations observed in the high-oxygen, low-density contours (Figure 3.4, lines 3-5) can also be seen in near-bottom fields suggesting this is the influence of the internal M2 tide (Suanda et al., 2014).

DO observations are lowest above the bottom in all sections (Figure 3.4). Upwelling source water, or off shore water along isopycnals that upwell on to the shelf, is higher in DO than over the shelf. This follows Adams et al., (2013) that report glider-measured source water DO concentrations, 2.2 ml l^{-1} at 26.5 kg m^{-3} in 2011, at the offshore station NH25 (Figure 3.1) Hence, an onshore near-bottom flow of source water is expected to be a source of DO for the near-bottom environment by flushing and replenishing low-DO shelf water.

Hypoxia

Near-bottom hypoxia (black contour in Figure 3.4b) is observed in each panel except for line 1, with cross-sectional hypoxic areas increasing from 0 km^2 in section 1 to 1.41 km^2 in line 7. Hypoxia is first observed in line 2 in two distinct locations: over the 60-80-m isobaths and the 120-140-m isobaths. By line 4, hypoxia is observed only upslope of the 80-m isobath. In the next line, 5, the hypoxic area extends down to 160 m. In line 6-8, hypoxia is observed down to the full depth range of the Slocum gliders, although the hypoxic area and median hypoxic height above the bottom varies (Table 3.1). In line 9, hypoxia is again present in two distinct zones as observed in lines 2 and 3. Finally, in line 10 near-bottom mid shelf DO levels have increased significantly and hypoxia is only observed on the outer shelf.

The 26.5 kg m^{-3} isopycnal is observed on the shelf in line 1 and offshelf in lines 2-10 with increasing depth. This behavior is also observed in shallower isopycnals. The onshore upward tilt of interior isopycnals and oxygen contours is observed in lines 1-8. In line 9, the 3.5 ml l^{-1} and 25.8 kg m^{-3} isopleths are flat. By line 10, a downward tilt is observed, indicative of the fall transition to downwelling-favorable conditions and poleward geostrophic flow. This is expected since line 10 was sampled directly after a strong poleward wind event (Figure 3.2a), characteristic of the fall transition to downwelling-favorable conditions. The vertical profile of density during line 10 (Figure 3.4e) shows a well-mixed top and bottom 20 m indicating strong and deep mixing in both boundary layers.

As shown in Figure 3.4d, near-bottom density decreases throughout the glider line sequence on the 80-m isobath. In 2011, offshore source waters (NH25; Figure 3.1) at densities upwelling on to the shelf were found to have a strong relationship of a 0.32 ml l^{-1} increase in DO per 0.1 kg m^{-3} density decrease (Adams et al., 2013). However, the decrease in near-bottom density observed in the 10 glider

lines is not associated with an increase in near-bottom DO (Figure 3.4b,d). This is due to the strong influence of shelf processes and local respiration on intraseasonal near-bottom DO variability.

As presented in Section 3.4.1, time-integrated currents (Figure 3.2c) indicate that the onshore return flow during late summer 2011 occurs at ~30-m water depth over the 80-m isobath, not in the BBL. From the vertical profiles of density over the 80-m isobath (Figure 3.4e), stratification is near-constant at 30-m which indicates that this is an interior depth, outside of the surface and bottom mixed layers, except in section 10. Note that DO at 30-m, the return flow depth, is above the hypoxic threshold in each glider line (Figure 3.4b).

Filtered Density and Absolute velocity

Filtered density lines (Figure 3.5a) compare well with hydrographic sections from previous NH-line studies which relied upon 12 CTD cast stations (e.g., Huyer et al., 2002). The filtered density sections clearly show the deepening of the 26.5 kg m^{-3} isopycnal throughout the 10 sections, also in the unfiltered density sections (Figure 3.4d).

Lines of glider-derived absolute N-S velocity, v_{abs}, are presented in Figure 3.5b. The strong equatorward (blue) surface flow observed offshore of the 80-m isobath in Figure 3.5b is the coastal upwelling jet which varies in strength and location throughout the 10 lines. Throughout the upwelling season, the coastal jet moves offshore and widens in cross-shelf extent following the 100-200 m isobaths around the Heceta and Stonewall Bank complex (Barth et al., 2005). Near-bottom poleward flow is observed on the shelf, although varying in strength and location in between glider sections.

N-S moored velocity, v_{NH10}, time series from the 80-m isobath is plotted in Figure 3.5c, to show the variability and structure of along-shelf currents throughout the

glider line sequence (Figure 3.5b). Each glider crossing of the 80-m isobath is marked by a black line. This data is also used in the v_{abs} and v_{NH10} mooring-data comparison in Figure 3.A1. Poleward near-bottom flows observed in Figure 5b are also observed in the v_{NH10} record in Figure 3.5c.

Vertical profiles of v_{NH10}, u_{NH10}, v_{abs}, and v_{geo} over the 80-m isobath are compared in Figure 3.5d. Negative vertical shear, or increasing N-S velocity with depth, is observed in each moored vertical profile, consistent with thermal wind and $\partial\rho / \partial x$ (Figure 3.4d). The same is true for the glider velocity profiles except for section 10 (Figure 3.5b).

Measured cross-shelf velocities and bottom Ekman transport

Low-pass filtered moored cross-shelf current data, u_{NH10}, is included as horizontal bars in Figure 3.5b over the 80-m isobath. Onshore flow is nonzero at interior depths, 40 – 60 m, for all lines (Figure 3.5b). Moored current records presented in Section 3.4.1, show a main return flow depth at 30 m when near-bottom flow becomes weak (Figure 3.2d). A seasonal decline in BBL cross-shelf transport, U_b^{Ek}, suggests that the BBL during the glider line sequence is arrested (Garret et al, 1993). U_b^{Ek} is calculated for each glider line from moored current record following the formulation presented in Section 3.4.1. The sign of U_b^{Ek} is indicated as a + or – sign in each panel of Figure 3.5b. The observed near-bottom cross-shelf flow at 60 m is the same direction as U_b^{Ek} except in glider line 10. The agreement is not as strong at 70 m for lines 1, 7, 8 and 10.

3.4.3. Physical versus biological drivers of intraseasonal DO variability

Variability of near-bottom DO observed in Figure 3.2c and 3.3b is quantified and investigated using the 10 glider lines presented in 3.3. Specifically, we focus on the difference between consecutive glider sections of DO and density 10 m above

the bottom (mab) at the mid self (80-m isobath; 0.2% slope; 18 km offshore) and the outer shelf (120-m; 0.7 %; 30 km offshore). The horizontal separation of these stations is 12 km. Potential mechanisms responsible for changes in observed DO between glider lines that can be estimated with extant data include local water-column respiration, cross-shelf advection and along-shelf advection. Other mechanisms that cannot be estimated here, such as vertical and horizontal mixing and benthic respiration, are addressed in the discussion.

Trend over glider sequence

Near-bottom DO data extracted from the unfiltered gridded glider sections shown in Figure 3.4b are lower at the outer shelf (120 m) than over the mid shelf (80 m) for the majority of the glider line sequence (Figure 3.6a). Lower DO water on the outer shelf is counter to the idea of higher-DO source water flowing onshore, replenishing near-bottom waters (Adams et al., 2013). Two hypotheses for why outer shelf DO concentrations are lower than over the mid shelf include (1) cross-shelf flow is offshore and near-bottom DO concentrations are declining en route to the outer shelf from local microbial respiration and (2) a low-DO along-shelf gradient is transported either north or south to the NH line. We evaluate these hypotheses using moored mid-shelf currents at NH10 and the glider data.

Time-integrated cross-shelf and along-shelf currents, or cumulative displacements (CD), are quantified in Figure 3.6c-d. The direction and magnitude of cross-shelf CD values are generally offshore and much less than 8 km (Figure 3.6c). Hence, offshore transport of low-DO mid-shelf water does occur during the majority of the glider sequence, as first shown in Figure 2d during August and September. However, the magnitude of cross-shelf CD, up to 8 km in the offshore direction, is smaller than the 12-km horizontal separation between the mid and outer shelf stations. Furthermore, even if offshore cross-shelf advection contributes to lower outer shelf DO concentrations, it is not large enough to explain the down-slope extension of the hypoxic shelf area observed in lines 5-8 (Figure 3.4b).

Along-shelf CD are variable in direction and magnitude in between the 10 glider lines. During glider lines 2-8, along-shelf CD is small and/or negative. This indicates equatorward flow, observed between 80-m crossings in Figure 3.5c. During glider lines 2-8 is when the down-slope extension of the hypoxic area occurs. If along-shelf advection of a low DO gradient caused this change, it would be from about 2-40 km north of the NH-line. Line 6 detoured far off course to the north of the NH line (Figure 3.1) and sampled hypoxic water all along the shelf (Figure 3.4b). This supports the hypothesis that the down-slope extension of near-bottom hypoxia resulted from low-DO water advected to the NH line from the north.

Change in outer shelf DO between consecutive glider lines

Observed DO rates of change are calculated in between consecutive glider lines in Table 3.2. Using the density-DO relationship of source water (NH25; Figure 3.1) presented in Adams et al., 2013, an expected DO rate of change based on the observed density change between lines is calculated as 0.32 ml l^{-1} per 0.1 kg m^{-3}. Similarly, the expected draw down of DO from respiration is estimated from an average respiration rate calculated at SH70, 0.026 ± 0.013 ml l^{-1} day^{-1} (Adams et al., 2013; F. Chan unpublished). The observed DO rates of change range from -0.13 to 0.29 and -0.45 to 0.10 ml l^{-1} day^{-1} on the mid and outer shelf regions, respectively. The magnitude of this large event scale variability of DO rates-of-change is similar for DO decreases and increases the mid and outer shelf. Moreover, this variability on short time scales is many times larger than the observed seasonal DO decline observed on the central Oregon shelf, ~0.01 ml l^{-1} day^{-1} (Adams et al. ,2013).

The largest change in outer shelf DO between any two consecutive glider lines is observed between lines 4 and 5 (Figure 3.6a-b). At 120-m, DO decreased by 0.72 ml l^{-1} in 2.8 days where as the 80-m DO values dropped by half that amount, 0.35

ml l^{-1} in 1.5 days (Figure 3.6b; Table 3.2). The respective DO decline rates of these sharp decreases are 0.45 ml l^{-1} day^{-1} and 0.13 ml l^{-1} day^{-1} which are several orders of magnitude larger than the average local respiration rate 0.026 ml l^{-1} day^{-1} (SH70; Adams et al., 2013; F. Chan unpublished). This rules out local respiration as the driving mechanism of the observed DO decrease between glider lines 4 and 5 at the mid and outer shelf stations, and also the sharp increase in hypoxic area down slope (Figure 3.4b).

Cross-shelf CD between the 80-m isobath crossings of glider lines 4 and 5 is -1.39 km (Table 3.4; Figure 3.6c). An offshore excursion this small cannot explain the observed down-slope extension of hypoxic area between lines 4 and 5 (Figure 3.4b). Furthermore, DO concentrations onshore of 120 m are higher during this time (Figure 3.6a-b), so cross-shelf advection of a gradient cannot be the driving mechanism of the extension of the hypoxic area down the slope. Since the N-S CD is negative, along-shelf advection of a low-DO gradient from the north is likely. Low-DO shelf water north of the line is observed in glider line 6 which sampled up to 14 km north of the NH line. Along-shelf advection of a gradient is the most plausible driving mechanism of the observed DO decline between glider lines 4 and 5. The magnitude of this gradient is the observed DO decline at 120-m divided by the along-shelf CD, 0.72 ml l^{-1} / 2.58 km or 0.28 ml l^{-1} per km. Similarly, the magnitude of the along-shelf DO gradient is only 0.14 ml l^{-1} per km over the 80-m isobath. Here we have assumed the mid shelf CD applies to the outer shelf. There is evidence from the COAST 2001 (Boyd et al., 2002) program that near-bottom currents are correlated strongly across the shelf with a 0.65 cross-correlation coefficient at zero lag.

Along-shelf maps of low-DO waters in the upper 200 m along the northern CCS indicate strong along-shelf gradients north of the NH line in September 2011 with a minimum north of the NH line over the shelf break (Peterson et al., 2013). This supports our hypothesis that equatorward along-shelf advection of a low-DO

water as the mechanism responsible for the large decline in DO observed between glider sections 4 and 5.

3.4.4. Cross-shelf variability of hypoxic observations (2006 – 2012)

3.4.4.1. Location of hypoxic measurements

The glider lines previously presented from 2011 are 10 out of 249 cross-shelf NH-line sections taken from April 2006 – December 2012. Hypoxia is observed in 133 glider lines total. The glider paths of those 133 lines are plotted in Figure 3.7a with the hypoxic section highlighted in blue. The large, along-shelf spread of glider lines are due to the slow vehicle speed of the Slocum gliders compared to the coastal currents. Hypoxia is observed each year in the data set and across the continental margin. A colored histogram map of hypoxic glider line sections in Figure 3.7a reveals areas across the shelf where hypoxia is recurrent (Figure 3.7b). The mid shelf, between the 50- and 80-m isobaths, is the region across the NH-line with the most hypoxic measurements, although hypoxia is also often observed in a second region on the outer shelf (120- to 200-m).

The vertical cross-section histogram of the 98 hypoxic glider lines across the NH line, 44.64 – 44.70°N, is shown in Figure 8a. Two distinct cross-shelf regions with prevalent hypoxic measurements are the mid (50-80-m isobaths) and outer shelf (120-200-m isobaths), similar to glider lines 2, 3 and 9 in Figure 3.4b. Hypoxia is observed over the mid-shelf in over 40% of the hypoxic glider lines whereas outer shelf hypoxia is observed in only 30% of hypoxic glider lines. Results presented in Section 3.4.3 indicated lower DO over the outer shelf. This is mostly likely a late-season result after onshore cross-shelf flow shuts down and near-bottom outer shelf waters are no longer replenished with source water.

The vertical histogram of 56 hypoxic glider lines sampled north of 44.70°N is shown in Figure 3.8b. Similar to the NH line, two distinct hypoxic areas are

observed. This is discussed further in 3.5. This was not observed during glider line 6 in Figure 3.4b where hypoxia was observed across the entire shelf width.

Hypoxia is observed offshore around station NH25 in less than 2% of the NH-line hypoxic glider lines. This station is often used as an upwelling source water location (Adams et al., 2013; Peterson et al., 2013). Infrequent hypoxia at NH25 is from near-bottom shelf hypoxic waters extending offshore as shown in glider line 7(Figure 3.4b). Since the top of the North Pacific oxygen minimum zone is at approximately 400-m water depth (Pierce et al., 2012), hypoxic measurements made in the top 200 m (e.g., Peterson et al, 2013) are attributed to shelf influence either from along-shelf or off-shelf advection and mixing.

3.4.4.2. Water mass properties of hypoxic measurements

Variability of water mass properties (DO, temperature, salinity, density and pressure) are presented at several isobath-crossings along the NH-line for all glider-measured hypoxic measurements (Table 3.4). Oxygen values of hypoxic measurements are more concentrated near the hypoxic threshold at 250-m isobath versus the 70-m isobath where there is a larger spread of DO values. This further supports the previous result of prevalent hypoxia over the mid-shelf throughout the 2006 to 2012 upwelling seasons.

Temperature, salinity and density all have more normal distributions with peaks warming, freshening and lightening onshore, respectively. Pressure indicates the depth over each isobath crossing where hypoxic measurements are recorded. Over the 50-m and 70-m isobaths, the majority of the measurements are made ~10 mab. The 100-m isobath distribution indicates that hypoxic measurements are also likely 20 mab. This could be due to higher average BML. Over the 200-m isobath, the pressure distribution of hypoxic measurements is very spread out from 100 – 190 m depths.

3.5. Discussion

3.5.1. Cross-shelf DO variability caused by along-shelf advection of gradients

Poleward advection

To the south of the NH line is the Heceta and Stonewall Bank complex (HSBC), a very productive, retentive area (Barth et al., 2005). During poleward advection, POM and hypoxic waters could be transported to the NH line from the Bank which sees persistent hypoxia ~3 months a year on the mid shelf (Adams et al., 2013). In fact, after a 20 km poleward CD between glider lines 1 and 2, near-bottom hypoxic water was observed over the mid and outer shelf regions (Figure 3.4b). Note the two distinct regions of hypoxia that are observed. The cross-shelf gap between the two NH-line prevalent hypoxic regions is directly to the north of Stonewall Bank. Bathymetry across the central-Oregon shelf from 44.75° to 44.5°N is shown in Figure 3.10.

Observations of bottom boundary layer mixing over Stonewall Bank are several orders of magnitude larger than the background shelf mixing rate under upwelling-favorable conditions early in the upwelling season (Nash and Moum, 2001). We posit that strong mixing during poleward flow around this feature also increases mixing rates in the BBL over the bank. Increased mixing would be a source of DO for the BBL. The high-DO signal observed in between the two cross-shelf hypoxic areas in Figures 3.7b and 3.8a-b are likely due to mixing over Stonewall Bank that is advected northward to the NH line. The gap between the two prevalent hypoxic areas on the NH line corresponds to a region of increased DO and decreased density (Fig. 3.8c-d) in average vertical cross-shelf sections corresponding to the hypoxic glider lines (Fig 3.8a). This further supports that higher DO water is vertically mixed into the BBL over Stonewall Bank and is advected northward to the NH line and even north of 44.7°N (Figure 3.8b).

3.5.2. Return flow depth

In the 2011 upwelling season, the onshore return flow depth over the mid shelf is near-bottom (70 m) until around day 190 (Figure 3.2d) where onshore flow is observed at 30-m water depth and near-bottom flow stalls. This results in a more retentive near-bottom environment, since the onshore flow of source water brings higher-DO water on to the shelf. This shutdown of cross-shelf near-bottom flow increases the risk for hypoxia. In data presented here, persistent hypoxia is not observed until after day 190 (Figure 3.2b), when the return flow depth is observed in the 31 m ADCP record. The mechanism that causes this switch in return flow depth is unknown.

In a two-dimensional upwelling model over a slope bottom, Lentz and Chapman (2004) find nonlinear cross-shelf momentum flux divergence to cause return flow below the surface boundary layer when the slope-Burger number, $S = N\alpha f^{-1}$, is 1.5 - 2. High values of S were found for Oregon coast data from 45°N where the shelf slope is steep and the bathymetry variations are small. Interior return flow is observed in a single cross-shelf velocity depth profile (Smith, 1981). To be consistent with the Lentz and Chapman (2004) prediction, S should be low early in the season when we observe BBL return flow and high late in the season when return flow is observed ~ 30 m. However, we find that stratification, and, therefore, S decrease throughout each upwelling season.

Another proposed mechanism for a change in BBL flow is the presence of an along-shelf pressure gradient. Chapman and Lentz (2005) find in a two-dimensional upwelling model that BBL flow acceleration due to an imposed along-shelf pressure gradient depends on S. In this model, vertical shear restricts the bottom friction from balancing the along-shelf pressure gradient even for low S values. Hence, along-shelf flow and the subsequent BBL flow continue to increase unbounded. From these model results, a decrease in BBL flow would correspond to a decrease in S. This is in fact what we observe over the mid shelf,

however a connection between an along-shelf pressure gradient and BBL transport has not been established.

Previous studies have identified the complicated 3-dimensional flow regime over the central-Oregon shelf. Smith (1981) found an imbalance between the onshore transport below the surface and the offshore surface transport from moored current data on the Oregon shelf and concludes the dv/dy continuity term cannot be neglected. Unsteady wind forcing and variations in bathymetric features are suggested as drivers of the 3-dimensionality of the flow regime in this region. Barth et al., (2005) attribute temporal variations in the wind-field to the 3-dimensional flow fields in this region. Coastal circulation along the NH-line is likely 3-dimensional due to the combination of temporal variations in wind-forcing and spatial variations in bathymetric features.

Future observational needs

With the addition of underwater gliders as observational platforms, fine-scale cross-shelf resolution of measurements has increased, however along-shelf resolution is still lacking. We have identified the lack of high-resolution (< 10 km) along-shelf DO data and of cross-shelf current data over the central-Oregon shelf. To date, no study has captured the along-shelf component to near-bottom DO variability on seasonal time scales. As part of the NSF-funded Ocean Observatories Initiative (OOI) Endurance array, gliders will occupy one along-shelf and multiple cross-shelf transects over the Oregon and Washington continental shelf. This data should enable the fine-scale resolution across and along the continental shelf not currently possible.

3.6. Summary and Conclusions

Cross-shelf variability of near-bottom dissolved oxygen concentrations on intraseasonal and interannual time scales is resolved (<1 km) using Slocum glider lines along the Newport Hydrographic line. A sequence of 10 glider cross-shelf

sections spanning 50 days clearly shows large intraseasonal variability on day – month time scales. Late-season return flow depth is observed at 30-m while near-bottom cross-shelf flow is weakly offshore. The change in return flow depth is not associated with a change in stratification. Outer-shelf DO decreases during the sequence but cannot be linked with the cross-shelf advection of a gradient or draw down due to local respiration. Therefore, an along-shelf gradient is found to be responsible for the largest DO decline observed in the glider line sequence. Hypoxia is prevalent on the mid and outer shelf regions in two distinct regions. Enhanced mixing over the sharp topographic feature of Stonewall Bank to the south of the NH line is a likely cause of the separation of the two cross-shelf hypoxic zones.

3.7. Appendix A

Comparison of mid-shelf moored versus glider-derived N-S velocities

N-S velocities from the two different platforms, the NH10 mooring and the glider, are compared in Figure A1. Moored ADCP data are selected at the time of each glider 80-m isobath crossing (Table 1) and interpolated onto the glider depth grid (2-5 m vertical spacing). Depth-averaged velocities are calculated for the water depth range of 8 - 70 m since the top 7 m are not measured by the downward-looking ADCP.

The depth-averaged v_{geo} and v_{abs} over the 80-m isobath are plotted alongside the depth-averaged v_{NH10} at the time of each glider 80-m isobath crossing. Over all, v_{NH10} and v_{abs} compare qualitatively well, however v_{abs} has a weaker magnitude in most glider sections. This signal dampening is a result of filtering the glider data or the measurement of v_{abs} over several vertical glider profiles. The average of the difference between the glider-measured and moored N-S velocities at each depth in the vertical profiles (Figure 3.4d) are presented in Figure 3.A1b and Table 3.2. The depth-average v_{abs} is approximately 0.05 m s^{-1} more poleward than v_{NH10}, in

each glider lines except for 8 and 10. However, v_{geo} differences vary erratically and as large as 0.2 m s^{-1} more equatorward than v_{NH10}.

Depth-average and near-bottom (70 m) $v_{NH10\ and}\ v_{abs}$ are compared further in Figure 3.A1c. The depth-average linear regression line slope, 0.92, is much closer to 1 than the 70-m slope of 0.62, however, an offset of 0.05 m s^{-1} is found for both data sets. The rms deviations for the depth-average and 70-m regression analysis are 0.031 and 0.026 m s^{-1}, respectively. Previously reported linear regressions (offset -0.02 m s^{-1}) with similar r^2 values compared measured water velocities and calculated geostrophic velocities referenced to 500 dbar from NH10 at 30-m water depth (Huyer et al, 2005). The v_{abs} offset could be attributed to the shallow reference depth of the geostrophic calculation, 190 m or to compass inaccuracy.

3.8. Acknowledgements

Foremost we thank our OSU glider group colleagues, namely A. Erofeev, Z. Kurokawa, P. Mazzini, C. Ordonez, A. Sanchez and G. Salidias, T. Peavy, J. Brodersen and L. Rubiano-Gomez, for their combined +6 years of glider data collection efforts along the Newport Hydrographic line supported by National Science Foundation (NSF) Grants OCE-0527168 and OCE-0961999. A. Erofeev is additionally thanked for assistance with glider pilot training, optode calibration and glider data processing. Thanks to J. Jennings and A. Ross for their assistance with Winkler titrations for optode calibrations. In kind memory, M. Levine provided invaluable guidance and the COAST and NH10 mooring data. SH70 mooring data was collected through the MI_LOCO program funded by Gordon and Betty Moore Foundation (Grant # 1661). Thanks to Francis Chan for SH70 respiration rate data and thoughtful comments. Special thanks to W. Waldorf, C. Risien, and D. Langner with NH10 data processing and assistance in the field. We also thank Captain Mike Kriz, the crew of the R/V Elakha and the OSU Marine Technician group for their data collection efforts.

REFERENCES

[1] Adams, K. A., J. A. Barth, F. Chan (2013), Temporal variability of near-bottom dissolved oxygen during upwelling off central Oregon. Journal of Geophysical Research Oceans, 118, 4839-4854, doi:10.1002/jgrc.20361.

[2] Barnes, S. L., 1964. A technique for maximizing details in numerical weather map analysis. Journal of Applied Meteorology, 3, 396 – 409.

[3] Barth, J. A., S. D. Pierce, and R. M. Castelao (2005), Time dependent, wind-driven flow over a shallow mid shelf submarine bank. J. Geophys. Res., 110, C10S05, doi:10.1029/2004JC002761.

[4] Boyd, T., M.D. Levine, P.M. Kosro, S.R. Gard, and W. Waldorf (2002), Observations from Moorings on the Oregon Continental Shelf (May-August 2001), COAS Data Report 190, Reference 2002-6.

[5] Castelao, R. M., and J. A. Barth (2005), Coastal ocean response to summer upwelling favorable winds in a region of alongshore bottom topography variations off Oregon, *J. Geophys. Res*., 110, C10S04, doi:10.1029/2004JC002409.

[6] Chan, F., J. A. Barth, J. Lubchenco, A. Kirincich, H. Weeks, W. T. Peterson, B. A. Menge (2008), Emergence of anoxia in the California Current large marine ecosystem, *Science*, 319, doi:10.1126/science.1149016.

[7] Eriksen, C. C., Osse, T. J., Light, R. D., Wen, T., Lehman, T. W., Sabin, P. L., Ballard, J. W., Chiodi, A. M., Seaglider: a long-range autonomous underwater vehicle for oceanographic research, *Journal of Oceanic Engineering, IEEE*. 26(4), 424-436, doi: 10.1109/48.972073.

[8] Garau, B., S. Ruiz, W. G. Zhang, A. Pascual, E. Heslop, J. Kerfoot, and J. Tintore (2011), Thermal lag correction on Slocum CTD glider data. *J. Atmos. Oceanic Technol*., 28, 1065–1071.

[9] Garrett, C., P. MacCready, and P. B. Rhines, 1993: Boundary mixing and arrested Ekman layers: Rotating stratified flow near a sloping bottom. *Annu. Rev. Fluid Mech*., 25, 291–324.

[10] Grantham, B. A., F. Chan, K. J. Nielsen, D. S. Fox, J. A. Barth, A. Huyer, J. Lubchenco, and B. A. Menge (2004), Upwelling-driven nearshore hypoxia signals ecosystem and oceanographic changes in the Northeast Pacific, *Nature*, 429, 749-754.

[11] Gray, J. S., R. S. Wu, and Y. Y. Or (2002), Effects of hypoxia and organic enrichment on the marine environment, Mar. Ecol. Prog. Ser., 238, 249–279, doi:10.3354/meps238249.

[12] Huyer, A. (1976), A comparison of upwelling events in two locations: Oregon and Northwest Africa. *J. Marine Res.*, 34(4), 531-546.

[13] Huyer, A., R. L. Smith, and J. H. Fleischbein (2002), The coastal ocean off Oregon and northern California during the 1997–8 El Niño, *Progress in Oceanography,* 54, 311–341, doi: 10.1016/S0079-6611(02)00056-3.

[14] Huyer, A., J. H. Fleischbein, J. Keister, P. M. Kosro, N. Perlin, R. L. Smith, and P. A. Wheeler (2005), Two coastal upwelling domains in the northern California Current system, *J. Marine Res.*, 63, 901–929.

[15] Keller, A. A., V. Simon, F. Chan, W. W. Wakefield, M. E. Clarke, J. A. Barth, D. Kamikawa and E. L. Fruh (2010), Demersal fish and invertebrate biomass in relation to an offshore hypoxic zone along the US West Coast. *Fisheries Oceanography*, 19, 76–87. doi: 10.1111/j.1365-2419.2009.00529.x.

[16] Large, W. G., J. C. McWilliams, and S. C. Doney (1994), Oceanic vertical mixing: A review and a model with a nonlocal boundary layer parameterization, *Rev. Geophys*., 32, 363-403.

[17] Merckelbach, L.M., Briggs, R. D., Smeed, D.A., Griffiths, G., (2008) Current measurements from autonomous underwater gliders, *IEEE/OES 9th Working Conference on Current Measurement Technology,* 17-19 March 2008, doi:10.1109/CCM.2008.4480845.

[18] Nash, J. D., and J. N. Moum (2001), Internal hydraulic flows on the continental shelf: High drag states over a small bank, J. Geophys. Res., 106(C3), 4593–4611, doi:10.1029/1999JC000183.

[19] Pierce, S. D., J. A. Barth, R. K. Shearman, A. Y. Erofeev (2012), Declining Oxygen in the Northeast Pacific, *J. Phys. Oceanogr.*, 42, 495–501. doi:10.1175/JPO-D-11-0170.1.

[20] Pelland, N. A., C. C. Eriksen, C. M. Lee (2013), Subthermocline eddies over the washington continental slope as observed by seagliders, 2003–09. *J. Phys. Oceanogr.*, 43, 2025–2053. doi: http://dx.doi.org/10.1175/JPO-D-12-086.1.

[21] Reid, J. L., and A. W. Mantyla (1976), The effect of the geostrophic flow upon coastal sea elevations in the northern North Pacific Ocean, *J. Geophys. Res*., 81(18), 3100–3110, doi:10.1029/JC081i018p03100.

[22] Rudnick, D. L., and S. T. Cole (2011), On sampling the ocean using underwater gliders, *J. Geophys. Res*., 116, C08010, doi:10.1029/2010JC006849.

[23] Smith, R. L. (1981), A comparison of the structure and variability of the flow field in three coastal upwelling regions: Oregon, northwest Africa, and Peru, in *Coastal Upwelling, Coastal Estuarine Ser*., vol. 1, edited by F. A. Richards, pp. 107– 118, AGU, Washington, D. C.

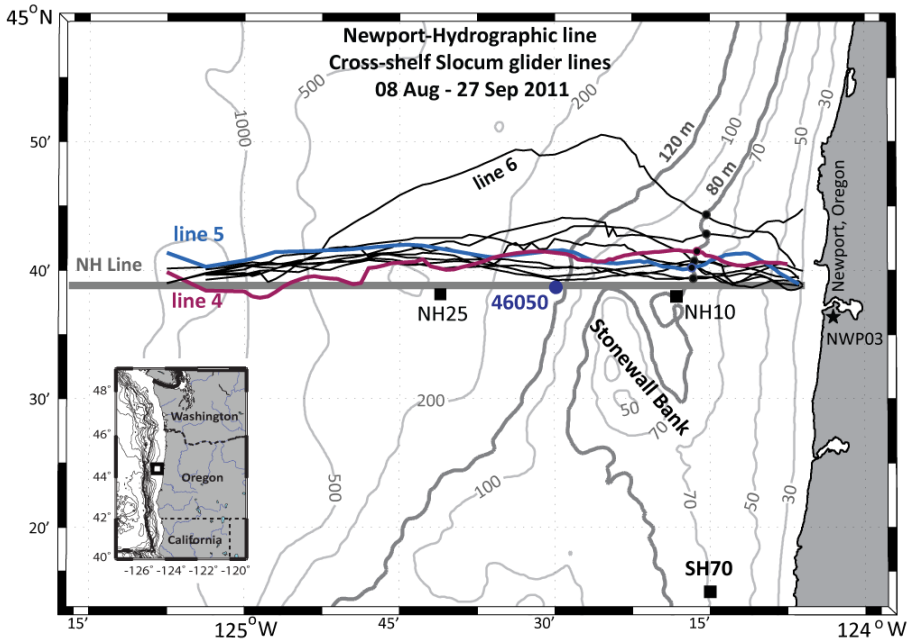

Figure 3.1: Central Oregon coast study map with glider tracks along the Newport Hydrographic line (NH line) from 10 sequential Slocum glider cross-shelf transects from late summer 2011. Glider lines span 2 – 90 km offshore (124.1 – 125.1°W). Mooring locations (black squares) are shown for the NH-line mid-shelf (NH10; 80-m water depth) and Strawberry-Hill line mid-shelf (SH70; 70-m water depth). Wind data were measured at NDBC buoy 46050 and at a coastal meteorological station, NWP03. The mid shelf (80 m) and outer shelf (120 m) isobaths are shown in bold. Black circles on the 80-m isobath indicate the locations of glider 80-m isobath crossings.

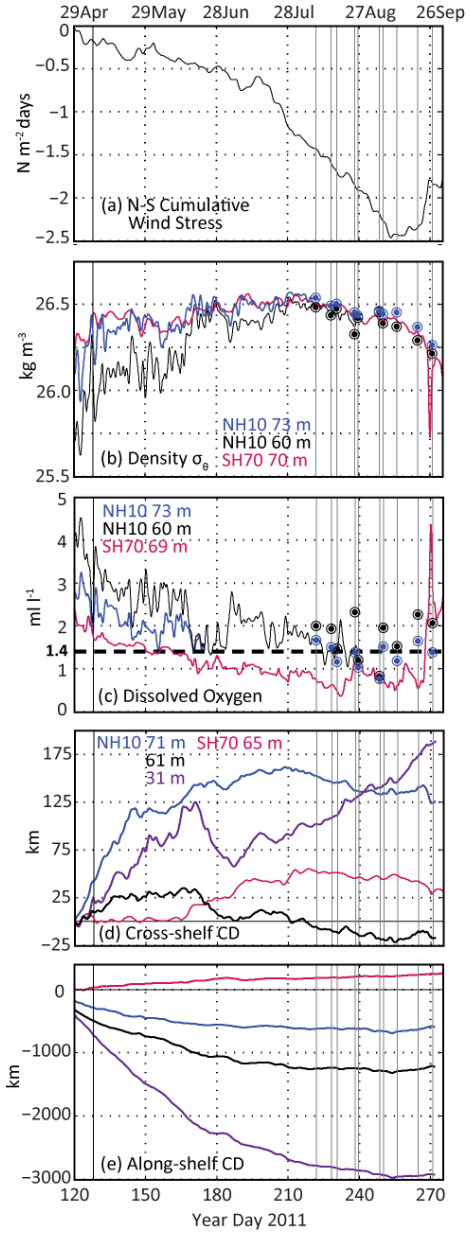

Figure 3.2: (a) 2011 upwelling season cumulative N-S wind stress (N m^{-2} days) from NDBC 46050 wind data. Mid-shelf mooring continuous time series from NH10 (44.65°N, 124.3°W; 80-m water depth) and SH70 (44.25°N, 124.25°W; 70-m water depth) of (b) potential density anomaly (kg m^{-3}), (c) dissolved oxygen (ml l^{-1}), (d) cross-shelf and (e) along-shelf cumulative displacement (CD) at several ADCP depth bins for NH10 and the near-bottom bin for SH70. Positive CD slope indicates onshore or poleward flow. The circles in (b) and (c) correspond to 70 m (blue) and 60 m (black) Slocum glider data at each 80-m isobath crossing in glider sections 1-10 (gray lines) (Figure 3.1). A solid black line at 07 May marks the 2011 spring transition as found in Adams et al., (2013).

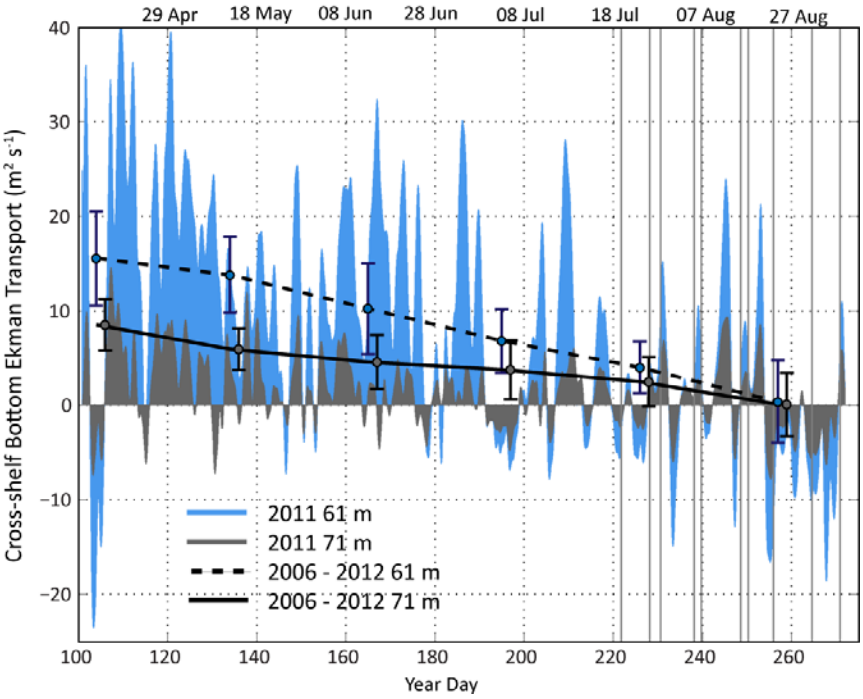

Figure 3.3: Time series of bottom Ekman cross-shelf transport (m^2 s^{-1}) at 20 mab (blue) and 10 mab (gray) in 2011 calculated from moored ADCP currents at the NH10 mooring (80-m water depth). Monthly means ± one standard deviation of bottom Ekman transport is also plotted at 20 mab (dashed) and 10 mab (solid) from 2006 – 2012 ADCP data. Gray vertical lines during August and September correspond to the 80-m isobath crossings of the 10 glider lines shown in Figure 3.1.

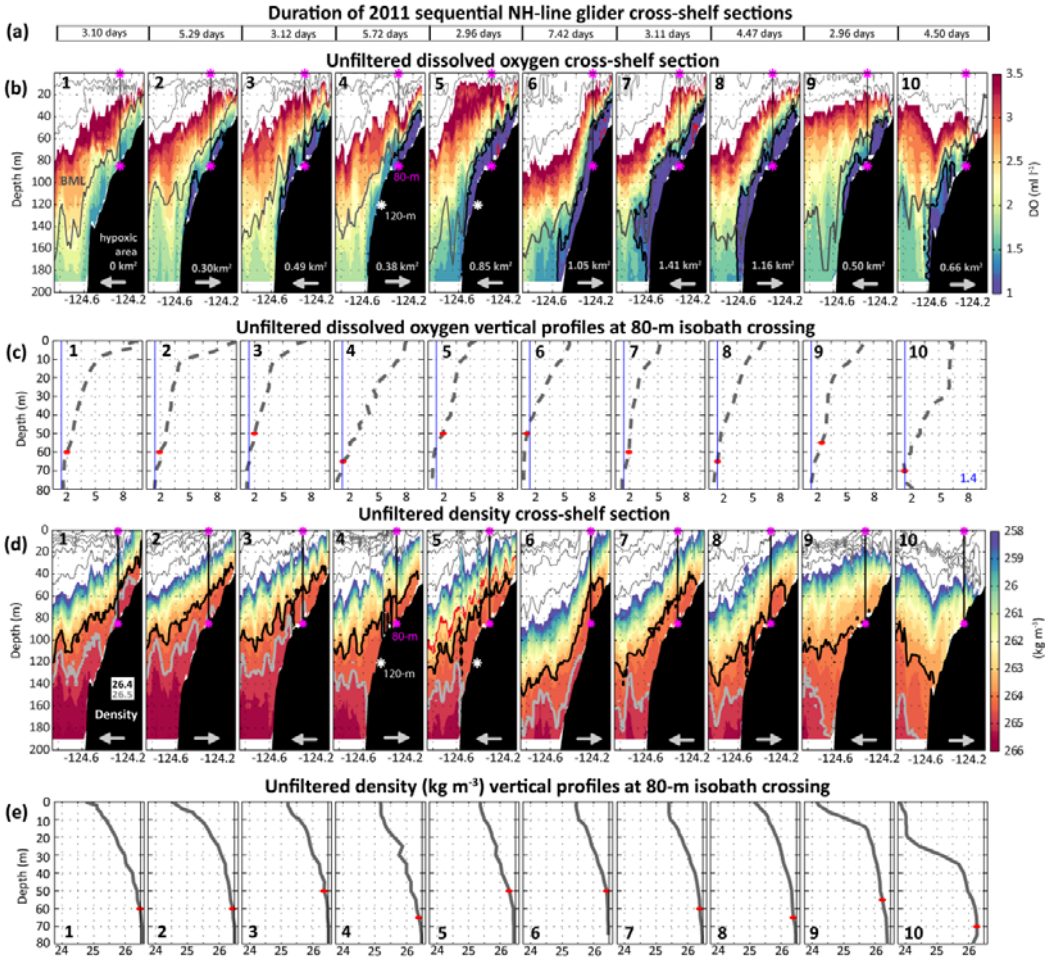

Figure 3.4: DO and density data for Slocum glider cross-shelf section sequence (1-10) along the NH-line, 08 Aug – 27 Sep 2011. (a) Duration of each glider line in days. (b) Dissolved oxygen (ml l^{-1}) data are color contoured for the concentration range 0-3.5 ml l^{-1}. The hypoxic contour (1.4 ml l^{-1}) is shown in black and the bottom mixed layer depth (BML) in dark gray. Shallow oxygen contours (5 and 7 ml l^{-1}) are plotted as light gray contours. The 80-m (120-m) isobath crossing is noted by pink (white) stars. The hypoxic cross-sectional area of each line is maximum (1.41 km^2) in line 7. (c) Depth profiles of DO at the 80-m isobath crossing are plotted with the hypoxic threshold in blue. (d) Potential density anomaly (kg m^{-3}) data are color contoured (25.8 – 26.6) and line contoured 23 – 25.8. Isopycnals 26.4 (black) and 26.5 (gray) are near-bottom. (e) Vertical profiles of density data at the 80-m isobath crossing with the 26.5 isopycnal shown in black. Red circles in (c) and (e) indicate the BML depth of each profile. Cross-shelf sections in (b) and (d) are organized offshore to onshore with an arrow indicating direction of glider path. Time increases left to right for even glider lines.

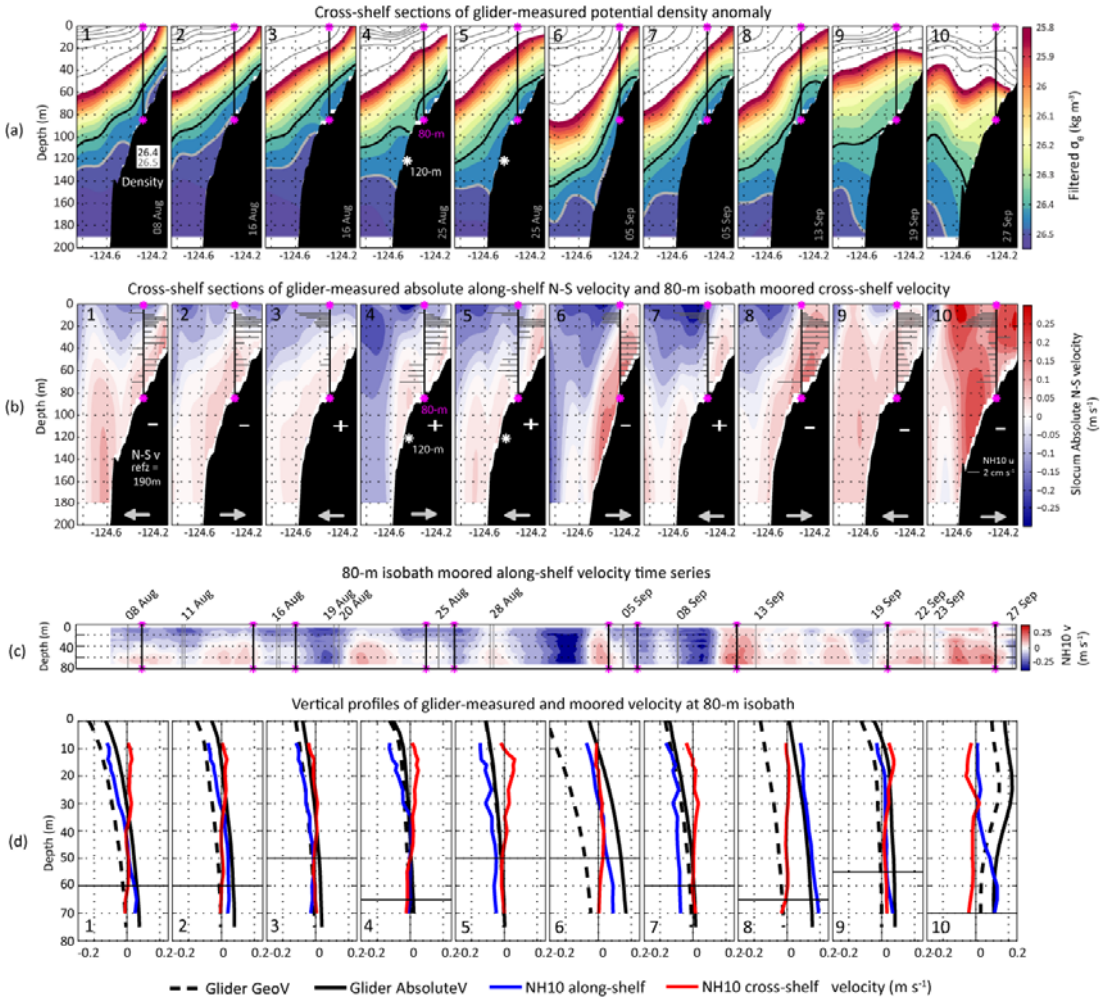

Figure 3.5:(a) Filtered potential density anomaly (kg m^{-3}) glider line sequence in Figure 3.4d. Isopycnals are color contoured, 25.8 – 26.6, and line contoured, 23 – 25.8. Near-bottom isopycnals are 26.4 (black) and 26.5 (gray). (b) Glider line sequence of absolute N-S velocity (geostrophic + glider-measured depth-averaged). The geostrophic velocity (not shown) reference depth is 190 m. Positive velocities are poleward. Depth profiles of NH10 cross-shelf velocity horizontal bars (gray) plotted over the 80-m isobath correspond to the time of the glider's 80-m isobath crossing (pink stars). Offshore (negative) E-W velocities are pointing left. For scale, a 2 cm s^{-1} vector is shown in line 10. The sign of cross-shelf bottom Ekman layer flow, values in Table 3.1, is shown in each panel as a + or – for onshore or offshore flow, respectively. (c) Mid-shelf mooring (NH10; 80-m water depth) ADCP along-shelf velocity (m s^{-1}) low-pass filtered (40-hr) time series for 7-73 m depth range. Gray lines indicate start and stop times of each glider line (1-10). The black lines and stars indicate glider 80-m isobath crossings. (d) Vertical profiles of glider geostrophic velocity (black dashed) referenced to

190 m, glider absolute velocity (black), and moored NH10 along-shelf (blue) and cross-shelf (red) velocities all over the 80-m isobath. The moored NH10 profiles were extracted from the continuous time series at the time of each glider line 80-m isobath crossing (Table 3.1).

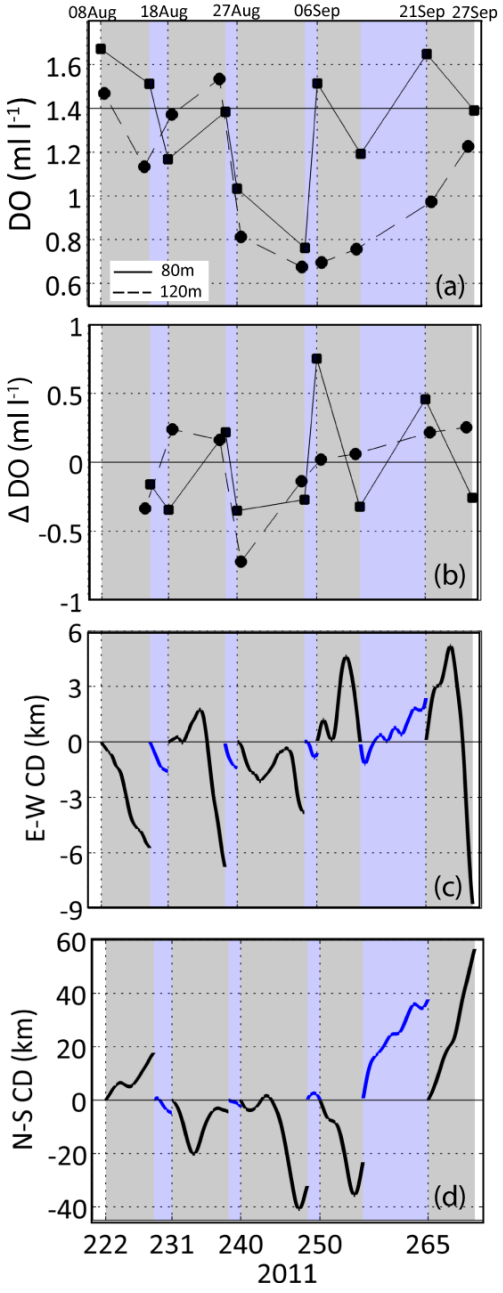

Figure 3.6:(a) Dissolved oxygen (ml l^{-1}) measured 10 m above the bottom at the 80-m (solid) and 120-m (dashed) isobath crossings of each glider line (Figure 2). (b) Change in near-bottom DO values 10 m above the 80- and 120-m isobaths

between consecutive glider lines. Mid-shelf mooring (NH10; 80-m water depth) time integrated (c) E-W and (d) N-S near-bottom (depth range 69-73 m) velocities between 80-m isobath glider crossings. Positive cumulative displacements are onshore and poleward. Alternating gray (blue) shading represents offshore- (onshore-) bound glider paths.

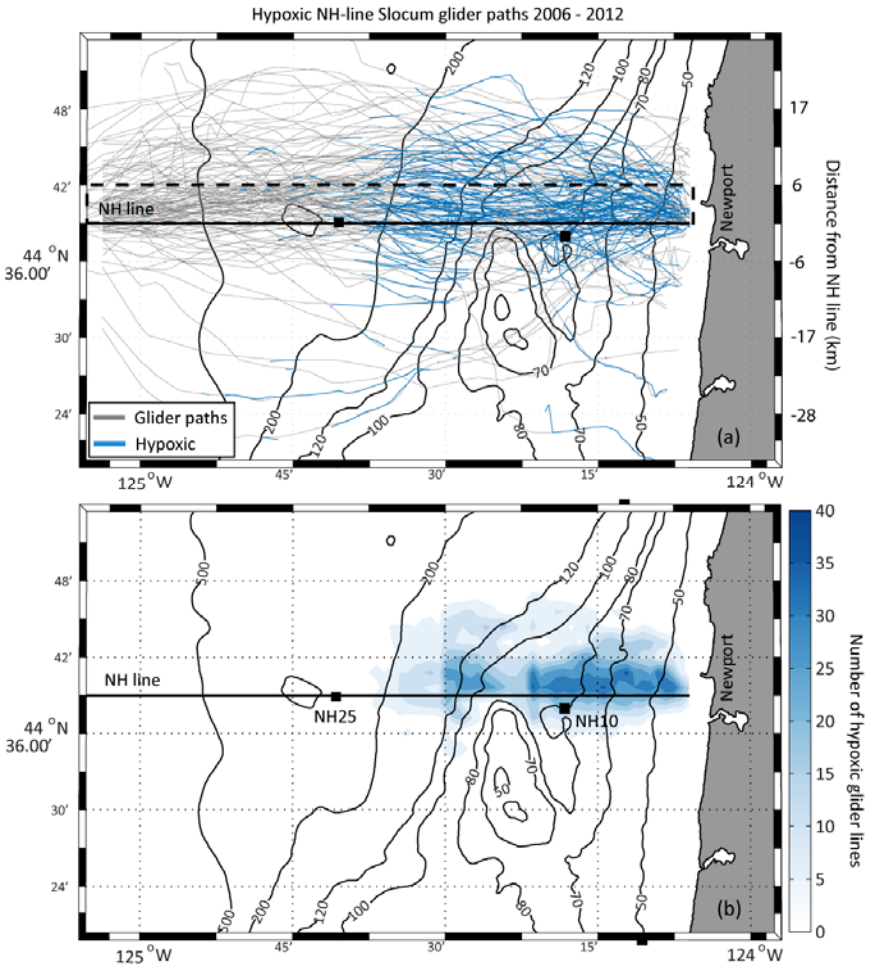

Figure 3.7: (a) Map of 133 Slocum glider paths in which hypoxia was measured along the NH-line from 2006 to 2012 in gray. Blue lines correspond to the section of each glider line where hypoxia was observed. Observations outside of the dashed box are not considered to be along the NH-line. (b) Colored histogram map of hypoxic glider line measurements of glider paths in (a) showing two separate prevalent hypoxic areas.

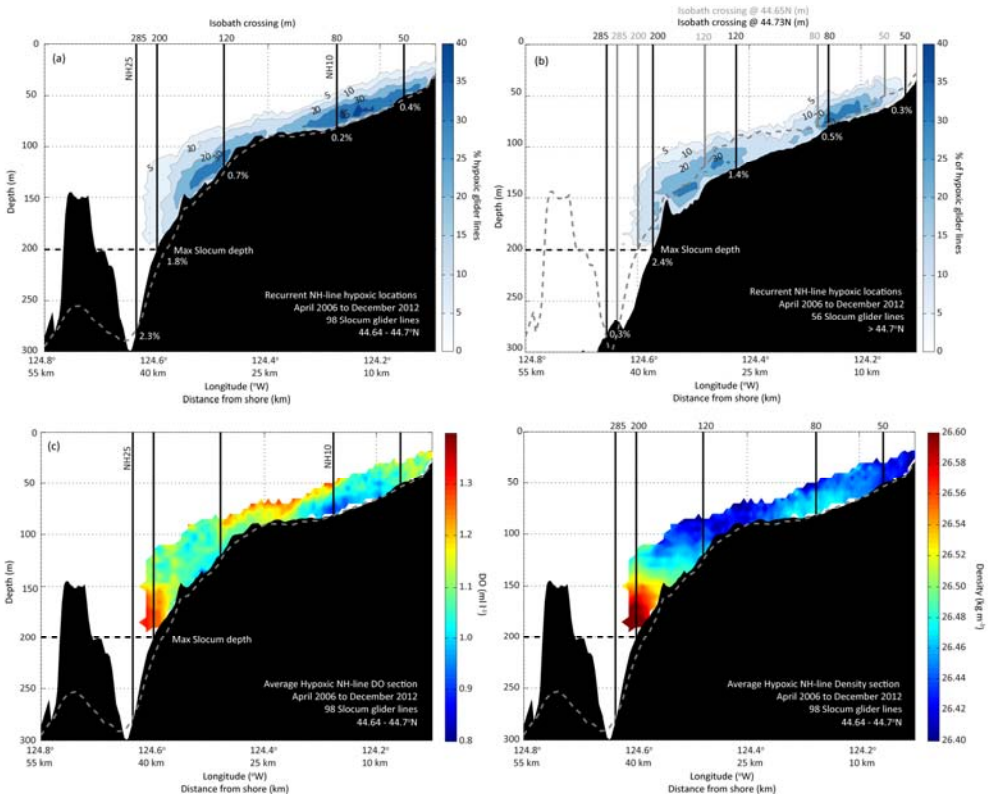

Figure 3.8: Sum of glider-measured hypoxic occurrences (blue) from 249 filtered, gridded Slocum-glider cross-shelf sections (2006 – 2012) along (a) the NH-line (44.64° to 44.7°N) and (b) north of the NH-line (>44.7°) for the top 200 m of the water column. The average glider-line bottom depth (dashed) is smoother and more monotonic than realistic bathymetry (black). Bottom slope (%) for the 50-, 80-, 120-, 200-, and 285-m isobath crossings along the NH-line, are based on the actual bathymetry (black). Bathymetry and isobath crossings in (b) are shown along 44.73°N (black) and along 44.65°N (NH-line) (gray). Average (c) DO and (d) density sections corresponding to the hypoxic glider lines shown in (a).

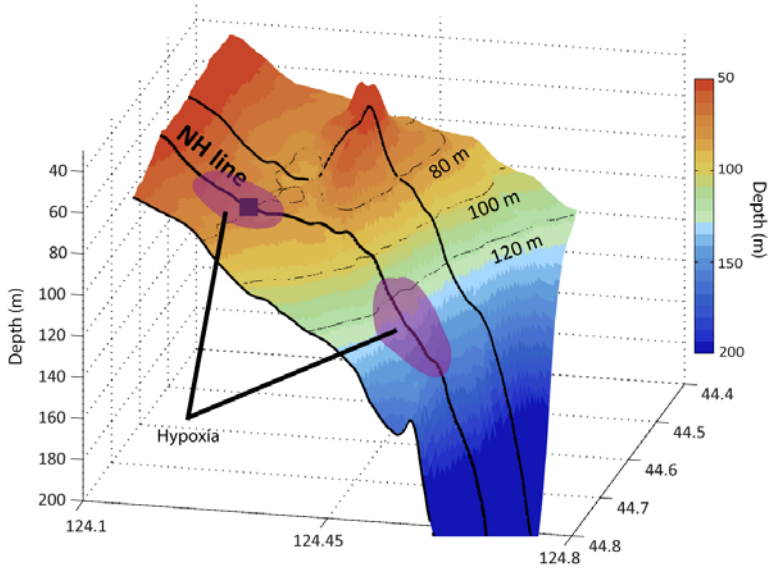

Figure 3.9: Central Oregon continental shelf bathymetry with latitudinal contours at 44.55°, 44.65° (NH line) and 44.75°N. The 80-, 100- and 120-m isobaths are also included in black. Hypoxic zones often observed on the NH line are on either side of the sharp topographic feature to the south, Stonewall Bank.

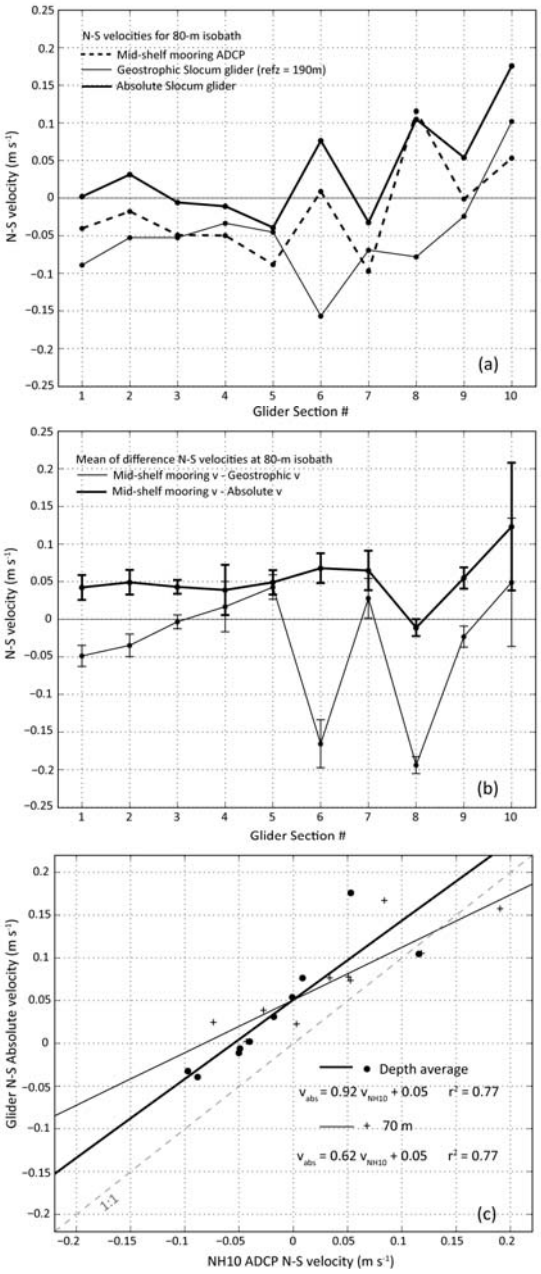

Figure 3.10: (a) Depth-averaged N-S velocities at the NH-line 80-m isobath from the mid-shelf NH10 mooring (dashed), Slocum glider geostrophy (black), and Slocum glider absolute (bold) for the NH-line glider sections (1-10) in Figure 1. (b) Mean and standard deviation of the difference between the mooring and glider N-S velocity vertical profiles at each 80-m isobath crossing. (c) NH10 mooring ADCP N-S velocities versus Slocum glider absolute N-S velocities, depth-averaged (circles) and 70-m (crosses). Linear regression lines and skills, r^2 values, are shown for depth-averaged (bold) and 70-m (black) N-S velocity data.

Table 3.1: 2011 Sequential Slocum glider cross-shelf section information. Times at inshore (NH1; 124.1°W) and offshore (NH45; 125.1°W) turn around points as well as times crossing the 80-m isobath area reported in GMT. Hypoxic area and height are calculated from unfiltered gridded oxygen data. Hypoxic area is calculated by integrating the cross-shelf and vertical extent of the hypoxic measurements in each unfiltered, gridded glider line. Hypoxic height is the distance from the shelf bottom to the hypoxic oxycline (Figure X.). Bottom mixed layer (BML) height at the 80-m isobath, also reported in meters above bottom (mab), requires a density difference of 0.02 kg m^{-3} between consecutive vertical bins. Bottom boundary layer (BBL) cross-shelf Ekman transport calculations from NH10 moored ADCP data.

	Inshore time	Offshore time	Duration	80-m isobath	Hypoxic area	Median hypoxic height	Hypoxic height 80 m	BML height 80 m	U_E BBL 80 m
Glider line #	Calendar Day Year Day	Calendar Day Year Day	days	Calendar Day Year Day	km^2	mab	mab	mab	$m^2\ s^{-1}$
1	08 Aug 00:16:01 221.01	11 Aug 02:44:36 224.11	3.10	08 Aug 19:30:08 221.81	0	n/a	n/a	20	-0.35
2	16 Aug 13:22:41 229.56	11 Aug 06:25:53 224.27	5.29	15 Aug 04:50:26 228.20	0.30	15±7	5	20	-0.51
3	16 Aug 17:15:11 229.72	19 Aug 20:07:20 232.84	3.12	17 Aug 15:03:53 230.63	0.49	15±7	20	30	0.32
4	25 Aug 20:08:55 238.84	20 Aug 02:41:36 233.11	5.72	25 Aug 03:12:15 238.13	0.38	15±6	20	20	0.13
5	25 Aug 20:37:58 238.86	28 Aug 19:36:10 241.82	2.96	26 Aug 18:01:23 239.75	0.85	25±8	25	20	0.88
6	05 Sept 10:16:31 249.43	29 Aug 00:11:33 242.01	7.42	04 Sept 14:59:37 248.62	1.05	30±8	40	30	-1.00
7	05 Sept 10:56:57 249.46	08 Sept 13:34:47 252.57	3.11	06 Sept 06:31:47 250.27	1.41	25±16	10	20	0.81

Glider line #	Inshore time Calendar Day Year Day	Offshore time Calendar Day Year Day	Duration days	80-m isobath Calendar Day Year Day	Hypoxic area km^2	Median hypoxic height mab	Hypoxic height 80 m mab	BML height 80 m mab	U_E BBL 80 m $m^2 s^{-1}$
8	13 Sept 01:43:28 257.07	08 Sept 14:25:19 252.60	4.47	11 Sept 23:24:23 255.98	1.16	25±16	15	15	-1.29
9	19 Sept 19:02:54 263.79	22 Sept 18:05:37 266.75	2.96	20 Sept 15:34:09 264.65	0.50	15±9	5	25	-0.58
10	27 Sept 19:39:54 267.32	23 Sept 07:34:56 271.82	4.50	26 Sept 20:00:44 270.83	0.66	25±17	5	10	-0.49

Table 3.2: Change in observed DO10 m above the bottom at the 80-m and 120-m isobaths from glider-measured DO (Figure 6a). Discrete observed DO rates of change (Δ DO per Δ time) are calculated. Estimates for density-driven (Δ 0.32 ml l^{-1} per Δ 0.1 kg m^{-3}) and biologically-driven (2.6 x 10^{-2} ml l^{-1} day^{-1}) DO rates of change are calculated based on Adams *et al*. (2013). Observed DO decline rates are bold if larger than 2.6 x 10^{-2} ml l^{-1} day^{-1}.

	Δ time 80m isobath	Observed Δ DO 70/80m	Observed Δ DO rate 70/80m	Estimated Density Δ DO 70/80m	Estimated Biological Δ DO 70/80m
Glider lines	days	ml l^{-1}	10^{-2} ml l^{-1} day^{-1}	ml l^{-1}	ml l^{-1}
2-1	6.4	-0.16	**-3.02**	0.15	-0.17
3-2	2.4	-0.34	**-9.44**	-0.03	-0.06
4-3	7.5	0.22	3.49	0.16	-0.20
5-4	1.5	-0.35	**-12.50**	0.06	-0.04
6-5	8.9	-0.27	**-3.38**	-0.09	-0.23
7-6	1.6	0.75	28.85	0.04	-0.04
8-7	5.7	-0.32	**-6.96**	-0.02	-0.15
9-8	8.7	0.46	4.69	0.27	-0.23
0-9	6.2	-0.26	**-5.42**	0.34	-0.16

	Δ time 120m isobath	Observed Δ DO 110/120m	Observed Δ DO rate 110/120m	Estimated Density Δ DO 110/120m	Estimated Biological Δ DO 110/120m
Glider lines	days	ml l^{-1}	10^{-2} ml l^{-1} day^{-1}	ml l^{-1}	ml l^{-1}
2-1	5.3	-0.33	**-5.16**	-0.08	-0.14
3-2	3.6	0.24	10.00	0.004	-0.09
4-3	6.3	0.16	2.13	0.13	-0.16
5-4	2.8	-0.72	**-45.00**	0.02	-0.07
6-5	8.0	-0.14	-1.57	-0.07	-0.21
7-6	2.6	0.02	1.25	0.13	-0.07
8-7	4.6	0.06	1.05	0.01	-0.12
9-8	9.8	0.22	2.53	0.13	-0.26
0-9	4.8	0.25	4.03	0.32	-0.13

Table 3.3: Time integration of NH10 (44.65°N, -124.3°W, 80-m water depth) N-S and E-W measured near-bottom average (69-73 m) water velocities between sequential glider section 80-m isobath crossings yields cumulative displacements (km). Positive values are poleward (north) and onshore (east). Time integration starts at 80-m isobath crossing of one line and stops at 80-m isobath crossing of next line (i.e., section 1 to 2). Values are plotted in Figure 6b-c.

	ADCP time integration start time	N-S 80m Cumulative Displacement	E-W 80m Cumulative Displacement
Glider lines	Year Day 2011 GMT	km	Km
2-1	221.81	17.72	-5.73
3-2	228.20	-4.81	-1.57
4-3	230.63	-4.38	-6.76
5-4	238.13	-2.58	-1.39
6-5	239.75	-32.12	-3.80
7-6	248.62	0.10	-0.62
8-7	250.27	-23.21	-0.02
9-8	255.98	37.70	2.36
0-9	264.65	56.63	-8.76

Table 3.4: Mean and standard deviation of glider-measured hypoxic water mass properties sampled along the NH line from 2006 to 2012, as shown in Figure 8.

Isobath (m)	Latitude (°N)	Longitude (°W)	DO (ml l^{-1})
50	44.66 ±0.04	124.14 ±0.01	1.12 ±0.2
80	44.67 ±0.04	124.26 ±0.01	1.01 ±0.3
120	44.70 ±0.05	124.45 ±0.05	1.11 ±0.2
200	44.69 ±0.05	124.58 ±0.02	1.13 ±0.2
250	44.67 ±0.03	124.63 ±0.02	1.25 ±0.1

Isobath (m)	Temperature (°C)	Salinity	σ_θ (kg m^{-3})	Pressure (m)
50	7.58 ±0.2	33.85 ±0.06	26.44 ±0.07	40 ±8
80	7.49 ±0.3	33.88 ±0.06	26.47 ±0.07	64 ±9
120	7.51 ±0.3	33.87 ±0.10	26.46 ±0.10	106 ±11
200	7.34 ±0.4	33.93 ±0.05	26.53 ±0.09	154 ±25
250	7.27 ±0.3	33.94 ±0.05	26.55 ±0.08	155 ±24

Table 3.5: Difference between depth-average and 70-m water depth NH10 moored ADCP and glider-derived N-S velocities during the 10 glider lines shown in Figure 1.

Glider line #	Depth-average		70-m depth	
	$v_{abs} - v_{NH10}$	$v_{geo} - v_{NH10}$	$v_{abs} - v_{NH10}$	$v_{geo} - v_{NH10}$
1	0.042 ± 0.016	-0.049 ± 0.014	0.021	-0.064
2	0.049 ± 0.016	-0.035 ± 0.015	0.043	-0.038
3	0.043 ± 0.009	-0.003 ± 0.009	0.066	0.020
4	0.039 ± 0.033	0.017 ± 0.033	0.020	-0.003
5	0.049 ± 0.016	0.043 ± 0.016	0.045	0.039
6	0.068 ± 0.020	-0.166 ± 0.032	0.083	-0.131
7	0.065 ± 0.026	0.028 ± 0.026	0.098	0.062
8	-0.011 ± 0.011	-0.194 ± 0.011	-0.033	-0.216
9	0.055 ± 0.014	-0.023 ± 0.014	0.027	-0.051
10	0.123 ± 0.085	0.049 ± 0.085	-0.013	-0.087

4. Along-shelf differences in upwelling source water properties over a submarine bank and implications for shelf hypoxia

Katherine Adams, John A. Barth, and R. Kipp Shearman

Geophysical Research Letters
2000 Florida Avenue, N.W., Washington DC 20009, USA
To be submitted

4.1. Abstract

Spicy, oxygen-depleted California Undercurrent (CU) water flows northward along the Oregon coast on isopycnal surfaces that upwell onto the continental shelf each summer. Along-shelf differences in spice and dissolved oxygen (DO) of slope and shelf waters off Oregon are investigated along two cross-shelf transects – the Newport Hydrographic line (NH; 44.65°N) and the Umpqua River line (UR; 43.7°N). In between the 100-km along-shelf stretch that spans these two cross-shelf lines is Heceta Bank (HB), a sharp topographic feature where the 200-m isobath detours sharply from a N-S orientation to an E-W orientation as the shelf width increases by a factor of two. Glider observations from the 2008 upwelling season reveal increased spiciness along upwelling isopycnals on the UR-line slope and shelf compared to the NH line. A remarkably strong spice and poleward velocity signal is observed just offshore of the shelf break, 0.05 kg m^{-3} and 0.1 m s^{-1}, respectively. North of the bank, however, the poleward core is weaker and the spice maximum is diffuse and farther offshore, suggesting the along-shelf mixing of water masses between the NH and UR lines. Implications for shelf DO concentrations are investigated. Although the spice-density relationship differs north-to-south, the DO-density relationship of near-bottom slope waters is similar. Strong, local respiration effects may alter the DO concentrations of near-bottom waters over the slope. A difference in spice is also observed on the shelf, however a change in near-bottom DO is indiscernible. We attribute this to the strong effects of shelf processes, namely mixing and respiration.

Introduction

Heceta Bank (HB) on the central-Oregon shelf rapidly widens and complicates the continental shelf bathymetry in the area between the Newport-Hydrographic (NH; 44.65N) and the Umpqua River (UR; 43.7°N) lines (Figure 4.1). Previous studies have identified this topographic feature as an area with irregular coastal circulation (Castelao and Barth 2005), high-productivity (Barth et al., 2005) and persistent seasonal hypoxia (Adams et al., 2013). The equatorward coastal upwelling jet follows the widening isobaths around HB, creating a lee region where re-circulating currents are observed (Barth et al., 2005; Castelao and Barth 2005). Model runs over HB during downwelling-favorable conditions find the resulting poleward jet shoals and does not follow isobaths as closely as the equatorward upwelling jet (Whitney & Allen, 2009). However, effects of HB on summertime deep poleward flows have not been well studied.

The poleward-flowing California Undercurrent (CU) is observed along the continental slope of the U.S. West coast during the wind-driven coastal upwelling season in the California Current System (Hickey, 1979). An along-shelf survey conducted in 1995 suggests the central-Oregon shelf just north of HB as a region where the CU separates from the shelf-break and discontinues from the coherent signal observed 400 km to the south of HB (Pierce et al, 2001).

On the NH line, north of HB, an average poleward core velocity of 0.05 cm s^{-1} over 100-300 m depths has been calculated from repeat cross-shelf hydrographic sections (Huyer et al., 2007). The coarse cross-shelf spacing of these sections, 18 – 36 km, is approximately equal to the core width, ~20 km (Pierce et al, 2000). To the south of the NH line, the poleward core tends to be stronger and farther offshore (Pierce et al, 2000; Huyer et al., 2005).

Along the NH line, the water transported via the CU has been identified as approximately 30-40% Pacific Equatorial Water (PEW) along the 26.5 kg m^{-3} σ_θ;

PEW is warm, salty and oxygen-depleted compared to North Pacific Upper water, NPUW, (Thomson and Krassovski, 2010). A metric often used to quantify the warm and salty quality of water is spice (kg m^{-3}) (Flament, 2002). From ~40 – 45N, Pierce et al. (2000) finds an average spice range of -0.2 to -0.1 kg m^{-3} along the 26.5 kg m^{-3} isopycnal.

Since CU flows are found at isopycnals that upwell onto the continental shelf (Huyer et al., 1979; Adams et al., 2013), water transported in the CU may influence source water properties and shelf DO concentrations. Thomson and Krassovski (2010) find a strong relationship between the %PEW and dissolved oxygen (DO) concentrations in the Gulf of Alaska. However, the relationship between poleward flows, spice and DO concentrations on the Oregon shelf has not been studied. Furthermore, a connection between offshore spice and onshore DO has not been identified either. With the recent decade of near-bottom hypoxia on the central-Oregon shelf, it is possible that the CU influences shelf DO concentrations (Barth et al., 2014).

The relative N-S contribution of upwelling source water is a possible mechanism of climate-forced DO variability and subsequent reorganization of coastal ecosystems and formation of coastal hypoxia along the CCS. In the North Pacific, DO levels are declining and are expected to continue (Whitney et al., 2007). To the south, the California Undercurrent has shoaled and increased in volume (Meinvielle & Johnson, 2013). It is important to identify locations along the CCS that are sensitive to a change in relative N-S contributions to source water and locations that may be more sensitive to other mechanisms of change, such as change in wind forcing.

Using high-resolution underwater glider lines, we investigate along-shelf differences in spice, DO and subsurface currents between the NH and UR lines during the 2008 upwelling season. Particularly of interest is whether a high spice

signal corresponds to a low DO signal of slope and shelf waters along upwelling isopycnals. Hypothetically, higher spice and lower DO source water may influence shelf hypoxia by lowering the starting DO concentration that is affected by microbial respiration throughout the season.

4.2. Data & Methods

Two Teledyne Webb Research Electric Slocum (SL) gliders and one University of Washington Seaglider (SG) (Eriksen et al., 2001) sampled cross-shelf transects off central Oregon. Each SL sampled conductivity, temperature, pressure (Sea-Bird Electronics, Inc. SBE 41CP) and dissolved oxygen (Aanderaa optode 3835) in the top 200-m of the water column. Thermal-mass corrections for the unpumped conductivity cell measurements were made following Garau et al., 2001. The SG sampled conductivity, temperature, pressure (Sea-Bird Electronics, Inc. SBE 41CP) and dissolved oxygen (Clark-electrode, SBE43F) in the top 1000-m of the water column. The SG base station code thermal-mass corrections were used. Aanderaa optode dissolved oxygen sensors were calibrated with Winkler titration samples in the laboratory, pre- and post-deployment. The SBE43F DO sensor aboard the SG was factory calibrated prior to the 2008 deployment. The placement of the SBE43F DO sensor on the SG vehicle body is within a re-circulating, wake region which results in a glider-speed dependent low-bias of DO measurements (Nicholson, 2009). A correction was developed from SG deployment data with an optode and a SBE43F sensor installed.

Each SL and SG cross-shelf transect was mapped to a telescoping longitude-depth grid based on the depth-dependent horizontal separation of glider dive-climb pairs. The grid spacing ranges from 0.5-5 km in the horizontal and 2-25 m in the vertical. Mapped data was filtered using a 2-D Gaussian filter (Barnes, 1964) with decorrelation radii of 10 km and 5 m, in the horizontal and vertical respectively. UR and NH glider lines are mapped to the same longitude-depth grid, thus distance from shore differs between the two line locations.

Cross-path geostrophic velocities were calculated from the conductivity, temperature and pressure fields with a reference depth of 700 m for SG and 190 m for SL data, respectively. Geostrophic velocities are calculated over the shelf by extrapolating geopotential anomaly from offshore values (Reid & Mantyla, 1976). The N-S component of geostrophic velocity was retained and adjusted by the N-S component of dead-reckoned depth-average velocity (Todd et al, 2009) to obtain a N-S absolute velocity.

Thermohaline variations along constant potential density surfaces are identified using the state variable spice (π; kg m^{-3}). In T-S space, the slopes of spice isopleths are defined as equal and opposite to slopes of potential density surfaces, referenced to the surface, per Flament (2002). Positive and negative spice values indicate warm and salty or cold and fresh waters, respectively. Observational studies along the California Current System have used spice as a water mass tracer for Pacific Equatorial Water (PEW) that is transported poleward during summertime via the California Undercurrent (Meinvielle and Johnson 2013; Thompson and Krassovski 2010; Collins *et al*., 2000; Pierce *et al.,* 2000). This northward-flowing PEW signal is warm and salty, or spicy, compared to the North Pacific Upper water (NPUW) in the southward-flowing California Current. Spice anomalies are calculated from the mean spice NH-line calculated from 64 SG cross-shelf transects collected during June – September of 2008 to 2012. Each SG line was mapped and filtered as described above.

4.3. Results

During the upwelling season of 2008, underwater gliders sampled two cross-shelf lines 100 km apart, the Newport-Hydrographic line (44.65°N) and the Umpqua River line (43.7°N) (Figure 4.1). The top 200 m of each line was measured by a Slocum glider (SL), while a Seaglider (SG) alternated between the two lines sampling the top 1000 m of the water column.

September 2008 Seaglider line

Two SG lines from late September 2008 are shown in Figure 4.2. Along the NH line, high spice water is observed in a wide band around 200-m depth. Poleward flow of 0.05 m s^{-1} is observed against the continental slope from 200 to 550 m. Isopycnal tilt of the 27 kg m^{-3} σ_θ is observed around 600 m. Deep dissolved oxygen (DO) contours behave similarly to deep isopycnals. At 200-m depth, DO decreases towards shore. Spice anomaly for this NH-line section is near-zero below 100-m depth indicating this NH-line section is similar to the 5-year summertime mean (Figure 4.3).

One hundred km to the south, UR-line fields are remarkably different to the NH line observations described above (Figure 4.2). The spice maximum, 0 - 0.12 kg m^{-3}, is especially high for this latitude (Pierce et al., 2000; Meinvielle & Johnson, 2013). Unlike the NH line fields, the spice maximum is closer to the core of the poleward flow, 0.1 m s^{-1}. A second spice maximum on the shelf is also observed. Separation of isopycnals at approximately 150 m coincides with the poleward core.

In Figure 4.4, T-S diagram of vertical profiles over the respective 500-m isobaths of the NH and UR lines presented in Figure 4.2 are shown. Although the shape of each T-S profiles is similar, spice is higher along the UR-line profile. Around 50-m depth the NH line profile has a salinity minimum, associated with the Columbia River plume (Barnes et al., 1972). The UR line profile salinity minimum is not as fresh as the NH line and is nearly 1°C warmer. The water-mass properties between 100 and 200 m on the UR line are more similar than on the NH line, where the separation between 100 and 200 m is much greater in T-S space. This supports the hypothesis that the spicy water mass observed on the UR line mixes with North Pacific Upper water as it is advected northward. The 5-year mean T-S profile over the NH-line 500-m isobath is similar to the September 2008 T-S

profile at depths greater than 200 m. At 100-m depth, the September 2008 NH-line profile is warmer and spicier, yet falls within one standard deviation of the mean.

Along the 26.5 kg m^{-3} isopycnal, the spiciness of the UR and NH 2008 T-S profiles, sampled 100 km apart, differ by approximately 0.15 kg m^{-3}. This is nearly three times the size of the along-shelf gradients observed previously (Pierce et al., 2000) along this isopycnal.

2008 Slocum glider lines

Along-shelf differences of water mass properties on the continental shelf are investigated from 22 NH and 20 UR cross-shelf transects sampled by Slocum gliders in the 2008 upwelling season. Spice and DO data sampled in the top 200 m of the water column from each 300-m isobath crossing are averaged into 0.05 kg m^{-3} density bins. The density-spice and density-dissolved oxygen relationships for the two cross-shelf lines are then compared (Fig. 4.5).

Spiciness of UR-line waters is higher than NH-line waters for densities 26.4 – 26.6 kg m^{-3} (Figure 4.5a). This density range is observed on the shelf during upwelling. Higher spice along isopycnals is indicative of a larger percentage of PEW (Thomson and Krassovski, 2010) on the UR line than on the NH line. The decrease in spice along the NH line could be due to the mixing of northward flowing PEW in the California Undercurrent with the southward flowing North Pacific Upper water (NPUW). Alternatively, the PEW signal could be transported farther offshore on the NH line, e.g., by subsurface eddies (Pelland et al., 2013), and therefore not observed over the 300-m isobath.

Although an along-shelf difference in spice is very clear over the slope, a difference in source water DO concentrations between the NH and UR lines is not apparent (Figure 4.5b). This is likely due to the small DO difference between

water masses at this location. The NH-line is approximately 40% PEW at 200-m water depth (Thomson and Krassovski, 2010). Therefore water at this location is nearly half PEW and NPUW. The spice difference is large enough to discern but the DO concentration of the two mixing water masses is too small to distinguish.

Differences on the shelf are examined using the Slocum glider data 10 m above the 100-m isobath. Time series of near-bottom spice is higher on the UR line throughout the upwelling season. Therefore, the high spice signal observed in source water on the UR line (Figure 4.5a) influences water mass properties over the shelf.

Although the magnitude of spice is higher on the UR line, the behavior of the spice time series is similar for the NH and UR lines (Figure 4.6a). Spice decreases during the first part of the upwelling season and subsequently increases from year day 175 to the end of the observational record at each line. This is due to the change in the direction of the flow after the spring transition. Prior to the start of upwelling, poleward winds drive predominantly poleward flows on the shelf, which transport spicy, southern waters northward. After upwelling begins, less-spicy, northern waters are carried southward. It is interesting that mid-season the spice signal strengthens. This is most likely due to the increase in spice in the northern CCS throughout the upwelling season from mixing with PEW transported via the CU. This means that the less spicy water mass, NPUW, which flows southward past the NH-line is less pure and more mixed with spicy PEW over the course of the upwelling season. Hence spice near the bottom along the NH and UR lines increases throughout the season since the spiciness of the equatorward-flowing water increases. Alternatively, the late season increase in spice could be due to a spin up time of the CU which is not well understood.

The time series of near-bottom DO is similar between the UR and NH lines but does not show an offset in magnitude as observed in spice (Figure 4.6b). This

result is similar to what was found for the source water over the 300-m isobath (Figure 4.5b).

To further examine shelf water mass properties, spice-DO and DO-density relationships are shown (Figure 4.6c-d). The spice-DO relationship shows higher spice on the UR line while the DO-density relationship is quite similar between lines. Hypoxic, DO < 1.4 ml l^{-1}, measurements are more prevalent on the UR line, however we are not presenting two continuous time series so caution must be taken upon interpretation.

In fact, the majority of the hypoxic measurements on the UR line correspond to densities that are rarely observed along the NH line, > 26.6 kg m^{-3} (Figure 4.6d). Deeper waters upwell once the coastal jet migrates offshore late in the upwelling season and a cyclostrophic balance at the southern end of the Bank is established (Barth et al., 2005; Castelao and Barth 2005). Denser waters on the UR line are only observed in the middle of the season. This may be when the cyclostrophic balance is first established. However, this dense water is not observed later in the season (not shown). This denser water has a lower source water DO signature (Figure 4.5b), 2.0 ml l^{-1} versus 2.2 ml l^{-1} at 26.5 kg m^{-3}. A lower source water DO concentration increases the likelihood for hypoxia to develop since microbial respiration on the shelf decreases DO levels from the source water level. Another possible contributor to low DO water on the UR line may be from equatorward advection of near-bottom waters over Heceta Bank. Persistent hypoxia has been observed on the Bank for three months each year (Adams et al., 2013). This is due to the high signal of shelf microbial respiration on near-bottom DO concentrations (Adams et al., 2013).

4.4. Discussion & Summary

Data along the Newport Hydrographic (NH) and the Umpqua River (UR) cross-shelf transects off of central Oregon, are compared during the 2008 upwelling season. Spaced 100 km apart, these two lines straddle Heceta Bank, a sharp topographic feature that affects the course of the upwelling jet and may cause disturbances in deep poleward flows. Differences in the magnitude and location of the subsurface poleward velocity and spice maximums, characteristic of the California Undercurrent (CU), are observed between these lines. A stronger (0.1 m s^{-1}), spicier (0.05 kg m^{-3}) CU signal is observed on the UR line. Spiciness along the UR line is also higher over the continental shelf throughout the 2008 upwelling season, indicating upwelling source water is more influenced by CU water south of HB than to the north, along the NH line. This is likely due to mixing of CU water with surrounding North Pacific Upper water triggered by flow-topography interactions over the southern portion of HB. Near-bottom spice-DO relationship is investigated, however a clear trend is not distinguished since the shelf respiration signal shelf dominates the DO variability.

Since central-Oregon is located between the two water mass endpoints, is likely that the DO signature of the water masses is masked by respiration and mixing leaving behind an indistinguishable difference. This is not true for the Gulf of Alaska where a clear high spice and low DO relationship was found (Thomson and Krassovski, 2010). This latitudinal dependence on DO difference between water masses has implications for how locations will be affected by future changes in DO concentrations along the CCS. Significant changes in the DO concentration of either PEW or NPUW may be buffered off central-Oregon but severe off locations closer to the north or south. Although, variability in N-S water mass contribution to upwelling waters is posited to be a strong driver of DO dynamics in the CCS, it appears that the strength of this mechanism may be highly variable. Other mechanisms resulting from climate variability and change, such as change in upwelling wind forcing, may have a greater affect on DO

dynamics in locations where DO dynamics are less sensitive to N-S source water variability.

Although spice is higher along the UR line throughout the 2008 upwelling season (Figure 4.5a), the spicy water mass observed in late September (Figure 4.2) is anomalously high. Positive spice values are rarely observed this far north, except during strong El Niño years (Huyer et al., 2002). Without additional years of data, the uniqueness of the 2008 observation cannot be determined. Furthermore, the weak CU signal observed over the NH line is likely due to its location north of HB. Although there is a long and growing time series along the NH line, it results in a view of the CU influenced by an abrupt submarine bank just upstream. Therefore, additional cross-margin observation transects in the northern California Current would be helpful in providing a "cleaner" view of the CU.

There are very few long-term monitoring stations that sample the full continental margin, such as the NH line, along the CCS. The time scales dominating the along-shelf variability of the CU cannot be determined from extant data sets due to scarcity and/or paucity. The addition of continuous monitoring stations along the CCS would enable resolution of seasonal and interannual variability of the along-shelf gradients in CU concentrations, rather than the single season or multi-decadal approaches (e.g., Pierce et al., 2000; Meinvielle and Johnson 2013) used previously.

To understand the flow-topography interaction between the CU and HB, additional modeling and monitoring should be conducted. Simultaneous cross-shelf sections would resolve the temporal variability of the along-shelf difference in CU signals. Investigation using local ocean model runs with high-resolution bottom topography that accurately represents HB bathymetry, currently underway, will shed light on the behavior of the CU as it encounters the southern portion of HB.

4.5. Acknowledgements

The OSU glider group operations were supported by National Science Foundation (NSF) Grants OCE-0527168 and OCE-0961999. We acknowledge our OSU glider group colleagues, namely A. Erofeev, Z. Kurokawa, P. Mazzini, C. Ordonez, A. Sanchez and G. Salidias, T. Peavy, J. Brodersen and L. Rubiano-Gomez, for their glider data collection and processing efforts. Thanks to J. Jennings and A. Ross for their assistance with Winkler titrations for optode calibrations. We also thank Captain Mike Kriz, the crew of the R/V Elakha for their data collection efforts.

REFERENCES

[1] Adams, K. A., J. A. Barth, F. Chan (2013), Temporal variability of near-bottom dissolved oxygen during upwelling off central Oregon. *J. Geophys. Res.*, 118, 4839-4854, doi:10.1002/jgrc.20361.

[2] Barnes, S. L., 1964. A technique for maximizing details in numerical weather map analysis. *Journal of Applied Meteorology*, 3, 396 – 409.

[3] Barth, J. A., S. D. Pierce, and R. M. Castelao (2005), Time dependent, wind-driven flow over a shallow mid shelf submarine bank. *J. Geophys. Res*., 110, C10S05, doi:10.1029/2004JC002761.

[4] Barth, J. A., R. K. Shearman, A. Y Erofeev, S. D. Pierce, F. Chan and K. Adams, 2014. Upwelling-driven continental shelf hypoxia: Underwater robotic gliders signal change. In preparation.

[5] Castelao, R. M., and J. A. Barth (2005), Coastal ocean response to summer upwelling favorable winds in a region of alongshore bottom topography variations off Oregon, *J. Geophys. Res*., 110, C10S04, doi:10.1029/2004JC002409.

[6] Eriksen, C. C., Osse, T. J., Light, R. D., Wen, T., Lehman, T. W., Sabin, P. L., Ballard, J. W., Chiodi, A. M., Seaglider: a long-range autonomous underwater vehicle for oceanographic research, *Journal of Oceanic Engineering, IEEE*. 26(4), 424-436, doi: 10.1109/48.972073.

[7] Garau, B., S. Ruiz, W. G. Zhang, A. Pascual, E. Heslop, J. Kerfoot, and J. Tintore (2011), Thermal lag correction on Slocum CTD glider data. *J. Atmos. Oceanic Technol*., 28, 1065–1071.

[8] Hickey, B.M., 1979. The California Current System, hypotheses and facts. *Progress in Oceanography*, 191–279.

[9] Huyer, A., R. L. Smith, and J. H. Fleischbein (2002), The coastal ocean off Oregon and northern California during the 1997–8 El Niño, *Progress in Oceanography,* 54, 311–341, doi: 10.1016/S0079-6611(02)00056-3.

[10] Huyer, A., E. J. C. Sobey, R. L. Smith (1979), The spring transition in currents over the Oregon continental shelf. *J. Geophys. Res.*, 84, 6995–7011.

[11] Meinvielle, M., and G. C. Johnson (2013), Decadal water-property trends in the California Undercurrent, with implications for ocean acidification, *J. Geophys. Res*., 118, 6687–6703, doi:10.1002/2013JC009299.

[12] Nicholson, D. (2009), Nitrogen, oxygen and the noble gases as tracers of upper-ocean productivity and air-sea gas fluxes, Ph.D. dissertation, University of Washington, Seattle, Washington, U.S.A.

[13] Pelland, N. A., C. C. Eriksen, C. M. Lee (2013), Subthermocline eddies over the Washington continental slope as observed by seagliders, 2003–09. *J. Phys. Oceanogr.*, 43, 2025–2053. doi: http://dx.doi.org/10.1175/JPO-D-12-086.1.

[14] Pierce, S. D., R. L. Smith, P. M. Kosro, J. A. Barth, and C. D. Wilson (2000), Continuity of the poleward undercurrent along the eastern boundary of the mid-latitude North Pacific. *Deep-Sea Res.*, 47B**,** 811–829.

[15] Reid, J. L., and A. W. Mantyla (1976), The effect of the geostrophic flow upon coastal sea elevations in the northern North Pacific Ocean, *J. Geophys. Res.*, 81(18), 3100–3110, doi:10.1029/JC081i018p03100.

[16] Thomson, R. E., and M. V. Krassovski (2010), Poleward reach of the California undercurrent extension. *J. Geophys. Res.*, 115, C09027, doi:10.1029/2010JC006280.

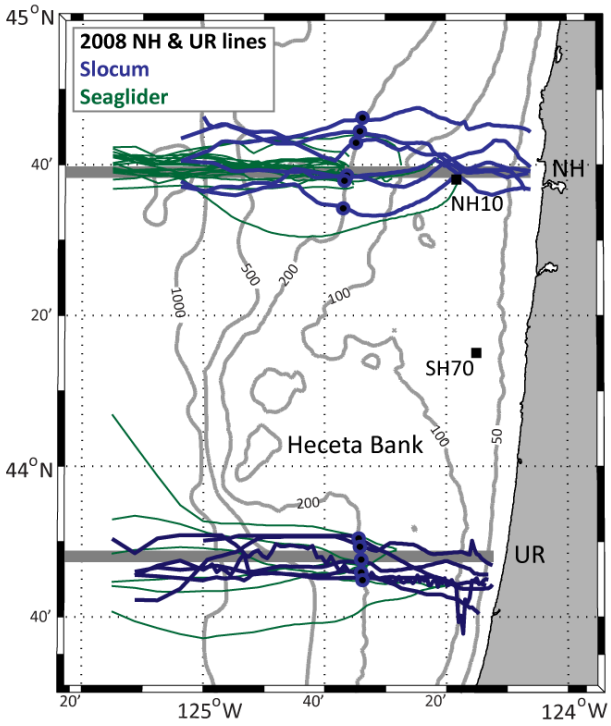

Figure 4.1: Central-Oregon continental shelf map with 2008 Slocum (blue) and Seaglider (green) cross-shelf transects along the Newport-Hydrographic (NH; 44.65°N) and the Umpqua-River (UR; 43.7°N) lines. The 200-m isobath crossings are demarcated with circles. Note, Heceta Bank is the stretch of shelf where the 200-m isobath is the farthest from shore.

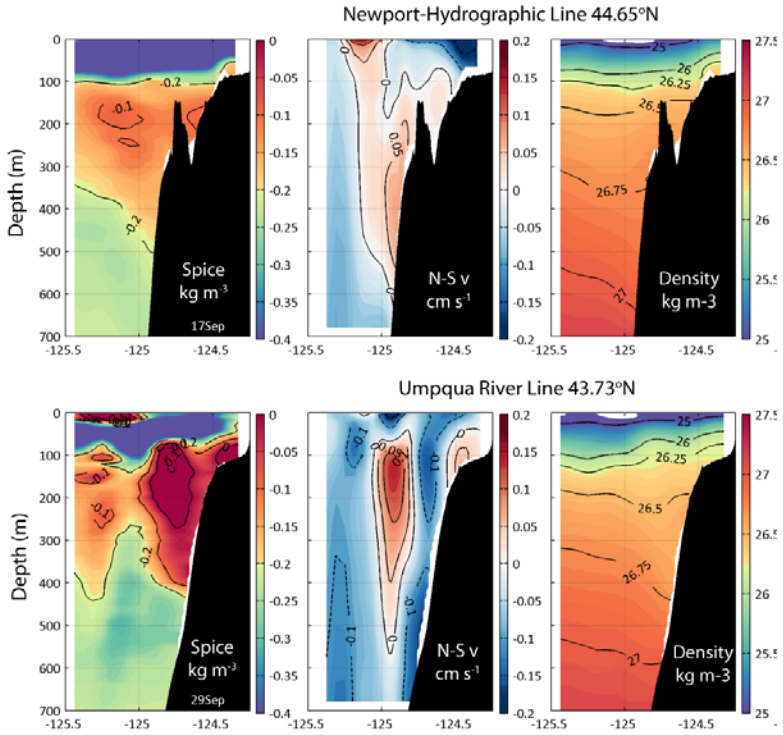

Figure 4.2: Cross-shelf transects of spice, N-S velocity, and potential density anomaly (top) Newport-Hydrographic line on 17 September 2008 and the (bottom) Umpqua-River line on 29 September 2008.

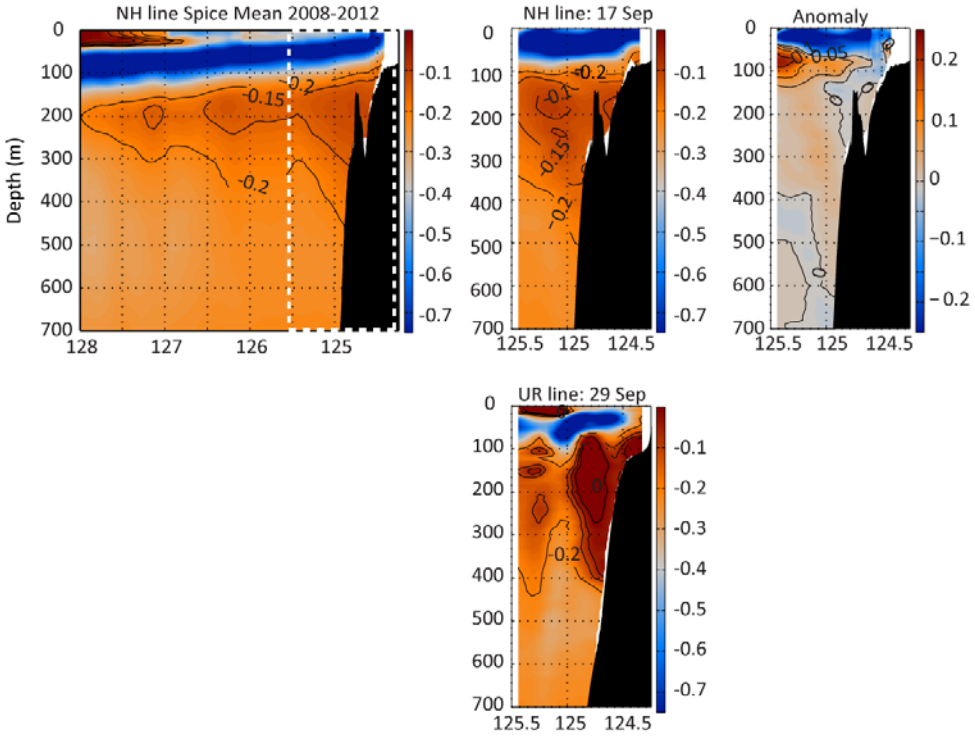

Figure 4.3. Mean vertical cross-section of spice (kg m^{-3}) along the NH line from 64 Seaglider sections, 2008 to 2012. The white dashed box indicates the coverage of the 17 September 2008 glider line and the corresponding spice anomaly panel. The UR line from 29 September 2008 is also included.

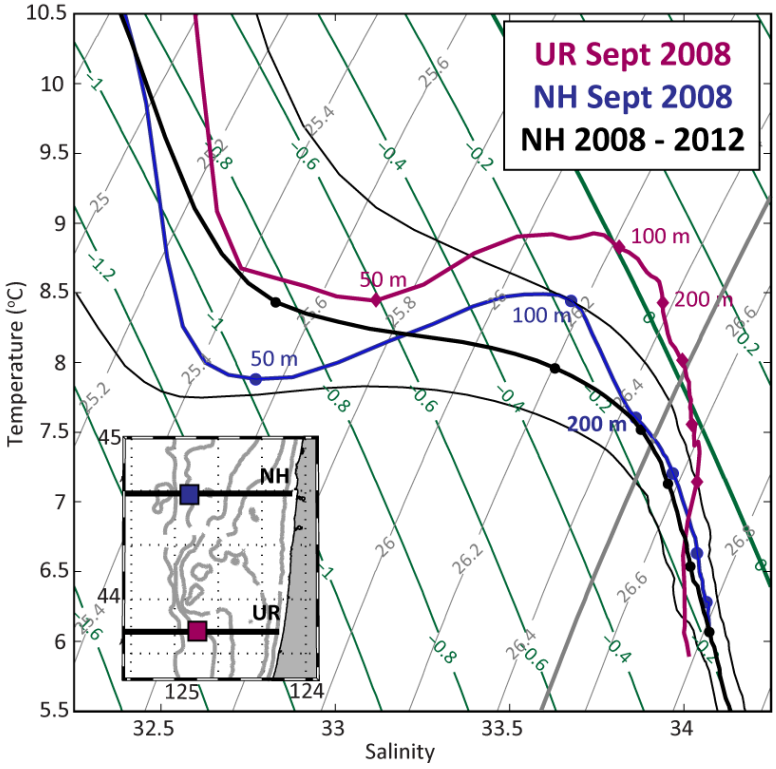

Figure 4.4: T-S diagram of vertical profiles over the 500-m isobath in the September 2008 cross-shelf NH line (blue) and UR line (red) in Figure 4.2. The 5-yr June – September mean (thick black) and standard deviation (thin black) of the NH-line 500-m isobath depth profile is included. Spice (kg m^{-3}) and potential density anomaly (kg m^{-3}) contours are green and gray, respectively. A map inset shows the location of the 500-m isobath crossing for the NH and UR line vertical profiles.

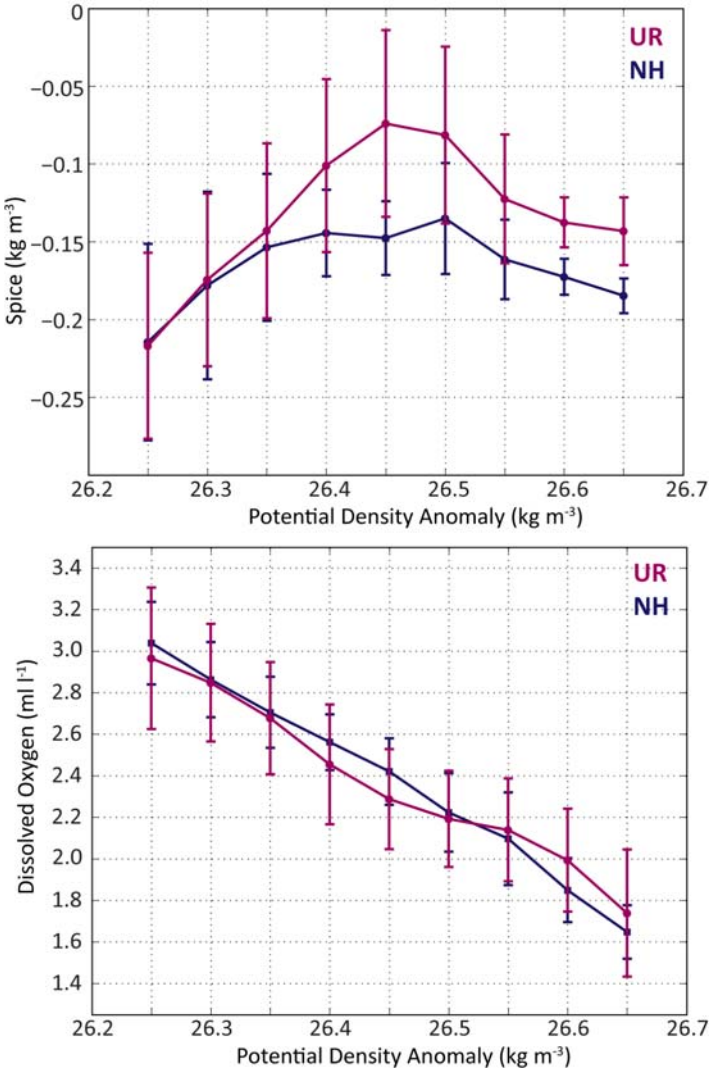

Figure 4.5: Spice-density and DO-density relationships for data sampled along the 300-m isobath of the NH (blue) and UR (red) lines in 2008. Mean values are plotted for each 0.05 kg m^{-3} density bin along with error bars representing one standard deviation.

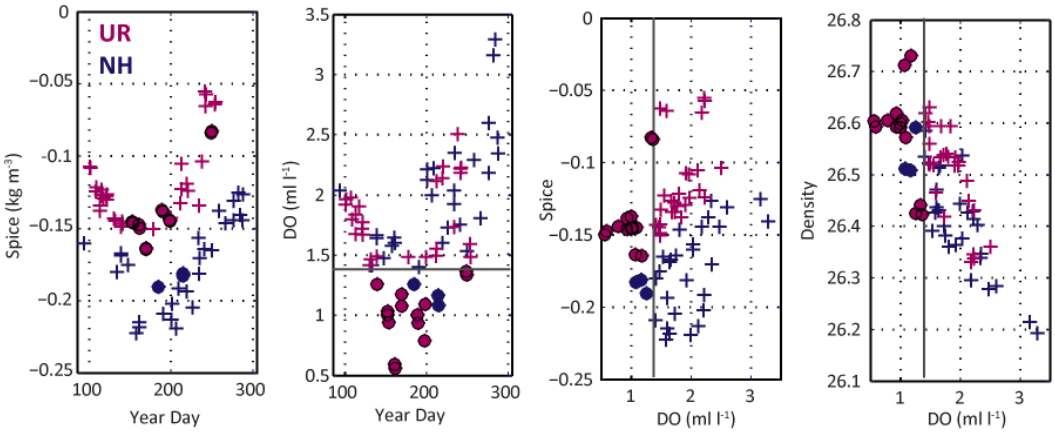

Figure 4.6: (a) Time series of near-bottom (10 mab) spice (kg m^{-3}) at the 100-m isobath along the UR (red) and NH (blue) lines. Measurements corresponding to DO concentrations below the hypoxic threshold (1.4 ml l^{-1}) are shown as filled circles. (b) Same as (a) for dissolved oxygen. (c) Spice-DO and (d) Density-DO relationships for the data in previous panels.

5. Summary

In this dissertation, observations from the central Oregon shelf have been presented and analyzed to better understand the influence of coastal currents and water-column stratification on near-bottom dissolved oxygen concentrations during upwelling. High-resolution moored continuous time series and underwater glider data allowed for analyses on fine temporal and spatial scales not possible in previous studies.

In Chapter 2, near-bottom continuous time series data is presented for three coastal moorings on the Oregon shelf. This is the first time series analysis of dissolved oxygen off Oregon. The majority of extant DO data sets are ship-based cast or bottle sample data. The high temporal resolution of a continuous time series for the 2009 – 2011 upwelling seasons allowed for an analysis on tidal, event-scale and interannual time scales. The observed spring transition does not coincide with the shift in local wind stress, thus a spring transition based on source water temperature is used. Near-bottom DO variability on tidal time scales is higher on the inner shelf than the mid shelf, however tidal currents were found to be higher of the Bank, along the Strawberry-Hill line. The inner shelf DO variability is also much higher on event and seasonal time scales. Large fluctuations in temperature, salinity and dissolved oxygen coincide with intraseasonal wind oscillations in the 2009 upwelling season. Downwelling-favorable wind events flush the inner shelf, whereas the mid shelf records are minimally affected. A seasonal decline of near-bottom DO on the mid shelf of -0.01 ml l^{-1} day^{-1} is observed. This is only 30% of the expected decrease in DO from microbial respiration, -0.026 ml l^{-1} day^{-1}, calculated from bottle incubations of water samples from the same location in 2009. Hence, physical processes of mixing and advection are tempering biological shelf processes on the mid shelf and keeping the system from reaching anoxia in the three years observed.

Cross-shelf variability of near-bottom DO is investigated in Chapter 3 with underwater glider data from the NH line. Greater spatial resolution than extant data sets elucidated persistent large cross-shelf variability on scales of < 10 km. On the NH line, hypoxia is prevalent in two cross-shelf locations, the mid shelf and the outer shelf. The gap in between the two observed prevalent locations lies just north of a sharp topographic feature, Stonewall Bank, where enhanced mixing rates are observed. Mid shelf moored time series shows a change in near-bottom cross-shelf and along-shelf flow around July 2011. At this time, flows weaken near the bottom and a strong onshore flow just below the surface boundary layer is observed. This shut down of near-bottom flow in both along-shelf and cross-shelf directions has implications for near-bottom DO concentrations. The onshore transport of source water observed early in the season replenishes and flushes the near-bottom environment. When that flow shuts down, there is a greater risk for hypoxia. The change in return flow depth is not associated with a change in the slope-Burger number, which is an indicator of return flow depth in a simplified 2-dimensional model.

Along-shelf variability of slope and shelf water mass properties due to Heceta Bank is presented in Chapter 4. During the 2008 upwelling season, underwater Slocum and Seagliders sampled along the NH line and the Umpqua-River line (43.7°N), nearly 100 km to the south. These two lines straddle Heceta Bank, the widest part of the Oregon shelf. Values of spice were found to be much higher along the UR line than the NH line over the course of the upwelling season. That result holds for near-bottom shelf waters as well. However, the relationship between spice and DO on the shelf is difficult to distinguish since respiration on the shelf dominates DO variability throughout the season. Along the NH line, the mean spice signal is diffuse and weak. It is likely that Heceta Bank is a location of enhanced mixing for the California Undercurrent which brings spicy and oxygen-depleted water northward. Mixing from eddies that are shed from the California Undercurrent (Garfield et al, 1999) are also a likely mechanism of mixing around

the Bank. These eddies observed off Washington (Pelland et al., 2013) may contribute to half of the CU signal.

Future modeling and observational work is needed to answer questions left unanswered in this compilation of studies. First, the 3-dimensionality of the flow field in the area around Heceta Bank has been established previously and in this dissertation. The influence of an along-shelf pressure gradient or large along-shelf variations (e.g., dv/dy) are proposed but have not been quantified. Second, there is a need for more coupled physical-biogeochemical idealized model experiments to identify and quantify the control of individual physical and biological mechanisms on near-bottom DO variability. A model with realistic bottom bathymetry could also test the hypothesis of enhanced mixing of the California Undercurrent as it flows around Heceta Bank. Third, the mechanism responsible for the shutdown of the bottom Ekman layer late in the season after the coastal jet moves farther offshore was not identified in this dissertation. Further dynamical analyses, observations or modeling experiments are is necessary to explain this result. Lastly, near-bottom DO concentrations are affected by pelagic and benthic respiration although the relative contribution of the two to near-bottom DO concentrations is still unknown. Observations of the vertical gradient of respiration rates and near-bottom DO variability would allow us to discern these two processes to better understand the influence from bottom sediments. Water-column respiration rates presented in this work were based on samples taken at one location during one upwelling season. Further work should be conducted to investigate the spatial and temporal variability of the respiration signal on the Oregon shelf.

In the chapters above, near-bottom DO variability has been examined in an area of complicated bathymetry. Similar bathymetric features are found elsewhere in the wind-driven coastal upwelling regimes in Eastern Boundary Current systems

off NW Africa and Chile. However, some of the results presented above may also apply to locations of simple bathymetry or embayments. It is likely that bottom boundary layer flows affect DO dynamics off the Washington and California shelves. In locations of eutrophication-induced hypoxia, such as the Gulf of Mexico and Chesapeake Bay, the phyical:biological ratio determining DO decline found here is likely to be much lower due to the increase in stratification and decrease in advection found in those locations compared to an open coastal region.

Given more time and resources continued research efforts would focus on the collection and analysis of high-resolution bottom boundary layer observations. Bottom boundary layer dynamics are of utmost importance to near-bottom DO dynamics as presented in Chapter 3. The ADCP data presented in the chapters above cannot sample the bottom 10% of the water column due to sensor restrictions. An additional velocity measuring device could be added to the existing observational platform, SH70 to obtain near-bottom velocities. This additional sensor could also provide vertical velocity data which was not included here.

To measure and quantify all terms in a DO budget on the Oregon shelf during upwelling, a mooring array combined with glider lines could be employed. An array of moorings similar to the 2001 COAST program, which did not sample DO, with current, temperature, salinity and dissolved oxygen sensors at a few depths would help identify the along-shelf and cross-shelf variability of physical advection, stratification and near-bottom hypoxia. Gliders outfitted with microstructure sensors sampling within the array of moorings would allow us to isolate the contribution of vertical and horizontal mixing on DO variability, while providing high spatial resolution in between moorings. Respiration rates have to be estimated using ship-based sampling. This and other water chemistry samples taken bimonthly would give a baseline for the nutrient concentrations and the

biological respiration signal over the shelf. The ship-based sampling scheme allows opportunities to ground-truth moored and glider samples by calibration casts or water samples several times a season. This sampling is similar to although more involved and resource intensive than the Oregon-shelf portion of the 2009-2010 MI_LOCO program.

Identifying present-day drivers of hypoxia and quantifying the interplay between physical and biological mechanisms in low-DO areas are necessary steps for predicting future DO levels in a changing climate. Recent findings of declining oxygen concentrations in the North Pacific (Whitney et al., 2007; Pierce et al., 2012) are in part due to a low-frequency oscillation (Falkowski et al., 2011) that few observational records can fully resolve. However, unprecedented atmospheric carbon dioxide levels are affecting the biogeochemical signatures of waters exposed to the atmosphere around the globe. Future DO levels off Oregon will depend on several factors including upwelling source water concentrations, affected by atmospheric concentrations and thermocline depth (Deutsch et al, 2011), and on the upwelling winds and coastal currents.

6. Bibliography

[1] Adams, K. A., J. A. Barth, F. Chan (2013), Temporal variability of near-bottom dissolved oxygen during upwelling off central Oregon. Journal of Geophysical Research Oceans, 118, 4839-4854, doi:10.1002/jgrc.20361.

[2] Bane, J.M., Y. H. Spitz,, R. M. Letelier, and W. T. Peterson (2007), Intraseasonal oscillations in Oregon's coastal upwelling system: from the jet stream to zooplankton. *Proceedings of the National Academy of Sciences*, USA 104, 13262–13267.

[3] Barnes, S. L., 1964. A technique for maximizing details in numerical weather map analysis. Journal of Applied Meteorology, 3, 396 – 409.

[4] Barth, J. A., S. D. Pierce, and R. M. Castelao (2005), Time dependent, wind-driven flow over a shallow mid shelf submarine bank. J. Geophys. Res., 110, C10S05, doi:10.1029/2004JC002761.

[5] Barnes, S. L., 1964. A technique for maximizing details in numerical weather map analysis. Journal of Applied Meteorology, 3, 396 – 409.

[6] Barth, J. A., R. K. Shearman, A. Y Erofeev, S. D. Pierce, F. Chan and K. Adams, 2014. Upwelling-driven continental shelf hypoxia: Underwater robotic gliders signal change. In preparation.

[7] Barth, J. A., S. D. Pierce, and R. M. Castelao (2005), Time dependent, wind-driven flow over a shallow mid shelf submarine bank. J. Geophys. Res., 110, C10S05, doi:10.1029/2004JC002761.

[8] Bograd, S. J., C. G. Castro, E. Di Lorenzo, D. M. Palacios, H. Bailey, W. Gilly, and F. P. Chavez (2008), Oxygen declines and the shoaling of the hypoxic boundary in the California Current, *Geophys. Res. Lett.,* 35, L12607, doi:10.1029/2008GL034185.

[9] Boyd, T., M.D. Levine, P.M. Kosro, S.R. Gard, and W. Waldorf (2002), Observations from Moorings on the Oregon Continental Shelf (May-August 2001), COAS Data Report 190, Reference 2002-6.

[10] Castelao, R. M., and J. A. Barth (2005), Coastal ocean response to summer upwelling favorable winds in a region of alongshore bottom topography variations off Oregon, *J. Geophys. Res*., 110, C10S04, doi:10.1029/2004JC002409.

[11] Chan, F., J. A. Barth, J. Lubchenco, A. Kirincich, H. Weeks, W. T. Peterson, B. A. Menge (2008), Emergence of anoxia in the California Current large marine ecosystem, *Science*, 319, doi:10.1126/science.1149016.

[12] Connolly, T. P., B. M. Hickey, S. L. Geier, and W. P. Cochlan (2010), Processes influencing seasonal hypoxia in the northern California Current system, *J. Geophys. Res.*,115, C03021, doi:10.1029/2009JC005283.

[13] D'Errico,J.(2004),Inpaint_nans, (http://www.mathworks.com/matlabcentral/fileexchange/4551),MATLAB Central File Exchange. Retrieved 24 June 2012.

[14] Diaz, R. J., and J. Rosenberg (1995), Marine benthic hypoxia: A review of its ecological effects and the behavioural responses of benthic macrofauna, Oceanogr. Mar. Biol., 33, 245–303.

[15] Eriksen, C. C., Osse, T. J., Light, R. D., Wen, T., Lehman, T. W., Sabin, P. L., Ballard, J. W., Chiodi, A. M., Seaglider: a long-range autonomous underwater vehicle for oceanographic research, *Journal of Oceanic Engineering, IEEE*. 26(4), 424-436, doi: 10.1109/48.972073.

[16] Erofeeva, S. Y., G. D. Egbert, and P. M. Kosro (2003), Tidal currents on the central Oregon shelf: Models, data, and assimilation, J. Geophys. Res., 108, 3148, doi:10.1029/2002JC001615.

[17] Deutsch, C., H. Brix, T. Ito, H. Frentzel, L. Thompson (2011), Climate-forced variability of ocean hypoxia, *Science*, 333(6040), 336-339, doi:10.1126/science.1202422.

[18] Falkowski, P. G., et al., (2011), Ocean deoxygenation: Past, present, and future, *Eos Trans. AGU*, 92(46), 409.

[19] Garau, B., S. Ruiz, W. G. Zhang, A. Pascual, E. Heslop, J. Kerfoot, and J. Tintore (2011), Thermal lag correction on Slocum CTD glider data. *J. Atmos. Oceanic Technol*., 28, 1065–1071.

[20] Garfield, N., C. A. Collins, R. G. Paquette, and E. Carter, (1999), Lagrangian exploration of the California Undercurrent, 1992– 95. *J. Phys. Oceanogr.,* 29, 560–583.

[21] Garrett, C., P. MacCready, and P. B. Rhines (1993), Boundary mixing and arrested Ekman layers: Rotating stratified flow near a sloping bottom. *Annu. Rev. Fluid Mech*., 25, 291–324.

[22] Grantham, B. A., F. Chan, K. J. Nielsen, D. S. Fox, J. A. Barth, A. Huyer, J. Lubchenco, and B. A. Menge (2004), Upwelling-driven nearshore hypoxia signals ecosystem and oceanographic changes in the Northeast Pacific, Nature, 429, 749-754.

[23] Gray, J. S., R. S. Wu, and Y. Y. Or (2002), Effects of hypoxia and organic enrichment on the marine environment, Mar. Ecol. Prog. Ser., 238, 249–279, doi:10.3354/meps238249.

[24] Deutsch, C., Brix, H., Ito, T., & Thompson, L. (2011). Ocean Hypoxia, *Science*, 333, 336–339.

[25] Hickey, B.M., 1979. The California Current System, hypotheses and facts. *Progress in Oceanography*, 191–279.

[26] Huyer, A. (1976), A comparison of upwelling events in two locations: Oregon and Northwest Africa. *J. Marine Res.*, 34(4), 531-546.

[27] Huyer, A., E. J. C. Sobey, R. L. Smith (1979), The spring transition in currents over the Oregon continental shelf. J. Geophys. Res., 84, 6995–7011.

[28] Huyer, A., J. H. Fleischbein, J. Keister, P. M. Kosro, N. Perlin, R. L. Smith, and P. A. Wheeler (2005), Two coastal upwelling domains in the northern California Current system, *J. Marine Res.*, 63, 901–929.

[29] Huyer, A., R. L. Smith, and J. H. Fleischbein (2002), The coastal ocean off Oregon and northern California during the 1997–8 El Niño, *Progress in Oceanography,* 54, 311–341, doi: 10.1016/S0079-6611(02)00056-3.

[30] Keeling, R. F., A. Kortzinger, and N. Gruber (2010), Ocean deoxygenation in a warming world, Annu. Rev. Mar. Sci., 2, 199-229.

[31] Keller, A. A., V. Simon, F. Chan, W. W. Wakefield, M. E. Clarke, J. A. Barth, D. Kamikawa and E. L. Fruh (2010), Demersal fish and invertebrate biomass in relation to an offshore hypoxic zone along the US West Coast. *Fisheries Oceanography*, 19, 76–87. doi: 10.1111/j.1365-2419.2009.00529.x.

[32] Kirincich, A. R., J. A. Barth, B. A. Grantham, B. A. Menge, and J. Lubchenco (2005), Wind-driven inner-shelf circulation off central Oregon during summer, *J. Geophys. Res*., 110, C10S03, doi:10.1029/2004JC002611.

[33] Kirincich, A. R., and J. A. Barth (2009), Alongshelf Variability of Inner-Shelf Circulation along the Central Oregon Coast during Summer, *J. Phys. Oceanogr*., 35, 1380 – 1398, doi: 10.1175/2008JPO3760.1.

[34] Kosro, P. M., W. T. Peterson, B. M. Hickey, R. K. Shearman, and S. D. Pierce (2006), Physical versus biological spring transition: 2005, *Geophys. Res. Lett*., 33, L22S03, doi:10.1029/2006GL027072.

[35] Large, W. G., J. C. McWilliams, and S. C. Doney (1994), Oceanic vertical mixing: A review and a model with a nonlocal boundary layer parameterization, *Rev. Geophys*., 32, 363-403.

[36] Meinvielle, M., and G. C. Johnson (2013), Decadal water-property trends in the California Undercurrent, with implications for ocean acidification, *J. Geophys. Res*., 118, 6687–6703, doi:10.1002/2013JC009299.

[37] Merckelbach, L.M., Briggs, R. D., Smeed, D.A., Griffiths, G., (2008) Current measurements from autonomous underwater gliders, *IEEE/OES 9th Working Conference on Current Measurement Technology,* 17-19 March 2008, doi:10.1109/CCM.2008.4480845.

[38] Nam, S. H., and U. Send (2011), Direct evidence of deep water intrusions onto the continental shelf via surging internal tides, *J. Geophys. Res.*, 116, C05004, doi:10.1029/2010JC006692.

[39] Nam, S. H., H. J. Kim, and U. Send (2011), Amplification of hypoxic and acidic events by La Niña conditions on the continental shelf off California, *Geophys. Res. Lett*., 38, L22602, doi:10.1029/2011GL049549.

[40] Nash, J. D., and J. N. Moum (2001), Internal hydraulic flows on the continental shelf: High drag states over a small bank, J. Geophys. Res., 106(C3), 4593–4611, doi:10.1029/1999JC000183.

[41] Nicholson, D. (2009), Nitrogen, oxygen and the noble gases as tracers of upper-ocean productivity and air-sea gas fluxes, Ph.D. dissertation, University of Washington, Seattle, Washington, U.S.A.

[42] Osborne, J. J., A. L. Kurapov, G. D. Egbert, and P. M. Kosro (2011), Spatial and Temporal Variability of the M2 Internal Tide Generation and Propagation on the Oregon Shelf, *J. Phys. Oceanogr.*, 41, 2037–2062. doi:10.1175/JPO-D-11-02.1.

[43] Pawlowicz, R., B. Beardsley, and S. Lentz (2002), Classical tidal harmonic analysis including error estimates in MATLAB using T_TIDE, *Comput. Geosci*., 28, 929–937.

[44] Pelland, N. A., C. C. Eriksen, C. M. Lee (2013), Subthermocline eddies over the Washington continental slope as observed by seagliders, 2003–09. *J. Phys. Oceanogr.*, 43, 2025–2053. doi: http://dx.doi.org/10.1175/JPO-D-12-086.1.

[45] Pierce, S. D., J. A. Barth, R. E. Thomas, and G. W. Fleischer (2006), Anomalously warm July 2005 in the northern California Current: Historical context and significance of cumulative wind stress. *Geophys. Res. Lett*., 33, L22S04, doi:10.1029/2006GL027149.

[46] Pierce, S. D., J. A. Barth, R. K. Shearman, A. Y. Erofeev (2012), Declining Oxygen in the Northeast Pacific, *J. Phys. Oceanogr.*, 42, 495–501. doi:10.1175/JPO-D-11-0170.1.

[47] Pierce, S. D., R. L. Smith, P. M. Kosro, J. A. Barth, and C. D. Wilson (2000), Continuity of the poleward undercurrent along the eastern boundary of the mid-latitude North Pacific. *Deep-Sea Res.*, 47B**,** 811–829.

[48] Reid, J. L., and A. W. Mantyla (1976), The effect of the geostrophic flow upon coastal sea elevations in the northern North Pacific Ocean, *J. Geophys. Res*., 81(18), 3100–3110, doi:10.1029/JC081i018p03100.

[49] Reimers, C.E., H. T. Özkan-Haller, P. Berg, A. Devol, K. McCann-Grosvenor, and R. D. Sanders (2012), Benthic Oxygen Consumption Rates during Hypoxic Conditions on the Oregon Continental Shelf: Evaluation of the Eddy Correlation Method. *J. Geophys. Res.* 117, C02021, doi:10.1029/2011JC007564.

[50] Send, U. and S. H. Nam (2012), Relaxation from upwelling: The effect on dissolved oxygen on the continental shelf. *J. Geophys. Res.* 117, C04024, doi:10.1029/2011JC007517.

[51] Schlax, M. G., and D. B. Chelton (1992), Frequency domain diagnostics for linear smoothers. *J. Amer. Stat. Assoc.*, 87, 1070-1081.

[52] Smith, R. L. (1981), A comparison of the structure and variability of the flow field in three coastal upwelling regions: Oregon, northwest Africa, and Peru, in *Coastal Upwelling, Coastal Estuarine Ser*., vol. 1, edited by F. A. Richards, pp. 107– 118, AGU, Washington, D. C.

[53] Steindler L., M. S. Schwalbach, D. P. Smith, F. Chan, and S. J. Giovannoni (2011), Energy Starved Candidatus Pelagibacter Ubique Substitutes Light-Mediated ATP Production for Endogenous Carbon Respiration. *PLOS ONE* 6(5): e19725. doi:10.1371/journal.pone.0019725.

[54] Suanda, A. and J. A. Barth (2012), Observations of High-Frequency Internal Waves across the Oregon Inner Shelf, paper presented at 2012 Ocean Sciences Meeting, ASLO and AGU, Salt Lake City, Utah. http://www.sgmeet.com/osm2012/viewabstract2.asp?AbstractID=10085

[55] Tengberg A., J. Hovdenes, H. Andersson, O. Brocandel, R. Diaz, D. Hebert, T. Arnerich, C. Huber, A. Kortzinger, A. Khripounoff, F. Rey, C. Ronning, J. Schimanski, S. Sommer, A. Stangelmayer (2006), Evaluation of a lifetime-based optode to measure oxygen in aquatic systems. *Limnology and Oceanography methods*, 4, 7-17.

[56] Thomson, R. E., and M. V. Krassovski (2010), Poleward reach of the California undercurrent extension. J. Geophys. Res., 115, C09027, doi:10.1029/2010JC006280.

[57] Whitney, F. A., H. J. Freeland, and M. Robert (2007), Persistently declining oxygen levels in the interior waters of the eastern subarctic Pacific, Prog. Oceanogr., 75, 179-199, doi:10.1016/j.pocean.2007.08.007.

[58] Whitney, M. M. and J. S. Allen (2009), Coastal wind-driven circulation in the vicinity of a bank. Part II: modeling flow over the Heceta Bank complex on the Oregon coast, J. Phys. Oceanogr., 39, 1298-1316

[59] Winant, C. D., R. C. Beardsley, R. E. Davis, (1987), Moored Wind, Temperature,and Current Observations Made During Coastal Ocean Dynamics Experiments 1 and 2 Over the Northern California Continental Shelf and Upper Slope. *J. Geophys. Res., 92, C2,* 1569-1604.